

DISS. ETH NO. 24926

**New approaches to understand T cell activation and  
circumvent T cell dysfunction in cancer**

A thesis submitted to attain the degree of  
DOCTOR OF SCIENCES of ETH ZURICH

(Dr. sc. ETH Zurich)

presented by

**Tobias Wolf**

Dipl. Biochem.

Ernst-Moritz-Arndt University Greifswald, Germany

born on *01.10.1987*

Bad Saarow, Germany

accepted on the recommendation of

Prof. Dr. Antonio Lanzavecchia (examiner)

Prof. Dr. Federica Sallusto (co-examiner)

Prof. Dr. Manfred Kopf (co-examiner)

2018



## Contents

<b>1</b>	<b>Summary</b> .....	<b>6</b>
<b>2</b>	<b>Abbreviations</b> .....	<b>10</b>
<b>3</b>	<b>Introduction</b> .....	<b>14</b>
<b>3.1</b>	<b>T cells: mediators of cellular immunity</b> .....	<b>14</b>
3.1.1	T cell receptor .....	14
3.1.2	T cell generation .....	16
3.1.3	T cell receptor signaling .....	20
<b>3.2</b>	<b>T cell activation and exhaustion</b> .....	<b>23</b>
3.2.1	T cell activation .....	23
3.2.2	T cell differentiation .....	26
3.2.3	Metabolism fuels T cell immunity .....	28
3.2.4	Regulatory T cells and immune tolerance .....	33
3.2.5	T cell exhaustion .....	36
<b>3.3</b>	<b>Cancer immunology and immune therapy</b> .....	<b>38</b>
3.3.1	Cancer immunoediting.....	39
3.3.2	Influence of the tumor microenvironment on T cell immunity.....	42
<b>3.4</b>	<b>Immunotherapy to treat cancer</b> .....	<b>45</b>
3.4.1	Origins of cancer antigens .....	45
3.4.2	Cancer vaccines .....	47
3.4.3	Immune checkpoint blockade .....	47
3.4.4	Adoptive T cell therapy.....	48
3.4.5	Metabolism – a target to treat cancer .....	49
<b>3.5</b>	<b>Hepatocellular Carcinoma</b> .....	<b>51</b>
3.5.1	Anatomy of the liver .....	51
3.5.2	The etiologies of HCC .....	53
3.5.3	T cells in HCC.....	53
3.5.4	Immunotherapeutic approaches to treat HCC .....	56
<b>4</b>	<b>Aims</b> .....	<b>59</b>
<b>5</b>	<b>Individual contributions to the studies</b> .....	<b>60</b>
<b>6</b>	<b>Results and discussion</b> .....	<b>61</b>
6.1	Translation profiling reveals regulations underlying T cell naiveté and preparedness .....	61

6.1.1	Results .....	61
6.1.2	Discussion .....	72
<b>6.2</b>	<b>L-Arginine modulates T cell metabolism and enhances survival and anti-tumor activity .....</b>	<b>75</b>
6.2.1	Results .....	75
6.2.2	Discussion .....	81
<b>6.3</b>	<b>High-throughput T cell receptor (TCR) grafting for adoptive T cell therapies to treat cancer .....</b>	<b>83</b>
6.3.1	Results .....	83
6.3.2	Discussion .....	93
<b>7</b>	<b>Outlook .....</b>	<b>96</b>
<b>8</b>	<b>Experimental procedures .....</b>	<b>99</b>
8.1	Isolation of primary cells from buffy coats .....	99
8.2	Cell culture .....	99
8.3	Flow cytometry .....	100
8.4	Withdrawal assay .....	100
8.5	ATP measurement .....	100
8.6	Metabolomics .....	100
8.7	Metabolic flux experiments .....	101
8.8	Detection of amino acids and polyamines by HILIC LC-MS/MS .....	101
8.9	Sample preparation for proteome MS analysis .....	101
8.10	LC-MS/MS for analysis of proteome .....	102
8.11	Pulsed SILAC .....	103
8.12	Tumor processing .....	103
8.13	<sup>3</sup> H-arginine uptake assay .....	103
8.14	Quantitative determination of amino acid uptake and calculation of proteome incorporation .....	104
8.15	OCR measurement .....	104
8.16	Nitric oxide detection assay .....	104
8.17	Limited proteolysis and mass spectrometry .....	105
8.18	CRISPR/Cas9-mediated gene disruption .....	106
8.19	Analysis of phosphorylation level of 4E-BP and S6K1 .....	108
8.20	Cytokine assay .....	109
8.21	Glucose consumption assay .....	109

<b>8.22</b>	<b>Serial block-face scanning electron microscopy and 3D reconstruction of single layers.....</b>	<b>109</b>
<b>8.23</b>	<b>Measuring single cell densities.....</b>	<b>109</b>
<b>8.24</b>	<b>Estimation of transcript copy numbers.....</b>	<b>109</b>
<b>8.25</b>	<b>qPCR.....</b>	<b>110</b>
<b>8.26</b>	<b>Microfluidic device handling and droplet PCR.....</b>	<b>110</b>
<b>8.27</b>	<b>Design of CD4 and NFAT-GFP construct.....</b>	<b>114</b>
<b>8.28</b>	<b>Droplet generation with vortex mixer.....</b>	<b>114</b>
<b>8.29</b>	<b>MinION sequencing.....</b>	<b>114</b>
<b>8.30</b>	<b>Animal experiments.....</b>	<b>115</b>
8.30.1	Mice.....	115
8.30.2	Isolating and culturing of mouse CD8 <sup>+</sup> T cells.....	115
8.30.3	Adoptive T cell transfer and survival experiments.....	115
8.30.4	Tumor experiments: <i>in vitro</i> activation of T cells.....	116
8.30.5	Tumor experiments: <i>in vivo</i> priming of T cells.....	116
8.30.6	Experiments with <i>Arg2</i> <sup>-/-</sup> mouse T cells.....	116
8.30.7	Mouse experiments with dietary L-arginine.....	117
<b>8.31</b>	<b>Quantification and statistical analysis.....</b>	<b>117</b>
8.31.1	Analysis of proteomics data.....	117
8.31.2	Enrichment analysis.....	118
<b>9</b>	<b>References.....</b>	<b>119</b>
<b>10</b>	<b>Acknowledgements.....</b>	<b>137</b>
<b>11</b>	<b>Curriculum Vitae.....</b>	<b>139</b>

# 1 Summary

T cell activation is a crucial checkpoint of adaptive immune responses to infections or cancers. Chronic T cell activation and/or changes in the environment of T cell activation can lead to T cell dysfunction and to an impaired clearance of the pathogen. While the molecular changes occurring following activation are well studied, little is known about the mechanisms underlying naïve T cell preparedness and the metabolic changes associated with T cell activation.

By using a pulsed SILAC proteomic approach and RNA sequencing, we determined global translational activity and transcript abundances in naïve and activated human T cells. While the majority of the proteome of naïve T cells was stable, roughly 1 % of the proteins were rapidly renewed, including receptors and transcription factors that shape the identity of CD4<sup>+</sup> T cells and promote quiescence. Furthermore, we showed that despite the low translational activity of naïve T cells, they contain large numbers of unused ribosomes and TOP-mRNAs. Upon naïve T cell activation, TOP-mRNAs were rapidly engaged in an mTORC1-dependent manner. Thus, this study discloses different mechanisms supporting naïve T cell preparedness.

Secondly, I analysed the metabolic changes associated with naïve T cell activation. To do so, kinetics of the metabolome and proteome following stimulation of naïve T cells were generated. While numerous pathways were up-regulated upon activation, an increased arginine metabolism led to a drop in intracellular L-arginine concentrations. Elevating intracellular L-arginine levels were associated with prolonged survival capacity and improved anti-tumor response. Structural analysis allowed the identification of three transcriptional regulators (BAZ1B, PSIP1, TSN) that induced L-arginine-mediated prolonged survival. Thus, L-arginine is a key metabolic regulator in T cells and increased intracellular levels are associated with improved T cell survival and anti-tumor functionality.

Finally, we aimed to establish microfluidics-based grafting of TCRs (MIGOT) to overcome the limitation of initial TIL expansion. By using a microfluidic device, we were able to transfer TCRs from TILs onto a reporter cell line, which can be analysed

according to the specificity of the engrafted TCRs. MIGOT offers the possibility to link information about TCR diversity with specificity. Moreover, MIGOT allows the analysis of the TCR repertoire of TILs at the highest state of TCR diversity.

## **Zusammenfassung**

Die Aktivierung von T-Zellen ist entscheidend für die Kontrolle der adaptiven Immunantwort zum Schutz vor Infektionen oder Krebs. Werden T-Zellen chronisch aktiviert und/oder werden die Bedingungen der Aktivierung verändert, kann es zu einer Beeinträchtigung der T-Zell-Funktion führen. Die Folge kann eine ineffiziente Beseitigung von Krankheitserregern sein. Die molekularen Veränderungen, welche mit der Aktivierung von T-Zellen einhergehen, sind Gegenstand intensiver Forschung. Jedoch ist wenig bekannt, wie T-Zellen ihre Bereitschaft zur Immunantwort gewährleisten und wie T-Zellen ihren Metabolismus nach der Aktivierung umstellen.

Im ersten Teil dieser Arbeit wurden die Mechanismen, welche die Bereitschaft von naiven T-Zellen ermöglichen, untersucht. Dazu wurde die Translationsaktivität und die Häufigkeit von mRNAs in naiven und aktivierten T-Zellen mit Hilfe von Massenspektrometrie und RNA-Sequenzierungsmethoden analysiert. Das Proteom von naiven T-Zellen ist nahezu stabil und nur ca. 1% der Proteine werden häufig erneuert. Bei Proteinen mit hohem Umsatz handelte es sich unter anderem um Rezeptoren und Transkriptionsfaktoren, die Identität und Status von naiven CD4<sup>+</sup> T-Zellen prägen. Des Weiteren enthielten naive T-Zellen große Mengen an ungenutzten Ribosomen und mRNAs, was im starken Widerspruch zur geringen Translationsrate in diesen Zellen stand. Eine genauere Untersuchung der ungenutzten mRNAs zeigte, dass diese ein spezifisches Motiv (TOP-Motiv) enthielten. Sobald naive T-Zellen aktiviert wurden, erfolgte die Translation der TOP-mRNAs in einem mTORC1 abhängigen Prozess. Somit zeigt der erste Teil meiner Arbeit auf, dass die rasche Aktivierung von T-Zellen über verschiedene Mechanismen ermöglicht wird.

Da die Aktivierung von T-Zellen nicht nur mit einer Veränderung der Translationsaktivität einhergeht, sondern auch mit einer Umstellung des Metabolismus von T-Zellen, wurden im zweiten Teil der Arbeit die metabolischen Veränderungen, die mit der T-Zellaktivierung verbunden sind, untersucht. Die Veränderungen im Metabolom und Proteom in der frühen Phase der T-Zellaktivierung wurden massenspektrometrisch untersucht. Im Gegensatz zu allen



anderen Aminosäuren war die intrazelluläre Konzentration von L-Arginin nach Aktivierung verringert. Dies konnte auf eine erhöhte Aktivität des Argininstoffwechsels nach Aktivierung zurückgeführt werden. Eine Erhöhung der L-Argininkonzentration führte *in vitro* zu einer verlängerten Lebensdauer der T-Zellen. Des Weiteren zeigten L-Arginin behandelte T-Zellen eine verbesserte Antitumorantwort *in vivo*. Strukturelle Analysen zeigten, dass die verlängerte L-Arginin-vermittelte Lebensdauer von T-Zellen unter anderem von drei Transkriptionsfaktoren (BAZ1B, PSIP1, TSN) vermittelt wird. Der zweite Teil meiner Arbeit zeigt somit, dass L-Arginin eine wichtige Rolle in T-Zellen einnimmt und dass eine Erhöhung der L-Argininkonzentration einen positiven Effekt auf die Funktionalität der Antitumorantwort hat.

Aktuelle Protokolle zur Identifizierung von Tumor-spezifischen T Zellen sind auf eine *in vitro* Vermehrung von Tumor-infiltrierenden T-Zellen angewiesen. Allerdings können verschiedene Mechanismen innerhalb des Tumors die Proliferation von Tumor-infiltrierenden T-Zellen beeinträchtigen. Das Ziel des letzten Teils meiner Arbeit war es eine Methode zu etablieren, welche die Analyse der Antigen-spezifität von T-Zell-Rezeptoren ermöglicht, ohne jedoch auf die Expansion von Tumor-infiltrierenden T-Zellen angewiesen zu sein. Dazu wurde ein mikrofluidisches Chip-System entwickelt, womit T-Zell-Rezeptoren von primären T-Zellen auf Reporterzelllinien mittels Klonierungsmethoden übertragen werden können. Diese Methode ermöglicht es, Informationen bezüglich der Diversität der T-Zell-Rezeptoren mit deren Spezifität zu verknüpfen. Des Weiteren können Repertoires von T-Zell-Rezeptoren von Tumor-infiltrierenden T-Zellen zum Zeitpunkt der geringsten Klonalität analysiert werden.

## 2 Abbreviations

ACT	Adoptive cell transfer
AFP	$\alpha$ -fetoprotein
AIRE	Autoimmune regulator
ALL	Acute lymphoblastic leukemia
APC	Antigen-presenting cell
APS1	Autoimmune polyendocrine syndrome type 1
ASH	Alcoholic steatohepatitis
BCR	B cell receptor
BEC	S-(2-boronoethyl)-L-cysteine
CAR	Chimeric antigen receptor
CCR	CC-chemokine receptor
CD	Cluster of differentiation
CDR	Complementary determining region
CHX	Cycloheximid
CIK	Cytokine-induced killer cells
CLDN1	Claudin-1
CLP	Common lymphoid progenitors
CMP	Common myeloid progenitors
CSK	C-terminal SRC kinase
cSMAC	Central supramolecular activation cluster
CTA	Cancer/testis antigen
cTEC	Cortical thymic epithelial cell
CTLA4	Cytotoxic T-lymphocyte antigen 4
D	Diversity
DAG	Diacylglycerol
DC	Dendritic cells
ddPCR	Digital droplet PCR
DN	Double negative
DP	Double positive
dSMAC	Distal supramolecular activation cluster
ETP	Early thymic progenitor

FAO	Fatty acid oxidation
FasL	Fas ligand
FDA	Food and Drug Administration
FDR	False discovery rate
FOXO1	Forkhead box O
Foxp3	Forkhead box P3
FPKM	Frequency per kilobase of exon per million reads mapped
GATA3	GATA-binding protein 3
HA	Hemagglutinin
HBV	Hepatitis B virus
HCC	Hepatocellular carcinoma
HCV	Hepatitis C virus
HEV	High-endothelial venules
HIF1 $\alpha$	Hypoxia-inducible factor 1 $\alpha$
HSC	Hematopoietic stem cell
ICOS	Inducible co-stimulator
IFN	Interferon
IFN- $\gamma$	Interferon- $\gamma$
IL	Interleukin
IL-12R $\beta$	IL-12 receptor $\beta$
InCVAX	In situ cancer vaccine
Ins(1,4,5)P <sub>3</sub>	Inositol-1,4,5-triphosphate
ITAM	Immunoreceptor tyrosine-based activating motif
ITK	IL-2 inducible T cell kinase
iTreg	Induced Treg
I $\kappa$ B	Inhibitor of NF- $\kappa$ B
J	Joining
KLF2	Kruppel-like factor 2
LAG3	Lymphocyte activation gene 3
LAT	Linker for activation of T cells
LC-MS/MS	Liquid chromatography-coupled high resolution mass spectrometry
LCMV	Lymphocytic choriomeningitis virus
LFQ	Label-free quantification

LiP	Limited proteolysis
LPS	Lipopolysaccharide
LSEC	Liver sinusoidal endothelial cell
mDC	Myeloid dendritic cell
MDSC	Myeloid derived suppressor cells
MHC	Major histocompatibility complex
MIGOT	Microfluidic-based grafting of T cell receptors
MS/MS	Tandem mass spectrometry
mTEC	Medullary thymic epithelial cell
mTOR	Mechanistic target of rapamycin
mTORC1/2	mTOR complex 1/2
NASH	Nonalcoholic steatohepatitis
NDGC	<i>N</i> -dihydro-galacto-chitosan
NF-κB	Nuclear factor κB
NFAT	Nuclear factor of activated T cells
NOHA	N <sup>ω</sup> -Hydroxy-nor-L-arginine
nTreg	Natural T regulatory cell
OCLN	Occludin
OXPPOS	Oxidative phosphorylation
PCR	Polymerase chain reaction
PD-L1	Ligand of PD-1
PD1	Programmed cell death protein 1
pDC	Plasmacytoid dendritic cell
pgRNA	Pregenomic RNA
PHA	Phytohaemagglutinin
PI3K	Phosphoinositide-3-kinase
PLCγ1	Phospholipase Cγ1
PRR	Pattern recognition receptors
pSMAC	Peripheral supramolecular activation cluster
PtdIns(4,5)P <sub>2</sub>	Phosphatidylinositol-4,5-bisphosphate
RAG	Recombination activating gene
RASGRP	RAS guanyl-nucleotide releasing protein
RORγt	Retinoic-acid orphan receptor

ROS	Reactive oxygen species
SFK	SRC family kinases
SILAC	Pulsed stable isotope labeling by amino acids in cell culture
SMAC	Supramolecular activation cluster
SP	Single positive
SPRY2	Sprout homologue 2
SQSTM1	Sequestosome 1
STAT	Signal transducer and activator of transcription
T-bet	T-box expressed in T cells
TAA	Tumor associated antigen
TAM	Tumor-associated macrophages
TCR	T cell receptor
TGF	Transforming growth factor
T <sub>H</sub>	T helper cell
TIL	Tumor infiltrating lymphocyte
TIM3	T cell immunoglobulin domain and mucin domain-containing protein3
TME	Tumor microenvironment
TOP	5'-terminal oligopyrimidin
TRAIL	Tumor necrosis factor-related apoptosis-inducing ligand
TSA	Tumor specific antigen
TSSP	Thymic-specific serine protease
V	Variable
VEGF	Vascular endothelial growth factor
VLDL	Very low-density lipoprotein

## 3 Introduction

### 3.1 T cells: mediators of cellular immunity

The human body is challenged by an enormous variety of pathogens. The innate and adaptive immune system has evolved to encounter this threat. While the innate immune system recognizes conserved molecular structures shared by different pathogens or molecules released by damaged cells, the adaptive immune system displays a specific immune response to a variety of different microbial and non-microbial antigens. The humongous diversity, which is required for the latter system, cannot be achieved by coding sequences in the genome for every single antigen-receptor. Therefore, T cells, as well as B cells, undergo somatic rearrangement on the genetic loci for their antigen-receptor to ensure the required diversity. The antigen receptor of T cells is the T cell receptor (TCR)<sup>1</sup>.

#### 3.1.1 T cell receptor

The TCR is a heterodimer and can be divided into two classes:  $\alpha\beta$ TCRs and  $\gamma\delta$ TCRs, of which the latter only display 1 – 10% of the T cell repertoire<sup>2</sup>. The  $\alpha\beta$ TCR, as well as the  $\gamma\delta$ TCR, consists of two transmembrane proteins, which are connected via disulfide bonds between their extracellular parts. Each chain of the TCR has two immunoglobulin-like domains, the constant and the variable domain (Fig. 3.1). The variable domain of the TCR is encoded by variable (V), diversity (D) and joining (J) gene segments. In the human  $\beta$  locus 50 V, 2 D and 12 J gene segments and in the  $\alpha$  45 V and 50 J gene segments are encoded (Fig. 3.2). The constant domain is build by the extracellular region, a short hinge region, the transmembrane segment and the cytoplasmic tail<sup>1</sup>.

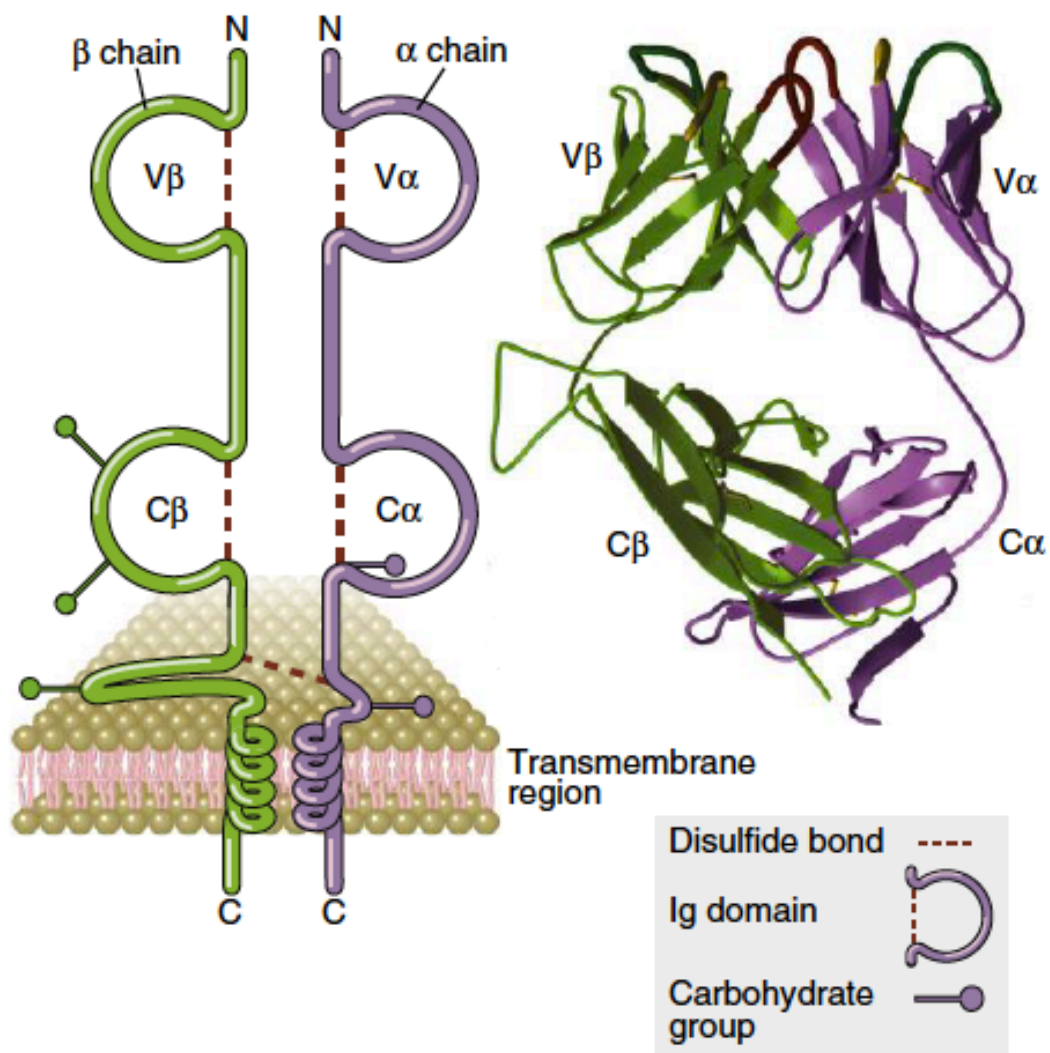


**Fig. 3.1: Structure of the T cell receptor.** Schematic structure of the  $\alpha\beta$  T cell receptor (left) shows the typical domains of a  $\alpha\beta$  T cell receptor. The interaction between TCR and peptide-MHC complex is mediated by the V regions. The image on the right site represents ax-ray crystallography-based ribbon diagram on the extracellular part of a TCR. Adapted from Abbas *et al.*<sup>1</sup>

TCR specificity and diversity is based on 3 loop regions of the molecule that interact with the peptide-MHC complex, known as complementary determining regions (CDR). By rearrangement of the gene segments to one exon, the imprecise junction of the V(D)J elements creates a highly diverse CDR3 joint region. The TCR  $\alpha$  chain requires a single rearrangement event connecting randomly a V and J gene segment. For the  $\beta$  chain DJ rearrangement occurs first, followed by its fusion to a random V segment (Fig. 3.2). The somatic rearrangement of the TCR leads to a theoretical diversity of  $\sim 10^{15}$  different TCRs. However, selection during the generation of mature T cells lead to a reduced diversity in the TCR repertoire, which is estimated to be  $2 \times 10^7$  TCRs in humans<sup>3</sup> and will be discussed in the next chapter.

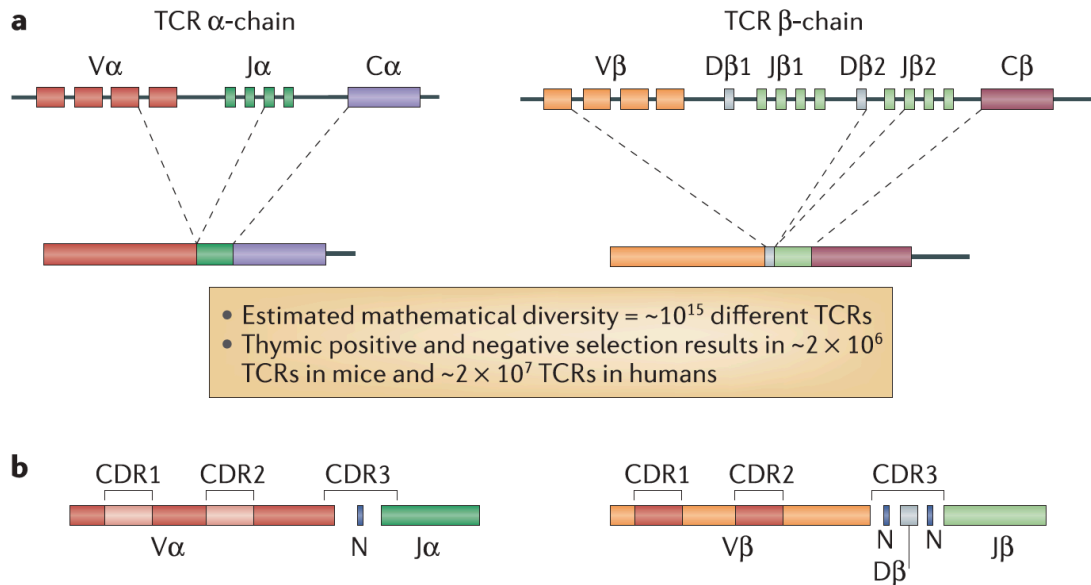


**Fig. 3.2: Generation of T-cell receptor diversity.** **a**) The TCR $\alpha$  chain is generated by somatic recombination of variable (V) and junctional (J) gene segments. In the case of the TCR $\beta$  chain, a diversity (D) gene segment is inserted between the V and J segments. The functional TCR is formed during T cell development by splicing the single segments together with the constant (C) region. **b**) Two Complement-Determining regions (CDRs) are located within each V gene segments. CDR3 is generated by the somatic recombination of V(D)J segments. These recombination leads to the addition of non-template-encoded nucleotides (N) at the V(D)J junctions. This process results in a mathematical diversity of  $10^{15}$  different TCRs. The actual number is reduced by negative and positive selection in the thymus to approximately  $2 \times 10^7$  different TCRs for each human. Adapted from Turner *et al.*<sup>4</sup>

### 3.1.2 T cell generation

T cells arise, like all blood cells, from pluripotent stem cells in the bone marrow. However, in contrast to other leukocyte populations, T cells do not mature in the bone marrow, but in the thymus. Therefore, they have been termed thymus-dependent (T) lymphocytes or T cells. The thymus is a bilobed organ that is located in the anterior mediastinum between the heart and the sternum<sup>1</sup>.

T cells originate from hematopoietic stem cells (HSCs), which are located in the bone marrow. HSCs give rise to all red and white blood cells. It has been shown that HSCs differentiate into common myeloid progenitors (CMP) and common lymphoid progenitors (CLP). CMP give rise to granulocytes, macrophages, megakaryocytes and erythrocytes. Whereas, CLPs can generate all lymphoid lineages, like innate lymphoid cells and natural killer cells, as well as B and T cells<sup>5,6</sup> (Fig. 3.3). This dual branch model is well established. However, more recent studies attenuated the stringent commitment to one of the two lineages. It has been shown that multipotent progenitor cells, which migrate into the thymus, can not only lead to the differentiation of cells



from the lymphoid compartment, but also to cells from the myeloid compartment like dendritic cells (DC) and erythrocytes<sup>7,8</sup>.

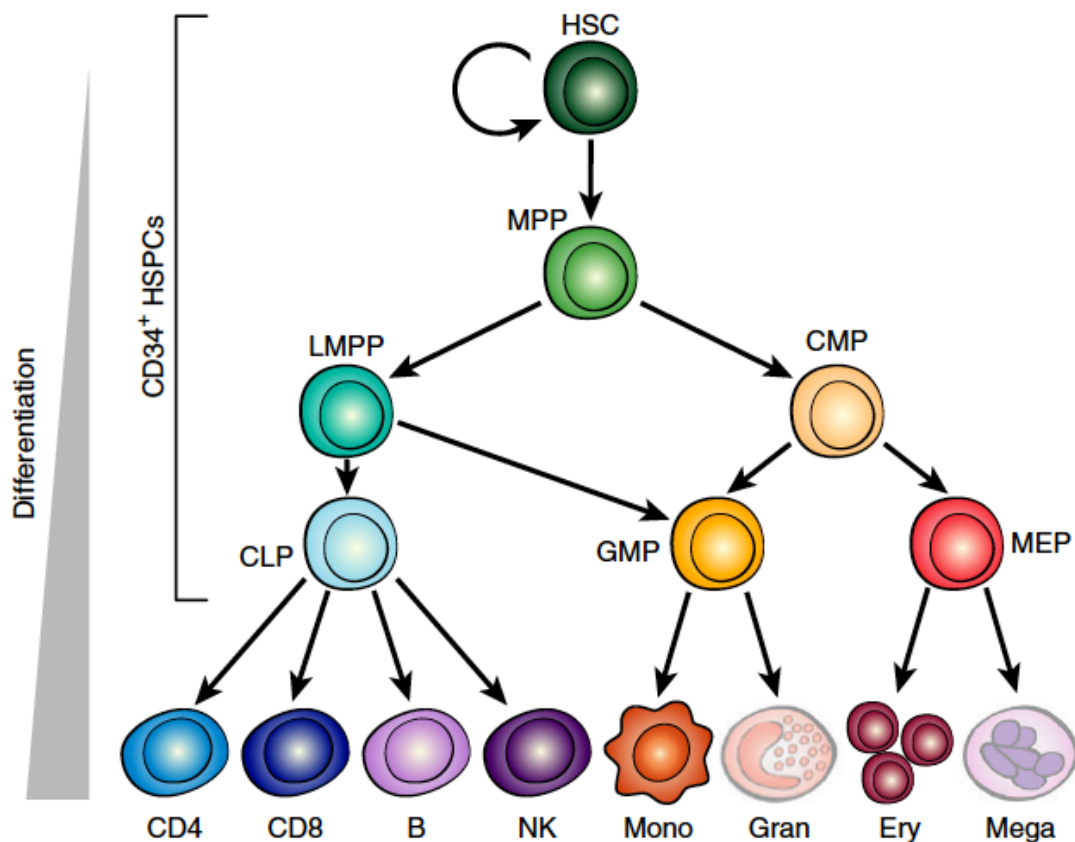


**Fig. 3.3: The hematopoietic hierarchy.** Lineage tree showing adult hematopoiesis and the branching points between lymphoid and myeloid cells. HSC = hematopoietic stem cell; MPP = multipotent progenitor; LMPP = lymphoid-primed multipotent progenitor; CMP = common myeloid progenitor; CLP = common lymphoid progenitor; GMP = granulocyte-macrophage progenitor; MEP = megakaryocyte-erythrocyte progenitor; CD4 = CD4<sup>+</sup> T cell; CD8 = CD8<sup>+</sup> T cell; B = B cell; NK = NK cell; Mono = Monocyte; Gran = Granulocyte; Ery = Erythrocyte; Mega = Megakaryocyte. Adapted from Corces *et al.*<sup>9</sup>

The final maturation of T cells occurs in a stepwise process in four compartments of the thymus. (i) The subcapsular zone contains predominantly cortical thymic epithelial cells (cTEC). (ii) The cortex is comprised of a mixture of cTECs, fibroblasts and macrophages. (iii) A stromal network of DCs and medullary thymic epithelial cells (mTEC) build the medulla. (iv) The corticomedullary junction consists of a dense network of endothelial cells. This region supports the rapid exit and entrance of thymocytes into the blood (Fig. 3.4). The initial progenitors of T cells in the thymus are called double negative (DN) cells, which can be distinguished by surface marker expression (CD25, CD44, CD117, CD4, CD8) into different subgroups<sup>10</sup>.

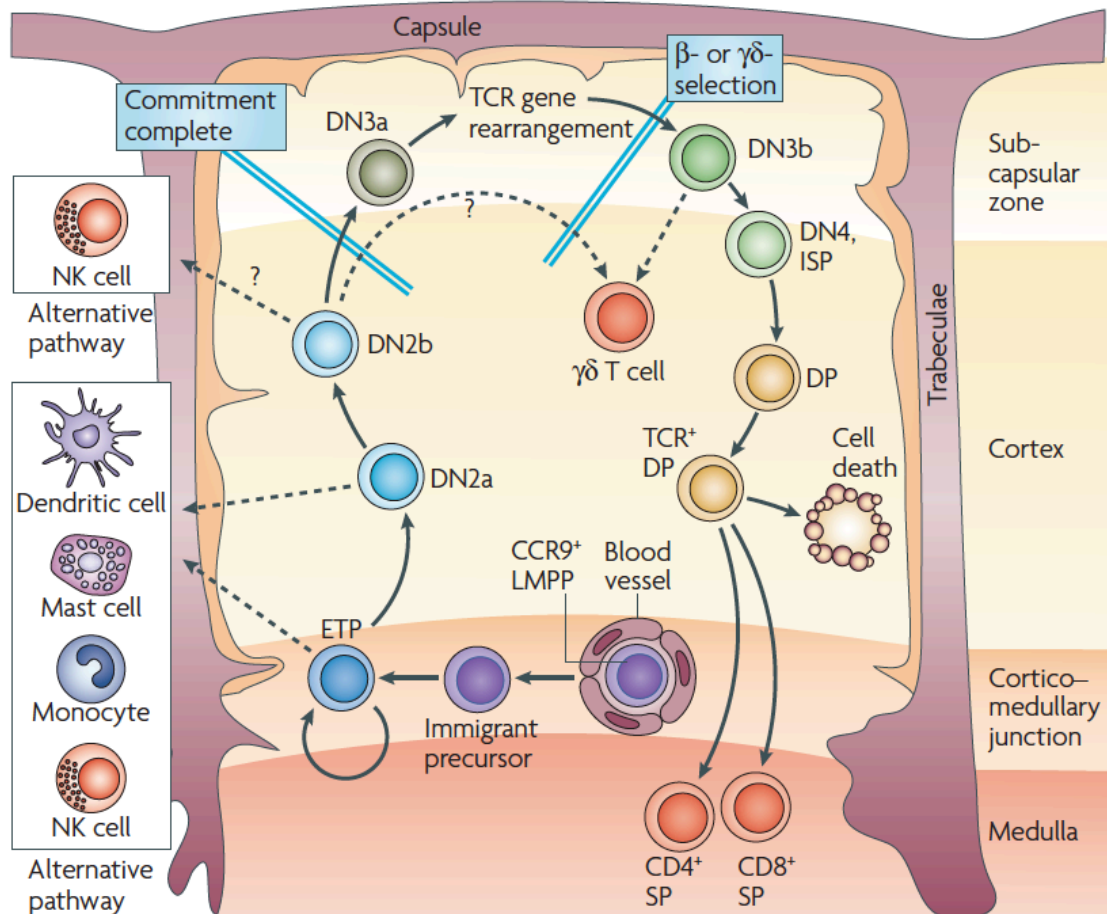


**Fig. 3.4: Stages in early T cell development.** Illustration showing the migration of T cell precursor cells through the thymus and their differentiation towards mature T cells. LMPP = lymphoid-primed multipotent progenitor; ETP = Early thymic progenitor; DN = double negative T cell; ISP = Immature single positive T cell; DP = Double positive T cell; SP = single positive T cell; Adapted from Rothenberg *et al.*<sup>11</sup>

DN1 cells are a heterogeneous population. DN1 are located in the corticomedullary junction, where they remain for several days and proliferate. During this time, DN1 cells become more restricted towards the T cell lineage<sup>12</sup>. It has been shown, that Notch1 signaling plays a crucial role in the early period of T cell maturation<sup>13,14</sup>. Notch1 inhibits the differentiation of early thymic progenitor (ETP) cells towards B cells or plasmacytoid DC and by this supports the T cell fate commitment. The microenvironment of the thymus supports also the Notch-dependent lineage commitment of early T cell progenitors. Depletion of the Notch ligand DLL4 on TECs inhibited T cell differentiation and induced the maturation of ETPs into B cells within the thymus<sup>13</sup>.

Following the initial restriction of ETP/DN1 cells to the T cell lineage, they leave the corticomedullary junction and migrate into the cortex, where they differentiate into

DN2 cells (CD24<sup>+</sup>, CD25<sup>+</sup>, CD44<sup>+</sup>, CD117<sup>+</sup>, CD27<sup>dim/hi</sup>). Fibroblasts and TECs support this process by providing stimulatory signals<sup>15,16</sup>. DN2 cells can be divided into two subgroups. DN2a (CD117<sup>hi</sup>) cells are able to give rise to DCs and NK cells. DN2b cells downregulate CD117, which correlates with a decreased potential to differentiate into DC<sup>17</sup>. Moreover, DN2b cells increase the expression of genes that initiate gene rearrangement at the TCR $\beta$ , TCR $\gamma$  and TCR $\delta$  loci. IL7 seems to be an important mediator of the development towards  $\alpha\beta$  T cells or  $\gamma\delta$  T cells. DN2 cells expressing high levels IL7R $\alpha$  seem to be biased to the  $\gamma\delta$  T cell lineage, whereas DN2 expressing low levels of IL7R $\alpha$  predominately give rise to  $\alpha\beta$  T cells<sup>18</sup>.

At the end of the DN2 stage, DN2b cells migrate into the subcapsular zone and further differentiate into DN3 cells (CD24<sup>hi</sup>, CD25<sup>hi</sup>, CD44<sup>low</sup>, CD117<sup>low</sup>). At the DN3 stage T cells are either committed to  $\alpha\beta$  or  $\gamma\delta$  T cell lineage. The  $\gamma\delta$  T cell fate specification is promoted by the recombination of *Tcrg* and *Tcrd* and the transcription factor Id3<sup>19,20</sup>. The transition of DN3a to DN3b cells displays an important checkpoint for  $\alpha\beta$  T cells, which is called  $\beta$ -selection and is associated with an increased expression of CD27. At this point, T cells are selected for the functional expression of TCR $\beta$  chain, components of CD3 and an invariant pT $\alpha$  chain. Cells that do not fulfill these requirements will undergo apoptosis<sup>21</sup>. DN3b thymocytes that passed the  $\beta$ -selection mature into the DN4 stage (CD24<sup>+</sup>, CD25<sup>-</sup>, CD44<sup>-</sup>, CD117<sup>-</sup>). These cells migrate back into the cortex, where they start to express CD4 and CD8 co-stimulatory molecules on their surface<sup>12</sup>. These cells, known as double-positive (DP) thymocytes, initiate again the expression of Rag genes, which leads to recombination of the *Tcra* locus.

Following the functional recombination of the TCR $\alpha$  chain, DP thymocytes are positively or negatively selected based on the specificity and binding strength of the TCR to self-peptides, which are presented in the context of major histocompatibility complexes (MHC) on cTECs, fibroblasts and DCs. During positive selection, only TCRs with a weak interaction are prevented from death by neglect resulting in the depletion of roughly 90 % of DP thymocytes.

Following positive selection, the DP thymocytes lose the expression of CD4 or CD8 and become CD4 single positive (SP) thymocytes (CD4<sup>+</sup>, CD8<sup>-</sup>) or CD8 SP

thymocytes (CD4<sup>-</sup>, CD8<sup>+</sup>). Lineage decision has to be matched with MHC specificity. This means that CD4 SP thymocytes recognize peptide-MHC-II complexes and CD8 SP thymocytes are restricted to MHC-I. Initially it was suggested, that qualitative and quantitative differences between MHC-I and MHC-II lead to lineage differentiation in DP thymocytes and to the loss of CD4 or CD8<sup>22</sup>. More recent data showed that CD4 lineage commitment requires a longer interaction with MHC molecules than the CD8 lineage. This led to the kinetic signaling model of lineage choice<sup>23,24</sup>. During the decision progress, the transcription factor GATA3 induces the expression of genes required for CD4 cell differentiation and the transcription factor Thpok, which partly suppresses CD8 lineage genes<sup>25-27</sup>. Runx3 has been described to be important to suppress CD4 expression and by this support CD8 lineage differentiation<sup>28</sup> (Fig. 3.5).

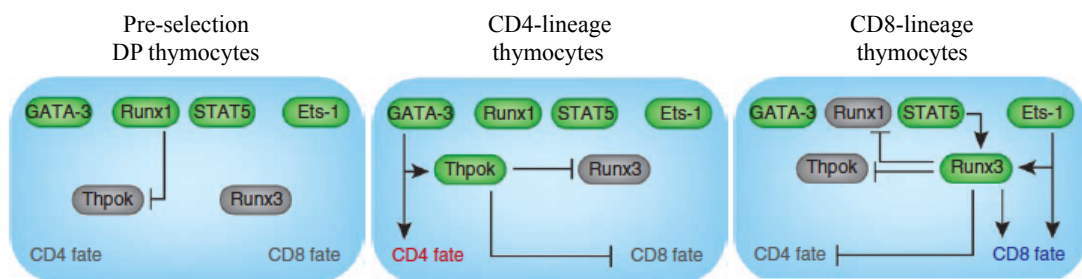


**Fig. 3.5: CD4-CD8 lineage differentiation.** Runx1 suppresses Thpok in pre-selection cells (left). When double-positive thymocytes differentiate into the CD4 lineage, GATA3 promotes Thpok expression, which is no longer suppressed by Runx1. Thpok inhibits the upregulation of Runx3 and CD8 differentiation (center). In CD8-differentiating cells, Ets1 promotes the expression of Runx3, which represses Thpok. In addition, STAT5 mediates IL-7 signaling to Runx3. Gray boxes represent proteins that are not expressed under the given situation. Adapted from Carpenter and Bosselut<sup>29</sup>

After CD4 and CD8 SP T cells migrated into the medulla, they undergo negative selection, where self-reactive T cells are eliminated. mTECs play a crucial role during this process, as they uniquely express AIRE (autoimmune regulator). This protein allows the expression of tissue-specific proteins in the thymus and the presentation of many tissue-specific peptides. As T cells that express a TCR with high affinity to self-antigens will be eliminated via the induction of death by apoptosis, the risk of generating autoreactive T cells is reduced. Mature T cells that passed positive and negative selection upregulate sphingosine-1-phosphate receptor 1, which allows them to exit the thymus and enter the circulation<sup>30</sup>.

### 3.1.3 T cell receptor signaling

After naïve T cells exit the thymus, they scan the body for pathogens. To transmit the signal after antigen encounter the TCR is embedded within the CD3 complex. This

multisubunit protein complex consists of the heterodimers CD3 $\epsilon\gamma$  and CD3 $\epsilon\delta$ , as well as one homodimer CD3 $\zeta\zeta$  (Fig. 3.6). After the stimulation of the TCR, the cytoplasmic tail of the CD3 molecules play a crucial role for the downstream signaling as it contains in total 10 immunoreceptor tyrosine-based activating motifs (ITAM). CD3 $\gamma$ , CD3 $\delta$  and CD3 $\epsilon$  contain each one ITAM and CD3 $\zeta$  contains three ITAMs<sup>31</sup>. ITAMs display phosphorylation sites, which are essential for the signaling cascade upon activation.

The TCR-CD3 complex has no intrinsic enzymatic activity and relies on the kinase activity of the SRC family kinases (SFK), especially LCK, to initiate signaling. This protein is associated with the co-receptors CD4 and CD8, which facilitate the extracellular interaction between TCR and peptide-MHC complex and bring intracellular LCK into close proximity to the ITAMs on the CD3 molecules. LCK is constitutively active in naïve T cells. However, two phosphorylation sites control the kinase activity of LCK. Phosphorylation of the activating tyrosine residue (Tyr394) leads to an open conformation and phosphorylation of the negatively regulating tyrosine (Tyr505) leads to a closed conformation, which results in the full or reduced kinase activity, respectively. The phosphorylation state of LCK is crucial for TCR activation. Two proteins have been shown to modulate the negatively regulating tyrosine residue of LCK. CD45 dephosphorylates Tyr505 and supports the activating state of LCK. In contrast, C-terminal SRC kinase (CSK) phosphorylates Tyr505 and inhibits the LCK activity. Further evidence for the crucial role of these two proteins came from mice experiment. Mice lacking CD45 fail to initiate TCR signaling and T cell specific CSK-deficient mice display constitutive TCR signaling<sup>32-34</sup>.

Following the phosphorylation of the ITAMs by LCK, the kinase SYK family tyrosine kinase ZAP-70 is recruited to the TCR-CD3 complex, where it gets activated through phosphorylation by LCK. Once Zap-70 is activated, it phosphorylates multiple targets including the scaffold protein linker for activation of T cells (LAT), which leads to the recruitment of other scaffold proteins, like SLP76 and GAD, and to the propagation of the TCR signaling by recruiting effector molecules like phospholipase C $\gamma$ 1 (PLC $\gamma$ 1) and the TEC family kinase IL-2 inducible T cell kinase (ITK)<sup>35</sup> (Fig. 3.6).

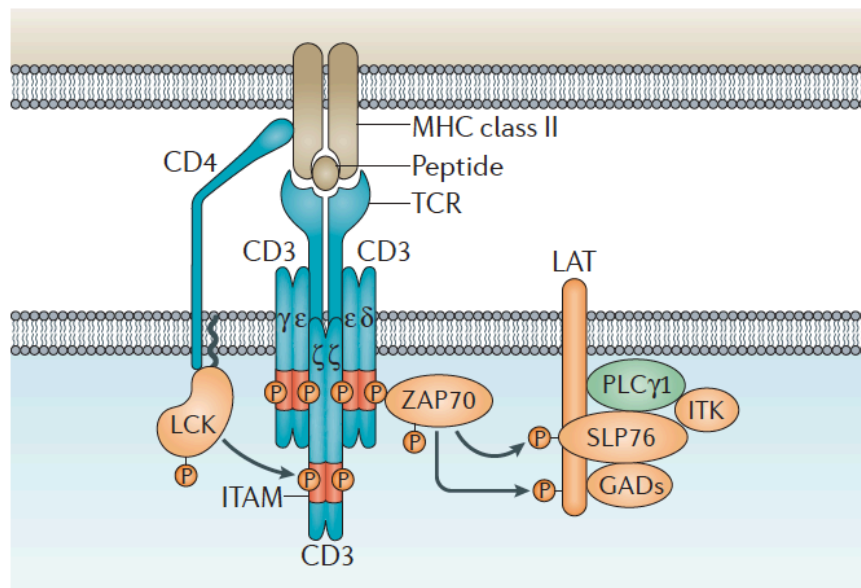


**Fig. 3.6: Overview of the early T cell receptor signaling.** The interaction of TCR with peptide-MHC on antigen presenting cells is stabilized by CD4 or CD8. LCK, which is associated with CD4 phosphorylates the immunoreceptor tyrosine-based activation motifs (ITAMs) on the intracellular part of the CD3 complex. This leads to the recruitment of ZAP70, which propagates the TCR signaling by phosphorylating multiple targets. Adapted from Li and Rudensky<sup>35</sup>

The multiprotein complex formed around LAT, called LAT signalosome, is an important signal branching point during T cell activation. Four major signaling pathways are induced at this point. The first one is the  $\text{Ca}^{2+}$  pathway.  $\text{PLC}\gamma 1$  metabolizes phosphatidylinositol-4,5-bisphosphate ( $\text{PtdIns}(4,5)\text{P}_2$ ) into inositol-1,4,5-triphosphate ( $\text{Ins}(1,4,5)\text{P}_3$ ) and diacylglycerol (DAG).  $\text{Ins}(1,4,5)\text{P}_3$  induces an increase in the cytosolic  $\text{Ca}^{2+}$  concentration, which leads to the activation of calcineurin and in consequence to the dephosphorylation of the nuclear factor of activated T cells (NFAT). In its dephosphorylated state NFAT is able to translocate into the nucleus. In addition, the  $\text{Ca}^{2+}$  pathway results in the production of DAG, which recruits various effector molecules to the cell membrane. One of them is the protein kinase  $\text{C}\theta$ , which initiates a signaling cascade that promotes the downstream ubiquitylation and degradation of the inhibitor of  $\text{NF-}\kappa\text{B}$  ( $\text{I}\kappa\text{B}$ ). This allows the transcription factor nuclear factor- $\kappa\text{B}$  ( $\text{NF-}\kappa\text{B}$ ) to translocate into the nucleus. Moreover, DAG also recruits the RAS guanyl-nucleotide releasing protein (RASGRP) to the cell membrane. RASGRP promotes the RAS mediated activation of the mitogen-activated protein kinase pathway (MAPK) and by this the activation of ETS family transcription factors. RAS can also activate the phosphoinositide-3-kinase (PI3K). PI3K metabolizes  $\text{PtdIns}(4,5)\text{P}_2$  into  $\text{PtdIns}(3,4,5)\text{P}_3$ , which leads to the inactivation of forkhead box O (FOXO1) and the activation of mechanistic target of

rapamycin complex 1 (mTOR1), which regulates cell growth and metabolic responses<sup>35</sup> (Fig. 3.7).

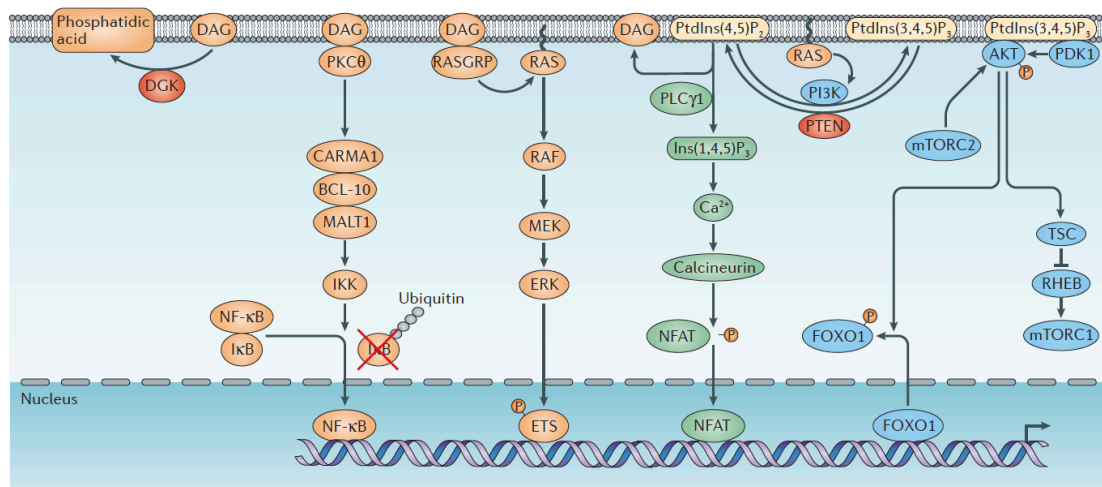


**Fig. 3.7: Propagation of T cell receptor signaling.** Lipid second messengers largely control the propagation of TCR signaling. The activation of phospholipase C  $\gamma$ 1 (PLC $\gamma$ 1) leads to the generation of inositol-1,4,5-trisphosphate (Ins(1,4,5)P<sub>3</sub>) and diacylglycerol (DAG). Ins(1,4,5)P<sub>3</sub> is required for the Ca<sup>2+</sup>-mediated activation of nuclear factor of activated T cells (NFAT). The formation of DAG start different signaling pathway, which in the end result in the activation of NF $\kappa$ B and ETS family transcription factors. The generation of phosphatidylinositol-3,4,5-trisphosphate (PtdIns(3,4,5)<sub>3</sub>) results in the inactivation of FOXO1 and the activation of mTOR. Adapted from Li and Rudensky<sup>35</sup>

## 3.2 T cell activation and exhaustion

### 3.2.1 T cell activation

To search for their cognate antigen, naïve T cells circulate through the body. In secondary lymphoid organs, like spleen, lymph nodes, tonsils and Peyer's patches, foreign, but also self contents of the blood, lymph and mucosa are displayed at the cell surface of antigen presenting cells (APC). DCs are the most potent APCs for naïve T cells. Beside the recognition of the cognate peptide-MHC complex, interaction of the T cell with surface receptors on interacting cells and sensing of soluble mediators modulate the clonal expansion and differentiation of naïve T cells into effector and memory T cells<sup>36</sup>.

Lymph nodes are highly compartmentalized lymphoid organs, which are located at vascular junctions. The lymph node is surrounded by lymphatic vessels, which deliver antigens and APCs. Several afferent lymphatic vessels allow the lymph and antigens to enter the lymph node, where it gets filtered through the lymphatic sinuses in the medulla<sup>37,38</sup>. Macrophages and B cells are the main cell types in the medulla. B cell lymphoid follicles are located at the outer cortex, whereas the inner paracortical area

consists of T cells and DCs. The majority of T cells enter the lymph nodes from the blood via specialized post-capillary venules, called high-endothelial venules (HEV). These cells support rolling, adhesion and arrest of T cells by expressing homing molecules. T cells that transmigrate into the paracortical area migrate further into the T cell zone of the lymph node. This migration depends on the sensing of a gradient of CCL18, CCL19 and CCL21 by the CC-chemokine receptor (CCR7). T cells that have not been activated within the lymph node exit it in a sphingosine-1-phosphate dependent manner and continue to migrate to screen the body for their cognate antigen<sup>1,39</sup>.

T cells show high motility within the T cell zone. Buosso and Robey estimated that a single DC has contact with up to 500 T cells per hour<sup>40</sup>. When a T cell encounters its cognate antigen, it stops migrating and several T cell surface proteins and intracellular molecules are immediately mobilized to the site of T cell-DC interaction. This leads to the formation of a bulls'-eye-like structure: the immunological synapse or supramolecular activation cluster (SMAC). SMACs contain a central cluster of TCR-pMHC and co-stimulatory molecules, called central SMAC (cSMAC). A ring of intergrins surrounds the cSMAC. This region is called peripheral SMAC (pSMAC) and stabilizes the binding of the T cell to the APC. The distal SMAC (dSMAC) is enriched with molecules with long extracellular domains, such as CD45 and CD43 (Fig. 3.8)<sup>1,41</sup>.

During the interaction of a T cell with the cognate peptide-MHC complex on an APC, the T cell requires three signals to become fully activated. Beside the TCR-peptide-MHC interaction (signal 1), co-stimulation via surface receptors (signal 2) and cytokines (signal 3) are essential for differentiation. The combination of these signals guides proliferating T cells into different fates of effector and memory function to generate an immune response that is optimal to clear the pathogen<sup>42</sup>.

Signal 1 is the initial trigger for T cell activation and induces the entry of T cells into the G<sub>1</sub> phase of the cell cycle. Moreover, Signal 1 leads to the expression of IL-2 and the  $\alpha$  subunit of the IL-2 receptor (IL-2R $\alpha$ , CD25). The expression of CD25 increases the affinity of the IL-2R to its target IL-2, which is an essential cytokine for T cell survival and growth. Irvine *et al.* showed that only one to three peptide-MHC



complexes are sufficient to induce effector function in a CD4<sup>+</sup> T cell. However, for the complete activation 10 peptide-MHC complexes are required<sup>43</sup>.

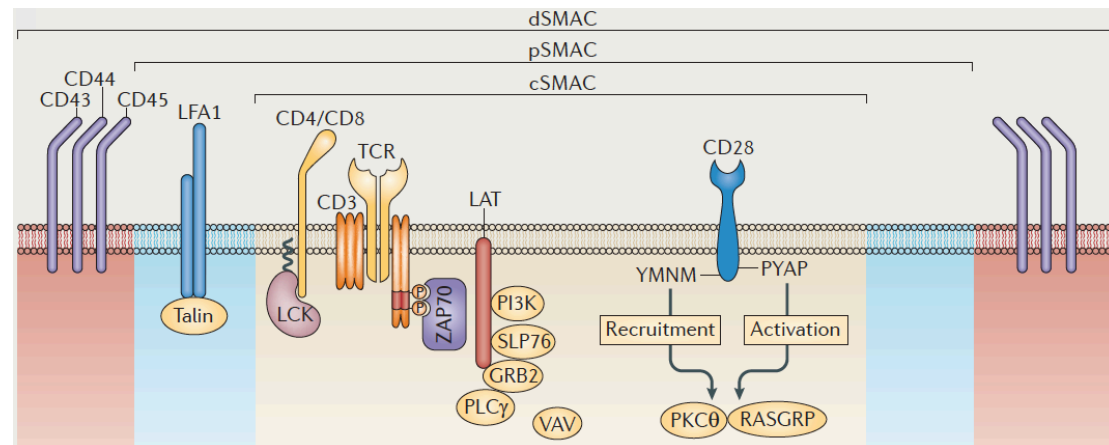


**Fig. 3.8: Overview of the immunological synapse.** The immunological synapse can be separated into central-supramolecular activation cluster (cSMAC), peripheral-(p) SMAC and distal-(d) SMAC. The TCR and costimulatory molecules are present in the cSMAC. Leukocyte function-associated antigen-1 (LFA1) and other adhesion molecules are expressed in the pSMAC. Large surface proteins like CD44 and CD45 are located in the dSMAC. Adapted from Chen and Flies<sup>44</sup>

T cells become anergic, if they only encounter signal 1. Therefore, a second signal by co-stimulatory molecules is required for the functional expansion of T cells. One of the best characterized and most important co-stimulatory molecules is CD28, which is constitutively expressed on all T cells in mice and on 95 % of CD4<sup>+</sup> T cells and 50 % of CD8<sup>+</sup> T cells in human<sup>45</sup>. CD28 interacts with members of the B7 family, B7-1 (CD80) and B7-2 (CD86). These molecules are expressed on APCs. CD28 carries two cytosolic motifs (YMN and PYAP) which recruit PKCθ and RASGRP after stimulation to promote T cell proliferation and survival<sup>44</sup>.

In contrast to CD28, the inducible co-stimulator (ICOS) is not constitutively expressed on naïve or resting T cells. Its expression is rapidly initiated after TCR stimulation and/or CD28 co-stimulation<sup>46,47</sup>. ICOS and CD28 are both members of the immunoglobulin superfamily and have a high homology, but unlike ICOS, stimulation of CD28 leads to the expression of IL-2. ICOS ligation results in a greater PI3K activity compared to CD28, which leads to an increased expression of the cytokines IL-4, IL-10, IFNγ and TNFα<sup>48</sup>.

The activation of T cells does not only result in the expression of co-stimulatory receptors. The inhibitory receptor cytotoxic T-lymphocyte antigen 4 (CTLA4) negatively regulates T cell activation and proliferation. CTLA4 is homologous to

CD28 and recognizes the same ligands, although with higher affinity. Competition of CD28 and its inhibitory counterpart for ligand binding controls the strength of T cell activation, in order to limit the proliferative response<sup>49</sup>.

CD40L (or CD154) is expressed by activated T cells and has a crucial role for B cell proliferation. The interaction of CD40L with its receptor CD40 induces the production of cytokines (IL-2, IL-4, IL-5) and mediates the differentiation of B cells into plasma cells<sup>50</sup>. CD40 is not only expressed on B cells, but also on DCs and monocytes. The stimulation of CD40 on DCs by CD40L on CD4<sup>+</sup> T cells can increase the ability of DCs to efficiently prime CD8<sup>+</sup> T cells, known as DC licensing<sup>51</sup>.

Cytokines (signal 3) have an important role in adaptive immunity. They are involved in the proliferation and differentiation of T and B cells. The cytokines that are present in the lymphoid organs drive the development of CD4<sup>+</sup> T cell subsets and shapes the immune response according to promote an efficient clearance of the pathogen.

### **3.2.2 T cell differentiation**

Experiments from Parish and Liew almost 50 years ago indicated for the first time that stimulated CD4<sup>+</sup> T cells consists of at least two populations, which have been later characterized as T helper (T<sub>H</sub>) 1 and 2 cells<sup>52</sup>. IL-12 and TNF $\alpha$  can induce the polarization of T<sub>H</sub>1 cells. These cytokines are produced by dendritic cells in response to infections with intracellular bacteria or viruses. IL-12 activates the signal transducer and activator of transcription (STAT) 1, which results in an increased expression of T-box expressed in T cells (T-bet). T-bet is the signature transcription factor (master regulator) of T<sub>H</sub>1 cells and mediates the up-regulation of IFN $\gamma$  production and the expression of the IL-12 receptor  $\beta$  (IL-12R $\beta$ ). This allows T cells to directly respond to IL-12 in a STAT4 dependent manner<sup>53</sup> (Fig. 3.9).

The polarization of T<sub>H</sub>2 cells is initiated by IL-4, which can be produced by activated naïve T cells, as a consequence of Jagged-1 mediated Notch signaling. Moreover, it has been shown that IL-25, produced by mast cells and macrophages in response to helminthes, can induce the production of IL-4 by stimulated naïve T cells itself<sup>54</sup>. IL-4 induced STAT6 activation leads to the up-regulation of GATA-binding protein 3

(GATA3) and c-maf. GATA3 in combination with an IL-2 dependent STAT5 activation leads to the production of IL-4 and the full differentiation of T<sub>H</sub>2 cells<sup>55</sup> (Fig. 3.9).

The discovery of T<sub>H</sub>17 cells as a third subset of CD4<sup>+</sup> polarized T cells has been initially shown by experiments that blocked T<sub>H</sub>1 and T<sub>H</sub>2 associated cytokines and transcription factors. IL-6 through STAT3 induces the expression of the retinoic-acid orphan receptor (ROR $\gamma$ t), which is the master transcription factor defining the T<sub>H</sub>17 subset. These cells produce IL-17 and IL-22, which promotes the recruitment of neutrophils and supports the immune response against extracellular bacteria and fungi<sup>56</sup> (Fig. 3.9).

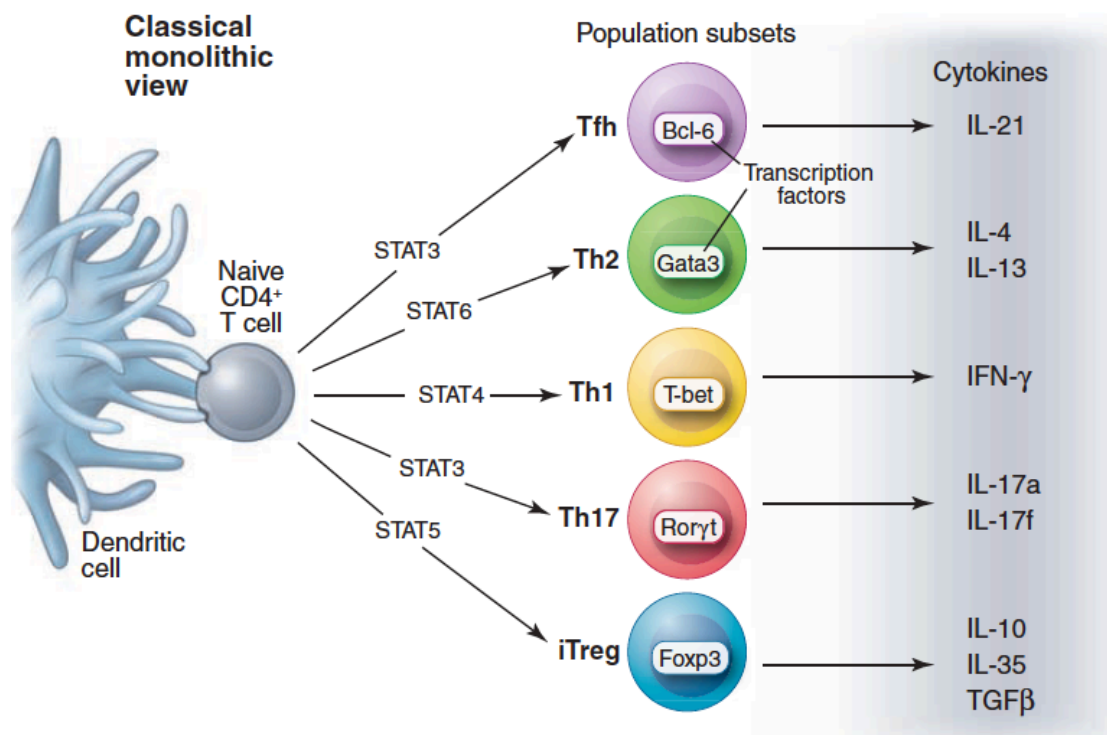


**Fig. 3.9: Helper T cell differentiation.** The graph displays the classical view of the lineages and master regulators. Initial studies indicated that the different subsets express lineage-defining transcription factors. However, recent studies revealed more flexibility in cytokine production than predicted by earlier work. Adapted from O’Shea and Paul<sup>57</sup>

The polarization of CD4<sup>+</sup> T cells induced by the encountered pathogen to the different subsets is not as strict as it has been suggested for many years. Becattini *et al.* identified *C. albicans*-specific T cells, which are mainly found in the T<sub>H</sub>17 compartment, with a T<sub>H</sub>1, T<sub>H</sub>1\* or T<sub>H</sub>2 phenotype. Moreover, they discovered T cell clones with identical TCR $\alpha\beta$ , but different surface marker and effector functions. This

supports the hypothesis that a proliferating T cell clone acquires different T cell fates as a result of stochastic stimulation and plasticity<sup>58,59</sup>. To this end, the early diversification of CD4<sup>+</sup> T cell phenotypes after pathogen encounter allows selection of a particular subset during the immune response<sup>60</sup>.

T cell activation results in the proliferation of the antigen-specific clones, called clonal expansion, thereby increasing the likelihood to eliminate the pathogen. During this process, the frequency of an antigen-specific clone can increase more than 50'000 fold. The majority of the expanded cells are effector cells that immediately act against the pathogen. However, roughly 10 % differentiate to memory T cells, which survive for long periods and in some cases for a lifetime. If a pathogen rechallenges the body, these memory T cells can respond rapidly and provide protection. IL-7 and IL-15 play crucial roles in the maintenance of memory cells<sup>1</sup>.

### **3.2.3 Metabolism fuels T cell immunity**

In the last years it has become increasingly clear that T cell fate and function is intimately linked to changes in the cellular metabolic programs. It has been shown that the T cell metabolism no longer exclusively displays the source for energy and molecular precursor for the production of biomolecules, but plays a crucial role in shaping T cell responses. The transition from naïve T cells to effector and memory T cells requires a dramatic metabolic remodeling process in order to comply with the metabolic demands. At every point of the life cycle of T cells, key metabolic pathways, like glycolysis, fatty acid oxidation or mitochondrial metabolism, have to be tightly controlled. Metabolic regulators, such as mTOR and AMPK, display a connection between cellular metabolism, T cell differentiation and function<sup>61</sup>.

Naïve T cells are assumed to be quiescent. Like other quiescent cells, naïve T cells rely on oxidative phosphorylation (OXPHOS) and fatty acid oxidation (FAO) (Fig. 3.10). It is assumed that 96% of the generated ATP in naïve T cells derives from OXPHOS<sup>62</sup>. Recent data suggest that quiescence of naïve T cells is actively maintained. The preservation of naïve T cells requires a balance between tonic TCR signals and IL-7, which is an essential pro-survival cytokine for naïve T cells<sup>63</sup>.

Furthermore, adenosine was shown to support naïve T cell development and survival via the prevention of IL-7R $\alpha$  down-regulation<sup>64</sup>.

Even though naïve T cells circulate in a quiescent state for many years through the body, after cognate antigen encounter they promptly initiate cell growth, proliferation, differentiation and effector functions. These processes are energetically demanding and require a metabolic reprogramming of the activated cell. Upon TCR-mediated stimulation, the expression of genes associated with glycolysis and glutaminolysis are up-regulated, as well as transporters required for the uptake of glucose, amino acids and glutamine<sup>65-67</sup>. The metabolism switches from a OXPHOS and FAO dependence, to aerobic glycolysis, pentose phosphate pathway and hexosamine pathway<sup>65</sup> (Fig. 3.10). Aerobic glycolysis leads to the generation of lactate, even though the oxygen would be sufficient to perform the catabolism of glucose via tricarboxylic acid (TCA) cycle and OXPHOS<sup>68,69</sup>. In comparison to OXPHOS, aerobic glycolysis is 9-fold less efficient in generating ATP. However, aerobic glycolysis mediates the maintenance of redox balance (NAD<sup>+</sup>/NADH) and results in the synthesis of metabolites essential for cell growth and proliferation<sup>68,70</sup>.

The changes in T cell metabolism upon activation are mediated by several transcription factors and signaling pathways. T cell stimulation and co-stimulation results in the activation of PI3K, which activates the serine/threonine kinase AKT and mTOR<sup>71</sup>. These two factors promote aerobic glycolysis and support effector T cell growth, differentiation and function<sup>72,73</sup>. The activation of mTORC1, which is one of two existing complexes of mTOR, results in the phosphorylation of 4E-BP1 and p70S6 kinase (S6K1), which in turn increases protein translation<sup>74</sup>. Moreover, mTORC1-mediated activation of sterol regulatory element-binding protein 2 (SREBP2) increases lipid synthesis<sup>75</sup>. The expression of nutrient transporter is controlled by Akt, which also can phosphorylate the glycolytic enzyme hexokinase II<sup>76-78</sup>.

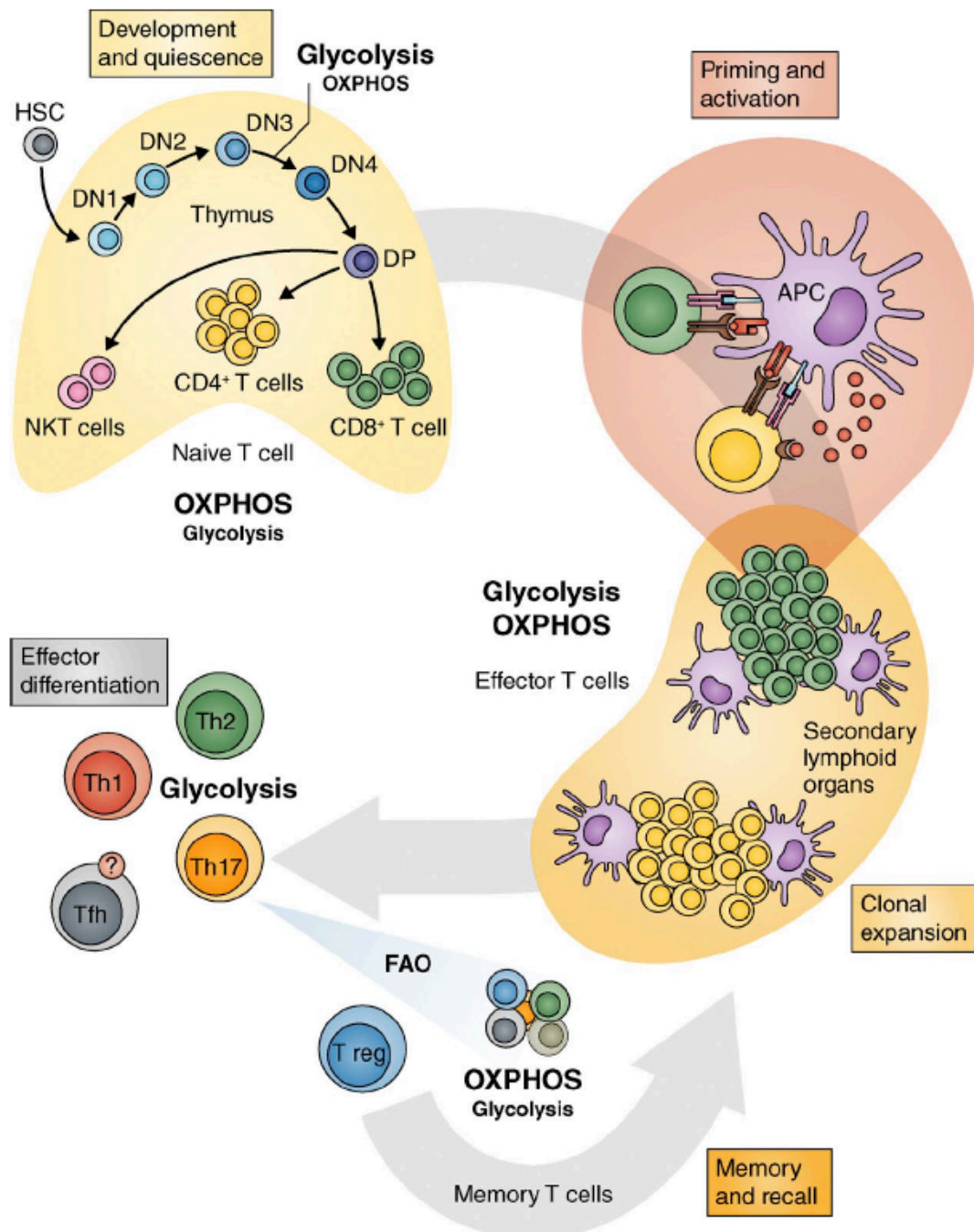


**Fig. 3.10: Metabolic programming during T cell maturation and activation.** While naïve T cells primarily rely on oxidative phosphorylation (OXPHOS), T cell activation induces a metabolic reprogramming, which is characterized by aerobic glycolysis. Glycolysis is suggested to promote the differentiation of  $T_H1$ ,  $T_H2$ ,  $T_H17$  and maybe  $T_{FH}$ . In contrast, an increased fatty acid oxidation (FAO) promotes the differentiation of  $T_{reg}$  (blue arrow). Memory T cells represent quiescent cells. However, re-stimulation leads to a rapid increase of glycolysis and OXPHOS. Adapted from Buck *et al.*<sup>78</sup>

Another important transcription factor for metabolic reprogramming is c-Myc. Originally described as an oncogene, it has been recently observed that c-Myc regulates the expression of proteins important for glycolysis and glutaminolysis<sup>65</sup>. c-Myc activates the transcription factor AP4, which prolongs the metabolic program initiated by c-Myc<sup>79</sup>. Furthermore, the hypoxia inducible factor-1 $\alpha$  (HIF-1 $\alpha$ ), which

responds to oxygen levels, increases glucose uptake upon T cell activation<sup>80,81</sup>. Promotion of HIF-1 $\alpha$  signaling by depletion of its negative regulator von Hippel-Lindau (VHL) results in increased glycolytic activity and improved anti-viral activity of CD8<sup>+</sup> T cells<sup>82</sup>.

The metabolism plays not only a crucial role during T cell activation, but for the differentiation of T<sub>H</sub> cells (Fig. 3.11). The first study indicating that T cell metabolism controls T cell differentiation derived from Kopf *et al.* They showed that blockade of mTOR pathway via rapamycin impairs the differentiation towards T<sub>H</sub>17 and promotes the generation of T<sub>regs</sub><sup>83</sup>. In line, the depletion of mTOR results in increased numbers of T<sub>reg</sub> cells upon activation, but not T<sub>H</sub>1, T<sub>H</sub>2 or T<sub>H</sub>17<sup>84</sup>. These results can be explained by findings from Michalek *et al.*, who showed that T<sub>H</sub>1, T<sub>H</sub>2 and T<sub>H</sub>17 cells have a higher glycolytic activity than T<sub>reg</sub> cells, which relied more on lipid oxidation<sup>85</sup>. T<sub>H</sub>17 cells show the highest glycolytic activity. The blockade of glycolysis by 2-Deoxy-D-glucose prevents the generation of T<sub>H</sub>17 and HIF-1 $\alpha$ -deficient mice further supported that glycolysis in T<sub>H</sub>17 is controlled by the mTOR-HIF-1 $\alpha$  pathway<sup>86,87</sup>. The differentiation of activated CD4<sup>+</sup> T cells into the T<sub>H</sub>1 or T<sub>H</sub>2 lineage depends on the activity of mTORC1 and mTORC2, respectively<sup>72,88</sup>. Initial activation of mTORC1 is also crucial for T<sub>H</sub>2 cell differentiation<sup>89</sup>. In contrast to T<sub>H</sub> subsets, T<sub>regs</sub> use lipid oxidation as primary source for energy<sup>85,86</sup>. The AMP-activated kinase (AMPK) has been suggested to play an important role for the metabolism of T<sub>reg</sub> cells. T<sub>reg</sub> show high levels of AMPK, which can inhibit mTORC1 activity via tuberous sclerosis 2 protein (TSC2)<sup>90</sup>. The activation of AMPK via metformin results in increased numbers of T<sub>reg</sub> *in vivo*<sup>91</sup>.

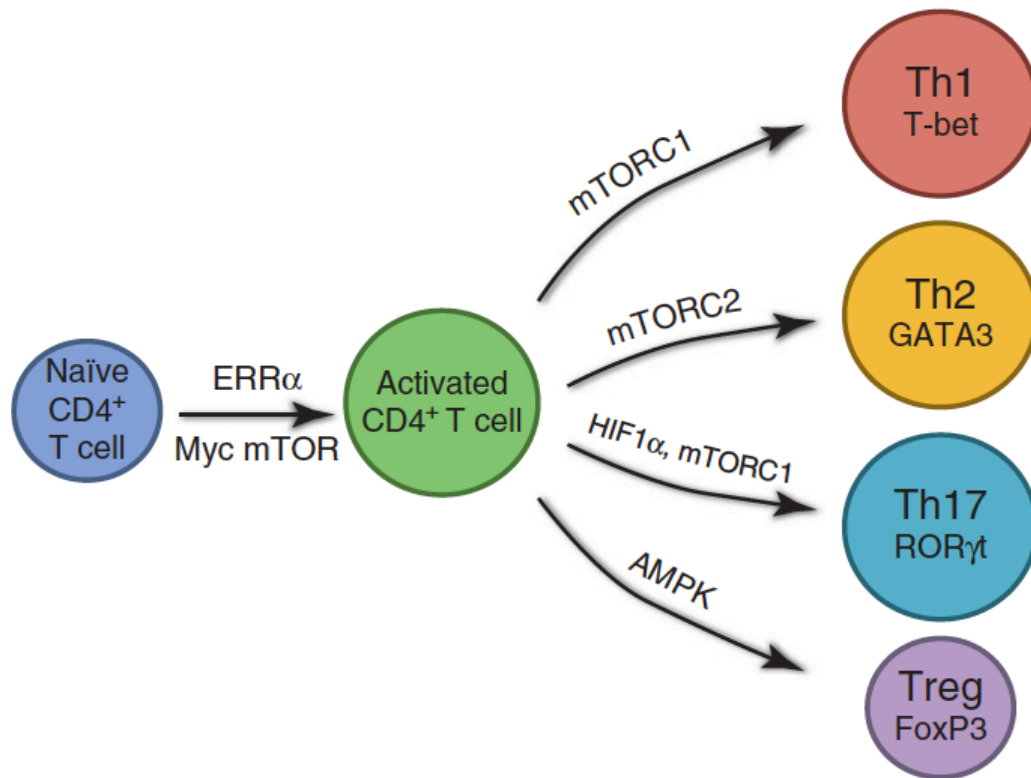


**Fig. 3.11: Signaling molecules associated with metabolic reprogramming and CD4<sup>+</sup> T cell differentiation.** Adapted from Gerriets and Rathmell<sup>92</sup>

After the antigen is cleared, the majority of effector T cells die by apoptosis. Only a small fraction converts into long-lived memory cells, which have a similar transcriptional profile than naïve T cells<sup>93</sup>. Memory T cells, just like naïve T cells, rely primarily on OXPHOS to meet their energetic demands. While the metabolic switch upon activation of naïve T cells is well investigated, less is known about the mechanism that allows glucose-addicted effector T cells to become memory T cells and switch back to OXPHOS. It has been suggested that the pro-survival cytokine IL-15 is an important factor for the shift back to OXPHOS and FAO. Memory CD8<sup>+</sup> T cells express high levels of eomesodermin (eomes), which promotes the up-regulation of the IL-15 receptor<sup>94</sup>. Signaling via this receptor in memory T cells increases the spare respiratory capacity (SRC), which represents the extra capacity to generate energy under stress conditions. A higher SRC has been linked with a beneficial effect on survival. Moreover, IL-15 promotes FAO<sup>95</sup>, which may be due to AMPK. Besides the up-regulation of specific proteins, data from Araki *et al.* suggest that T cells have to down-regulate the mTOR pathway in order to enter the memory pool<sup>96</sup>.



### 3.2.4 Regulatory T cells and immune tolerance

Somatic recombination enables the immune system to generate an enormous number of different T and B cells. This is the basis for the ability of the adaptive immune system to respond to a huge diversity of pathogen, but also contains the danger to damage healthy tissue, when T cells responding to self-antigens are not efficiently controlled. To handle this problem, the immune system has evolved processes that delete or inactivate self-destructive cells, called immunological tolerance.

The first step towards immunological tolerance occurs in the early life of a lymphocyte, called central tolerance. During negative selection in the thymus, self-reactive T cells undergo clonal deletion, clonal diversion, receptor editing or anergy. The thymic microenvironment plays a crucial role in these processes. As described above, positive selection relies on cTECs. However, mTECs and DCs are important for the clonal deletion and the differentiation of nTregs. Beside the antigen presentation of circulating and cell-associated proteins that are expressed in a variety of tissues, mTECs and DCs can present tissue-restricted proteins as well. Patients that carry a mutation in the AIRE gene suffer from a multiorgan autoimmune disease, known as autoimmune polyendocrine syndrome type 1 (APS1). It has been shown that the presentation of tissue-specific antigens by mTECs leads to the depletion of self-reactive CD8<sup>+</sup> T cells. However, the depletion of self-reactive CD4<sup>+</sup> T cells depends on DCs, which present mTEC-derived tissue-specific antigens<sup>97,98</sup>. The expression of AIRE in mTECs is induced upon stimulated RANK and CD40 by their ligands, which are expressed on mature CD4<sup>+</sup> T cells. RANK induced NF-κB activation not only results in the expression of AIRE, but also influences the differentiation and function of mTECs. Interestingly, tissue-specific antigen expression is not uniform through the mTEC population. Individual tissue-specific antigens are present in 1 – 3 % of entire mTEC population. The coordinated expression of different tissue-specific antigens within the mTEC population ensures a robust coverage<sup>99,100</sup>.

The majority of self-reactive CD4<sup>+</sup> T cells undergo clonal deletion within the thymus. However, a small fraction of self-reactive T cells differentiate into Tregs. This process is called clonal diversion. The decision if a cell undergoes clonal deletion or

clonal diversion depends on the strength and duration of TCR signals. Mice studies revealed that the generation of Tregs is abrogated in mice carrying a mutation in the LAT gene, while the formation of other T cells is not affected. This indicates that the development of Tregs requires a stronger TCR signal in the thymus than non-Treg T cells<sup>101</sup>. In addition to the affinity of the interaction between TCR and peptide-MHC, the microenvironment in the thymus also contributes to the generation of Tregs. The absence of mature mTECs, through a depletion of tumor-necrosis factor receptor-associated factor 6 or NF- $\kappa$ B inducing kinase blocks the development of Tregs<sup>102,103</sup>. Moreover, mTECs can prime thymic dendritic cells via the thymic stromal lymphopoietin to promote the generation of Tregs<sup>104</sup>. The transcription factor forkhead box P3 (Foxp3) is a master regulator of Treg development and function. However, different studies suggest that Foxp3 is not essential for the initial cell fate decision of Tregs. Mice lacking Foxp3 express Treg-associated surface molecules like CD25, but show no suppressive function *in vitro*. This suggests that Foxp3 plays an important role for the suppressive function and the stability of the Treg phenotype<sup>105-107</sup>.

Central tolerance is a crucial mechanism to prevent the formation of self-reactive lymphocytes, but it is not sufficient to eliminate all of them. T cells encounter food antigens, developmental antigens or antigens displayed during chronic infections for the first time in the periphery, which could lead to autoimmune responses and severe diseases. Therefore, peripheral tolerance is achieved by anergy and deletion of self-reactive T cells.

As described above, T cells rely on three signals to become fully activated. When a T cell recognizes their cognate antigen in the periphery without co-stimulation it induces an active repression of TCR signaling and IL-2 expression, leading to condition of long-term hyporesponsiveness in T cells, called anergy. The ubiquitin ligase Cbl-b has been linked with T cell anergy, as it induces the ubiquitination of TCR-associated molecules. Cbl-b deficiency in mice causes spontaneous T cell proliferation and autoimmunity. However, the mechanism that leads to the induction of Cbl-b for self-antigens, but not for pathogen-associated antigens is not understood so far. T cell anergy can also be induced by inhibitory receptors, like CTLA-4 and programmed cell death protein 1 (PD1). CTLA-4 mediates the control of the initial

CD4<sup>+</sup> T cell activation and acts as a mediator of the suppressive function of Tregs. In contrast, PD-1 has not directly been linked to the function of Tregs, but seems to be essential for the termination of peripheral responses of effector T cells<sup>1</sup>.

When T cells encounter their cognate antigen (e.g. self-antigen), they not only become anergic, but can also be deleted. The identification of self-antigens may directly induce the expression of Bim, which binds to pro-apoptotic effector proteins, predominately Bax and Bak. These factors oligomerize and increase the permeability of the mitochondrial membrane, which is inhibited by the co-stimulator- and survival factor-mediated expression of anti-apoptotic proteins, like Bcl-2 and Bcl-X<sub>L</sub>. The disrupted mitochondrial membrane allows the release of mitochondrial components, into to the cytosol, leading to activation of caspases. These proteins induce the fragmentation of DNA and finally the apoptosis of the cell. This procedure of cell death induction is the mitochondrial (or intrinsic) pathway. Beside this pathway, T cells can also be deleted via the death receptor (or extrinsic) pathway. Self-reactive T cells can encounter their antigens frequently in the periphery. This can induce the expression of Fas ligand (FasL) on the cell surface. The ligation of FasL with the receptor Fas (CD95) induces oligomerisation of the receptor, followed by the downstream activation of of caspase 8. Active caspase 8 not only induces apoptosis, but also a protein that binds Bax and Bak, known as Bid. The induction of the mitochondrial pathway supports and increases death receptor signaling<sup>1</sup>.

Several experimental settings indicate that naïve T cells can differentiate into Tregs and gain immune suppressive functions. Naïve T cells, which are activated in the presence of TGF-β *in vitro*, express Foxp3<sup>108,109</sup>. In contrast to nTreg, the expression of Foxp3 is unstable in induced Treg (iTreg). Laurance *et al.* indicated that the administration of IL-2 *in vivo* stabilizes the expression of Foxp3 in iTregs<sup>110</sup>. Also metabolites can affect the differentiation of naïve T cells. Retinoic acid is secreted by a subset of gut-resident dendritic cells. When these cells presented orally administrated antigens to naïve T cells, they induce the differentiation of Foxp3<sup>+</sup> Tregs. Moreover, it has been shown that retinoic acid inhibits the IL-6 dependent differentiation of Th17 cells. Therefore, retinoic acid may acts as an important mediator of oral tolerance<sup>111</sup>.

### 3.2.5 T cell exhaustion

During acute infections, T cells become activated and develop into effector T cells in order to eliminate the pathogen. When this aim is accomplished the majority of effector T cells die and only few cells differentiate into memory T cells. The formation of memory T cells occurs in the absence of the original antigen. When the immune system is not able to clear the infection, persistent antigen exposure impairs the development of memory T cells, resulting in exhausted T cells. T cell exhaustion was initially observed in mice with chronic viral infections<sup>112,113</sup> and has also been described for patients with HIV and HCV, as well as cancer patients. Exhausted T cells are characterized by a progressive and hierarchical loss of effector functions, increased levels of inhibitory receptors, an altered transcription factor expression and usage, metabolic disorders and inability to acquire features of quiescent cells<sup>114-117</sup> (Fig. 3.12). Mice studies with chronic lymphocytic choriomeningitis virus (LCMV) indicated that the level of antigen stimulation in combination with a missing CD4<sup>+</sup> T cell help and inhibitory receptor signaling contribute to the induction of T cell exhaustion<sup>118,119</sup>. It has been shown that CD8<sup>+</sup> T cells do not develop signs of exhaustion when they encounter a chronic LCMV strain for a short period (1 week). However, when continuous exposure (2 – 4 weeks) of CD8<sup>+</sup> T cells with the same strain lead to T cell exhaustion, which could not be reversed by removal of the antigen exposure<sup>120,121</sup>. The hypothesis that persistent TCR stimulation is a key mediator of T cell exhaustion has been supported by the discovery that proteins associated with TCR signaling, NFAT and sprout homologue 2 (SPRY2), are involved in the development of T cell exhaustion<sup>122-124</sup>.

Inhibitory receptors are an essential feature of adaptive immunity to prevent autoimmunity and induce self-tolerance. Although all activated T cells transiently express inhibitory receptors upon activation, exhausted T cells show a prolonged and high expression of several inhibitory receptors<sup>114</sup>. The intracellular pathways used by inhibitory receptors, such as PD-1 and CTLA-4, to promote T cell exhaustion are not clear. However, several mechanisms have been proposed by which inhibitory receptors regulate T cell function. First, inhibitory receptors disrupt the formation of microclusters and lipid rafts and sequester target receptors and ligands by ectodomain competition. A second mechanism that has been described is the modulation of

intracellular mediators, which can impair the signaling of the TCR and co-stimulatory molecules<sup>125-127</sup>. Third, the ligand binding of inhibitory receptors can result in the induction of inhibitory genes<sup>119</sup>. Beside PD-1 also other inhibitory receptors, like lymphocyte activation gene 3 (LAG3), 2B4 (or CD244), CD160, T cell immunoglobulin domain and mucin domain-containing protein 3 (TIM3) and CTLA-4, are expressed at high levels on exhausted T cells<sup>128</sup>. In general, the severity of exhaustion of T cells correlates with an increased number of inhibitory receptors. In line, the expression of an individual inhibitory receptor is not a clear sign of exhaustion, whereas the expression of several inhibitory receptors on one T cell is a basic aspect of T cell exhaustion.

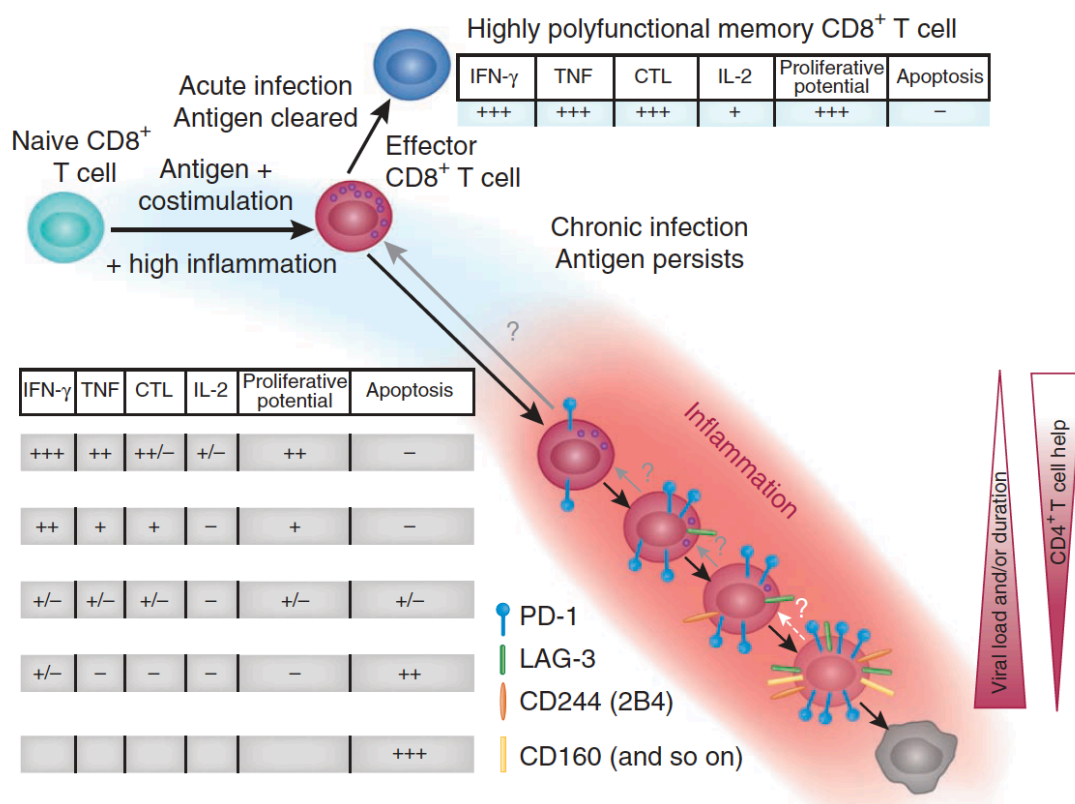


**Fig. 3.12: T cell exhaustion: A hierarchical overview.** Acute infections initiate the differentiation of naïve T cell towards effector T cells. When the acute infection is cleared, a small fraction of highly polyfunctional memory T cells will survive, which are able to produce a broad variety of cytokines, have a high cytotoxic potential and are maintained long term without antigen. In contrast, chronic infections fail to be cleared. As a consequence of the increase antigen and/or viral load, T cells undergo a hierarchical loss of effector functions. The severity of exhaustion is also characterized by an increased and more diverse expression of inhibitory receptors. When the viral load is too high and/or long, virus-specific T cells can be eliminated by apoptosis. The activity of each property is presented in a scale from high (++++) to low (-). CTL = cytotoxic potential of the cell. Adapted from Wherry<sup>114</sup>

Soluble molecules can also contribute to the development of exhaustion. These factors include immunosuppressive cytokines, like IL-10 and TGF $\beta$ , and

inflammatory cytokines, like type I interferons (IFN) and IL-6. Studies indicated that the interaction of IL-10 with its receptor mediates T cell exhaustion. If the interaction is blocked, T cell function is restored and the viral control during chronic infections is improved<sup>129,130</sup>. Moreover, when IL-10 signaling is blocked together with the PD-1 pathway, CD8<sup>+</sup> T cell exhaustion is reversed and the virus could be controlled better in mice<sup>131</sup>. This synergistic effect may be explained by the IL-10 production of monocytes following PD-1-PD-L1 interaction. Nevertheless, the specific mechanisms by which IL-10 shapes T cell exhaustion need further investigation. Another cytokine, which is associated with T cell exhaustion, is TGF $\beta$ . *In vivo* studies suggested that TGF $\beta$  signaling is involved during chronic LCMV infection, as the phosphorylation of SMAD2 in CD8<sup>+</sup> T cells was increased in chronically infected mice in comparison with acute infections<sup>132</sup>. However, current studies aiming at inhibition and blockade of the TGF $\beta$  signaling pathway resulted in a limited benefit of the treatment<sup>133,134</sup>.

The signaling of type I IFN, like IFN $\alpha$  and IFN $\beta$ , displays a crucial factor for antiviral functions during the early phase of infection. Surprisingly, recent data indicated that the blockade of these signaling pathways enhance control of chronic viral replication and reverse and/or prevent T cell exhaustion<sup>135,136</sup>. IFN type I signaling may be involved in the programming of T cells towards exhaustion, as a blockade of IFN $\alpha/\beta$  signaling during the first two weeks of infection prevents the development of T cell exhaustion.

Taken together, T cell exhaustion displays a distinct state of T cell differentiation, which has been associated with chronically infected patients. In the last years, several molecules have been linked with T cell exhaustion. However, the mechanisms leading to and more importantly reversing T cell exhaustion are poorly understood and need to be further investigated<sup>115</sup>.

### **3.3 Cancer immunology and immune therapy**

T cell exhaustion plays not only a role in patients with chronic infection, but also in cancer patients. Cancer is a global health problem and one of the most frequent causes of death worldwide. Tumors are characterized by the uncontrolled growth of

malignant cells within healthy tissue, which impairs the cellular integrity and function of the tissue. Malignant cells contain mutations in their genome, which result in massive proliferation, resistance to apoptotic death and escape from the hosts immune response<sup>1</sup>. The hypothesis that immune cells, especially T cells, can recognize and destroy malignant cells was proposed 60 years ago by Macfarlane Burnet and described as “immune surveillance”<sup>137,138</sup>. However, in the last years it has become increasingly clear that the immune system does not only eradicate malignant cells, but also can promote the growth of tumors. Schreiber and colleagues initially described this dual role of the immune system, called cancer immunoediting<sup>139,140</sup>. The most complex form of cancer immunoediting displays three stages. (i) In the initial stage, known as **elimination**, malignant cells are recognized by the innate and adaptive immune system resulting in the elimination of the malignant cells before clinical symptoms occur. (ii) When the immune system is not able to clear the entire tumor, the residual malignant cells enter the second stage of cancer immunoediting, called **equilibrium**, which is characterized by an immune-controlled growth of malignant cells without resulting in the clearance of the tumor. (iii) During this period, the immunological pressure may results in altered tumor cells, which can no longer be recognized by the immune system. The **escape** stage is associated with rapid growth, the establishment of an immunosuppressive tumor microenvironment and clinical symptoms<sup>141</sup> (Fig. 3.13). The single phases of cancer immunoediting are described in more detail in the following chapter.

### 3.3.1 Cancer immunoediting

Nascent tumor cells are recognized and destroyed by both, the innate and adaptive immune system in the initial stage of cancer immunoediting, known as elimination, which represents a modified version of the original theory of cancer immune surveillance. It has been shown that cells from the innate compartment, like NK cells, macrophages and DCs, as well as cells from the adaptive immune system, such as NKT, CD4<sup>+</sup> and CD8<sup>+</sup> T cells, are able to eliminate cancerous cells<sup>142,143</sup>. Moreover, also soluble factors can contribute to the elimination of a tumor. For example, the establishment of an anti-tumor immune response requires type I interferons (IFN- $\alpha/\beta$ ) and IFN- $\gamma$ . IFN- $\alpha/\beta$ , which generally target host cells, promote cross-presentation of tumor antigens by DCs. In contrast, host cells and tumors are affected by IFN- $\gamma$ , as it

enhances the differentiation of T<sub>H</sub>1 cells and CTLs and increases the expression of MHC-I on tumor cells<sup>144,145</sup>. When the immune system is able to clear the entire tumor, the elimination stage alone represents the cancer immunoediting.

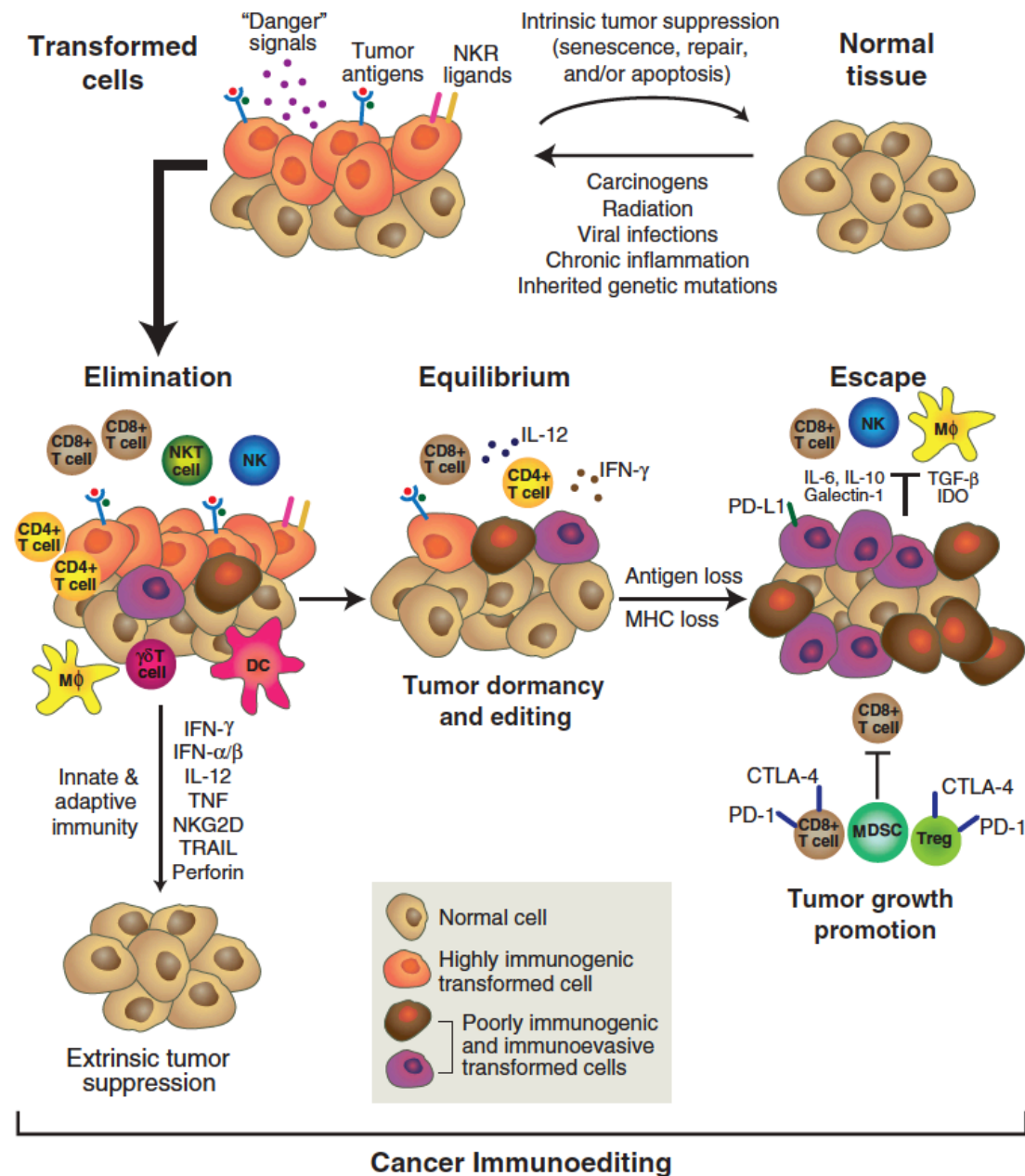


**Fig. 3.13: The cancer immunoediting hypothesis.** When a nascent malignant cell cannot be removed by intrinsic tumor suppressive mechanisms, cancer immunoediting occurs. In general, cancer immunoediting can be distinguished into three stages: elimination, equilibrium and escape. In the elimination phase immune cells recognize and destroy nascent tumor cells. If the tumor cells cannot be eliminated, the tumor cells enter the second stage of cancer immunoediting, known as equilibrium. In this phase the immune system controls the growth of tumor cells without eliminating it entirely. When the tumor cells reduce their immunogenicity they may enter the third stage, called escape. Massive proliferation and an immunosuppressive tumor microenvironment lead to the outgrowth of the tumor. Adapted from Schreiber *et al.*<sup>140</sup>



When malignant cells survive the elimination stage, they enter the second stage of cancer immunoediting (equilibrium). In this stage the tumor is clinically inconspicuous, as the outgrowth of cancer cells is controlled by the immune system. A clinical case from 2003 suggests that this stage is present in humans. Following the transplantation of kidneys from a cadaver donor, the two recipients developed malignant melanoma<sup>146</sup>. The transplanted kidneys were diagnosed as origin of the tumor, as the donor was cured from cancer 16 years before his death and was assumed to be cancer free. Unfortunately, the immunosuppressive therapy of the recipients led to the proliferation of the dormant resident malignant cells. 10 years ago, the group of Robert Schreiber published the first experimental data that the equilibrium phase exists<sup>147</sup>. They treated immunocompetent mice with low doses of the carcinogen 3'-methylcholanthrene. The majority of the mice had no clinically apparent tumor over a time period of 200 days. However, when they depleted the immune system by injection of monoclonal antibodies to T cells or IFN- $\gamma$  half of the mice developed rapidly growing tumors at the site of MCA administration. Strikingly, inhibition of the innate immune response did not initiate the outgrowth of cancer cells. As indicated by studies in mice and humans, the immune system can control malignant cells over years. Therefore, the equilibrium stage can represent the final step of cancer immunoediting<sup>141</sup>.

However, a reduced immunogenicity of the tumor cells can impair the host's immune response such that the tumor cells can no longer be controlled leading to the outgrowth of the tumor. In line, the tumor can become clinically apparent. In 2011, evading immune destruction has been recognized as one of the "hallmarks of cancer"<sup>148</sup>. Tumor cells can reduce their immunogenicity by intrinsic and extrinsic changes. For example, tumor cells can avoid immune destruction by down-regulation of MHC-I, reduced expression of co-stimulatory molecules and antigen loss<sup>149,150</sup>. Increased expression of STAT3 and the anti-apoptotic molecule Bcl-2 improves the resistance to survival and promotes survival of tumor cells<sup>151</sup>. Moreover, tumor cells can generate an immunosuppressive microenvironment. The influence of the tumor microenvironment (TME) on T cell function is described in the next chapter.

### 3.3.2 Influence of the tumor microenvironment on T cell immunity

Non-malignant cells, soluble factors and blood vessels, which surround and feed the tumor, generate the TME. It has been shown that also immune cells are present in the TME<sup>152</sup>. However, tumor-derived signals can mediate an environment in which anti-tumor function is suppressed. The TME is highly complex and contains cancer-associated fibroblasts, endothelial cells, myeloid cells, as well as cells from the adaptive immune system, like suppressive B cells, T<sub>regs</sub> and  $\gamma\delta$  T cells. Several mechanisms can promote tumor escape, like (i) the inhibition of tumor infiltration, (ii) chronic T cell stimulation, (iii) inhibitory molecules and cells, (iv) metabolic competition, (v) impaired antigen presentation and (vi) genetic mutations of the tumor<sup>153</sup> (Fig. 3.14).

T cell infiltration is a critical parameter to determine the “immunoscore” of a patient. A higher number of TILs has been linked to a higher “immunoscore” and is beneficial for the survival of the patient<sup>154,155</sup>. Therefore, solid tumors try to exclude T cells from the TME. T cell infiltration can be inhibited by the down-regulation of essential adhesion molecules like ICAM-1/2, VCAM-1 and CD34 on tumor endothelium<sup>156</sup>. The migration of T cells generally depends on chemokines. An important chemokine for the migration towards inflammatory site is CXCR3. Tumors expressing increased levels of CXCR3-ligands show a higher T cell infiltration, whereas tumors lacking these ligands show an impaired recruitment of T cells<sup>157,158</sup>. A recent publication by Peng and colleagues indicate that epigenetic changes in ovarian cancers may prevent the expression of chemokines required for T cell infiltration<sup>159</sup>. Moreover, some tumors express ligands for the death receptors on the vascular endothelium, which induces apoptosis in adhering lymphocytes<sup>160</sup>.

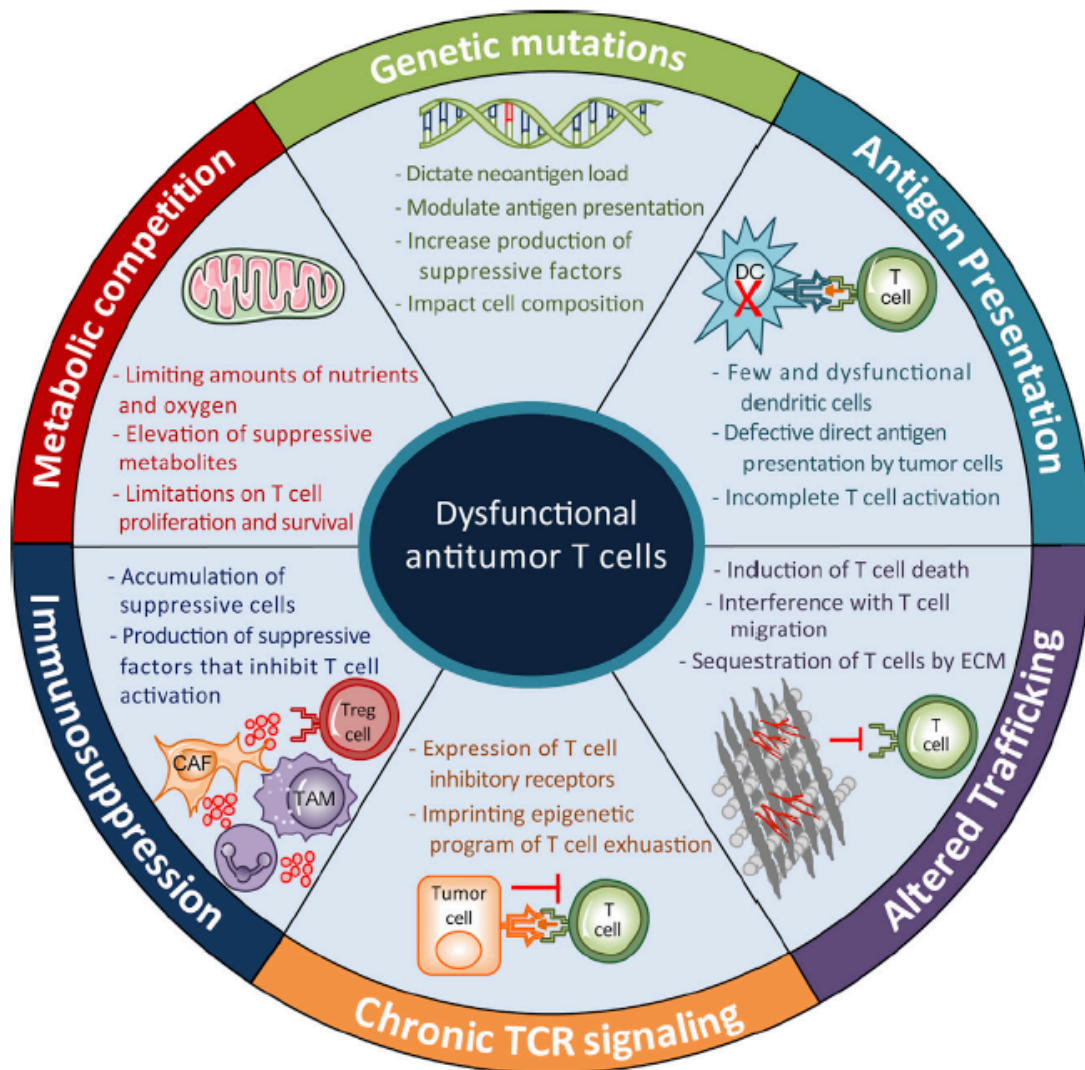


Fig. 3.14: Origins of T cell dysfunction in tumors. Adapted from Anderson *et al.*<sup>153</sup>

The different cell types within the TME can further mediate T cell suppression. Tumor-derived factors lead to the recruitment of tumor-associated macrophages (TAM) and granulocytes and promote the differentiation of myeloid cells into cells with anti-inflammatory function, like the production of the cytokines IL-10 and TGF- $\beta$ <sup>161</sup>. It has been shown that TGF- $\beta$  prevents the migration of T cells into the TME and impairs tumor-specific functions of CD8<sup>+</sup> T cells<sup>162</sup>. Stromal cells can impair T cell recruitment, inhibit T cell proliferation and induce the differentiation of T<sub>regs</sub><sup>163</sup>. A common feature of immunosuppression within the TME is an increased expression of inhibitory ligands. A well-characterized ligand, which also plays a role in chronic-viral infection induced exhaustion, is PD-L1. The interaction with its receptor on T cells results in reduced effector function of T cells. These findings indicate the complexity by which immunosuppressive cells mediate T cell dysfunction.

Rapidly proliferating tumor cells metabolize sugars, amino acids and fatty acids within the TME leading to an area of limited nutrient availability. Immune cells depend on these nutrients to establish complete functionality and therefore they are in strong competition with tumor cells for the few metabolites. One of these crucial metabolites is glucose. Like all briskly dividing cells, tumor cells require high amounts of glucose to meet their metabolic demands. The switch from cellular respiration to aerobic glycolysis of tumor cells was described for the first time 90 years ago<sup>164</sup>. This phenomenon was called Warburg effect. Tumor cells have a metabolic advantage over T cells, as they can express more surface molecules important for the uptake of nutrients. An overexpression of GLUT1, an essential transporter for the uptake of glucose, in tumor cells is associated with low CD8<sup>+</sup> T cell infiltration and poor prognosis of the patients<sup>165,166</sup>. The limited access of effector T cells to glucose within the TME directly impairs the proliferation, cytokine production and TCR signaling<sup>167-169</sup>. The metabolic environment within the tumor may also lead to increased numbers of T<sub>regs</sub> as these cells predominantly rely on oxidative phosphorylation.

Another metabolite that has been linked with the function of anti-tumor responses is arginine, which is converted into downstream metabolites by arginase (ARG) or nitric oxide synthase (NO). One of these enzymes or both are frequently up-regulated in solid tumors<sup>170</sup>. Interestingly, a reduced expression of Arg1 in TAMs led to a reduced tumor growth *in vivo*<sup>171</sup>. Higher levels of reactive nitrogen species can be a result from overexpression of NO. These are toxic for T cells<sup>170</sup>. In conclusion, the depletion of nutrients by rapidly proliferating tumor cells limits the function of effector T cells and displays another mechanism that allows tumor cells to escape from immune cell control.

Chronic stimulation of T cells within the TME can result in dysfunction, which is associated with an epigenetic program that has been described for exhausted T cells from patients with chronic viral infections<sup>172,173</sup>. Tumor-specific T cells frequently express inhibitory surface receptors, like PD-1, LAG3, and CTLA-4. As these molecules are also up-regulated upon functional T cell activation, scientists tried to identify genes initiating T cell dysfunction. A recent study suggests that

metallothioneins promote T cell dysfunction in a mouse model of sarcoma. However, if it is a mechanism restricted to sarcoma or a general mechanism is unclear<sup>174</sup>. Schietinger *et al.* published recently a study in which they showed that dysfunction of tumor-specific T cells is initiated already during the early stage of tumor malignancy. Interestingly, while T cell dysfunction was reversible by blockade of PD-1 in the early stage, application of an anti-PD-1 antibody did not rescue T cell function at an advanced stage<sup>153,175</sup>.

### **3.4 Immunotherapy to treat cancer**

Since the discovery that the immune system can recognize and destroy malignant cells, scientists tried to use the host's immune system to treat cancer patients, known as immunotherapy. In the last years, clinical studies proofed that immunotherapy can be a powerful tool to treat cancer patients leading to the approval of several immunotherapies for clinical use<sup>176-178</sup>. Immunotherapies aim to stimulate effector functions and/or inhibit suppressive mechanisms. Different strategies are currently under development to achieve this goal. They include cancer vaccines, antibodies against immune checkpoints, oncolytic viruses and adoptive T cell therapy (ATC). In particular, cancer vaccines and ACT rely on the identification of tumor-specific antigens to establish a functional immune response.

#### **3.4.1 Origins of cancer antigens**

The existence of tumor antigens, which can be detected by T cells, was initially described a quarter of a century ago<sup>179</sup>. In general, tumor antigens can be divided into three categories. (i) Tumor-associated antigens (TAA) describe proteins that are overexpressed in tumor cells and are expressed at low levels in normal cells. (ii) Cancer/testis antigens (CTA) arise from proteins that are expressed within the tumor and by reproductive tissue. These antigens are normally not presented by normal reproductive cells, as they do not express MHC-I. (iii) Tumor-specific antigens (TSA), also called neoantigens, are selectively expressed in tumor cells and derive from non-synonymous mutations<sup>141,180,181</sup>.

Many immunotherapies used TAAs and CTAs as targets, as these are commonly overexpressed in different types of cancer displaying the potential to treat a broad

range of patients. However, many studies targeting these antigens had no or just limited benefit for the outcome of the patients<sup>182</sup>. As TAAs derive from normal host proteins, central and peripheral tolerance mechanisms can deplete TAA-specific T cell. Moreover, it has been shown that the TCR affinity for TAAs is lower than for TSA<sup>183,184</sup>, which may correlate with a reduced T cell cytotoxicity and activation<sup>185</sup>.

A central concern of immunotherapies to TAAs and CTAs is the establishment of autoimmune responses to healthy tissues. Several studies have been published describing severe complications associated with immunotherapy to TAAs. A therapy to ERBB2, one of the most studied molecules in the field of cancer, resulted in respiratory failure and death, which was may due to a low expression of ERBB2 on lung epithelial<sup>186</sup>. A similar case report was published for the CTA MAGE-A3. The unknown expression of MAGE-A3 in the brain was the potential cause for severe neurological toxicity and death in treated patients<sup>187</sup>. These cases indicate the difficulties by using TAAs or CTAs as targets for immunotherapy. However, immunotherapies to TAAs have also resulted in tremendous clinical benefit for patients. The most prominent example is the therapy of acute lymphoblastic leukemia by engineered T cells recognizing CD19. In this case, the elimination of healthy CD19<sup>+</sup> B cells was managed with immunoglobulin replacement<sup>188</sup>.

TSAs are considered to be a more promising target for immunotherapy, as neonatigens derived from mutated proteins and the resulting antigens are theoretically foreign. Therefore, the risk to develop autoimmunity should be reduced in immunotherapies targeting TSAs<sup>189</sup>. The majority of neonatigens occur from mutations that result in no intrinsic growth advantage, called passenger mutations. Only few mutations support the cancer growth, known as driver mutations<sup>190</sup>. Driver mutations display a promising target for immunotherapy as it leads to the disruption of pathways, which are essential for tumor growth. In the last years, several studies indicated that a higher mutational load is associated with an improved anti-tumor response<sup>191,192</sup>. Moreover, therapeutic anti-tumor responses were described in a preclinical model using neonatigens as tumor vaccine<sup>193</sup>.

### 3.4.2 Cancer vaccines

The first approaches to stimulate the host's immune response against tumor cells have been therapeutic vaccines. In contrast to preventative vaccines against pathogen like hepatitis B virus or measles, cancer vaccine has to break the immune tolerance of tumor cells, which reduces the efficiency of the therapy<sup>194</sup>. The most promising results derived from vaccines with DCs that are loaded with tumor antigens *ex vivo* and then re-infused back into patients. In 2010, the FDA approved the cancer vaccine sipuleucel-T, which is a personalized cancer vaccine containing blood-derived DCs with DC-stimulating factors. Treatment of prostate cancer patients led to an improved survival in comparison to the control group<sup>176</sup>. Ott and colleagues described recently a personalized cancer vaccine for patients with melanoma leading to a strong T cell response without severe side effects<sup>195</sup>. The vaccine was personalized for the patients and contained neoantigens from the different patients. The identification of good antigens for cancer vaccine displays still the major challenge for cancer vaccine design. However, the identification of promising antigens does not assure the production of a protective immune response<sup>196,197</sup>. Further research is required to optimize the design of cancer vaccines in order to optimize the efficiency of these therapies.

### 3.4.3 Immune checkpoint blockade

One mechanism by which tumor cells prevent anti-tumor T cell responses is the expression of inhibitory receptors. In the last years these receptors have been identified as promising targets for immunotherapy. The blockade of immune checkpoint inhibitors, such as PD-1, PD-L1 and CTLA-4, resulted in significant efficiency in many types of cancers<sup>198</sup>. Different antibodies have been developed. The most prominent ones, are pembrolizumab and nivolumab, which target PD-1, and tremelimumab and ipilimumab, that block the CTLA-4 signaling<sup>199</sup>. The FDA and the European Medicines Agency approved the single treatment and the combination of these antibodies for metastatic melanoma, non-small cell lung cancer and renal cell carcinoma<sup>177,178</sup>. Interestingly, the combination of antibodies to CTLA-4 and PD-1 resulted in synergistic effects. A clinical phase II study showed that the combination results in an objective response rate of 61 %, while the monotherapy with ipilimumab shows an objective response rate of only 11 %<sup>200</sup>. These findings suggest that the

combination of immune checkpoint blockade with other therapies could be beneficial for the patient.

#### **3.4.4 Adoptive T cell therapy**

In general, the efficiency of immunotherapies relies on the presence of large numbers of tumor-specific T cells, which can migrate into the tumor and can selectively destroy cancerous cells. Adoptive cell transfer (ACT) represents an approach, where T cells, recognizing tumor-associated antigens, are identified and expanded *ex-vivo* and then infused into the cancer patient<sup>201</sup> (Fig. 3.15). The group of Steven Rosenberg isolated tumor infiltrating lymphocytes (TIL) from 93 metastatic melanoma patients. After the TILs were screened for tumor-reactivity, they were expanded *in vitro* and re-infused into the patients. 20 % of the treated patients showed a complete response after 3 years<sup>202</sup>. Beside the successful treatment of melanoma patients, the limited number of tumor-reactive TILs in other types of cancer is a massive limitation of ACT. To broaden ACT also to other types of cancer, gene-engineered T cells were used. TCR recognizing common TAAs like NY-ESO1 in cell sarcoma and melanoma patients, were grafted onto T cells from the patient's blood<sup>203</sup>. Chimeric antigen receptor (CAR) modified T cells represent a second class of engineered T cells used for ACT. CAR T cells have the advantage that they recognize antigens in an HLA-independent manner and therefore they are applicable for patients with different HLA haplotypes. Recently, the first CAR T cell therapy was approved by the Food and Drug Administration (FDA) to treat relapsing B-cell acute lymphoblastic leukemia (ALL) in children and young adults.



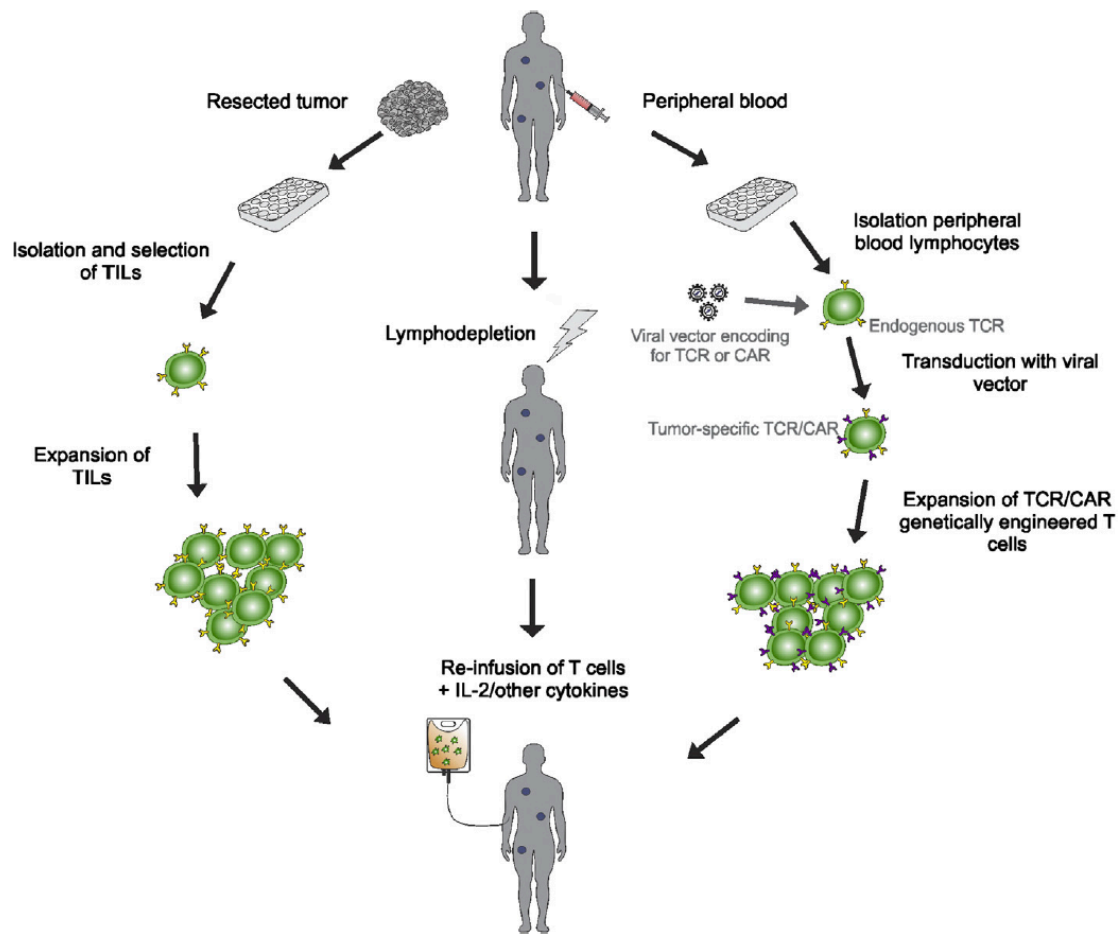


**Fig. 3.15: General schema for adoptive cell therapy (ACT).** Tumor-infiltrating lymphocytes (TILs) can be isolated and screened for tumor reactivity, followed by *ex vivo* expansion. Another source for T cells for ACT are peripheral blood T cells that are engineered in order to express a tumor-specific T cell receptor (TCR) or chimeric antigen receptor (CAR). After the patient undergoes lymphodepletion, the expanded anti-tumor T cells are re-infused in combination with cytokines, like IL-2. Adapted from Wayteck *et al.*<sup>204</sup>

### 3.4.5 Metabolism – a target to treat cancer

The success of ACT does not only depend on the identification of tumor-specific T cells, but also on the robustness and stability of the population. In the last years, it has become more and more evident that cellular metabolism influences T cell fate and function. It has been shown that nutrients are limited within the tumor microenvironment, which leads to T cell dysfunction, stress and apoptosis<sup>169,205,206</sup>. Therefore, methods that could improve the fitness and survival of cells, used for ACT, are urgently needed.

The mechanistic target of rapamycin (mTOR) plays a critical role in regulating T cell activation, differentiation and function<sup>207</sup>. The depletion of factors associated with mTORC1 or mTORC2 can inhibit the differentiation of naïve T cells into T<sub>H</sub>2 and

T<sub>H</sub>1/17, respectively<sup>72,88</sup>. The effect of the mTOR inhibitor rapamycin on T cell differentiation and function has varying effects. Whereas, it has been linked with the formation of CD8<sup>+</sup> T cell memory generation<sup>96</sup>, other studies indicated that rapamycin promotes Treg formation and T cell anergy<sup>208</sup>. First studies described the administration of rapamycin during cancer. Depending on the model, the inhibition of mTOR led to the promotion of effector T cells<sup>209</sup> or to the inhibition of effector T cells<sup>210</sup>.

The metabolism of T cells can also be influenced by antibody blockade of inhibitory receptors. It has been shown that ligand binding of PD-1 increased FAO and decreased glycolysis, which promoted longevity, but also dampened the effector functions<sup>211</sup>. Therefore, using immune checkpoint inhibitors may improve T cell function by enhancing glycolysis. Moreover, the blockade of metabolic pathways by small molecules displays another therapeutic possibility. Dichloracetate, an inhibitor of the kinase PDK1, selectively limited the survival and proliferation of T<sub>H</sub>17 cells in models of inflammatory bowel disease and experimental autoimmune encephalomyelitis<sup>212</sup>. Other studies used JPH203 and BCH, inhibitors of the amino acid transporter Slc7a5. This transporter is important for the differentiation and function of T<sub>H</sub>1/17 cells. The administration of these compounds dampened the response of inflammatory T cells<sup>66,209</sup>.

As described above, tumor-specific T cells are massively expanded *in vitro* to perform ACT. During this process, the proliferative capacity and effector function of these cells need to be maintained, as well as the capacity to form stable memory T cell populations in order to protect the patient in the future. The glycolytic activity of T cells could be an important parameter for the efficiency of ACT. It has been shown that T cells with a high glycolytic activity can accelerate exhaustion, whereas the inhibition of glycolysis improves CD8<sup>+</sup> T cell memory development. In the same line, when T cells are primed under conditions that promote mitochondrial metabolism and where glucose is limited, more T cells differentiate towards memory T cells and the anti-tumor response and persistence is improved<sup>213,214</sup>. In order to keep them alive, tumor-infiltrating T cells are cultured in medium containing IL-2. This may display a problem for ACT, as IL-2 promotes glycolysis and may promote terminal differentiation. Furthermore, culture conditions that result in mitochondrial

metabolism rather than glycolysis could be an advantage, as the majority of T cells that rely on glycolysis will die because nutrient starvation. Adding IL-7 and IL-15 to the culture medium could improve the longevity of adoptively transferred T cells<sup>215</sup>.

### 3.5 Hepatocellular Carcinoma

Liver cancer is a global burden and the sixth most common cancer worldwide with 782'000 new cases in 2012 and the highest incidence rates in Eastern Asia. Following lung cancer, liver cancer is the second most common cause of cancer-associated death worldwide<sup>216,217</sup>. The broad majority (70 – 90%) of liver cancers is hepatocellular carcinoma (HCC), which occurs in the setting of chronic inflammation (cirrhosis) (Fig. 3.16)<sup>218</sup>. The time point of diagnosis plays an important role for the survival of the patients. Whereas, patients with a diagnosis of HCC in an early stage showed an 5-year survival of 70 %, patients with a late-stage diagnosis had an overall 5-year survival of only 16 %<sup>219</sup>.

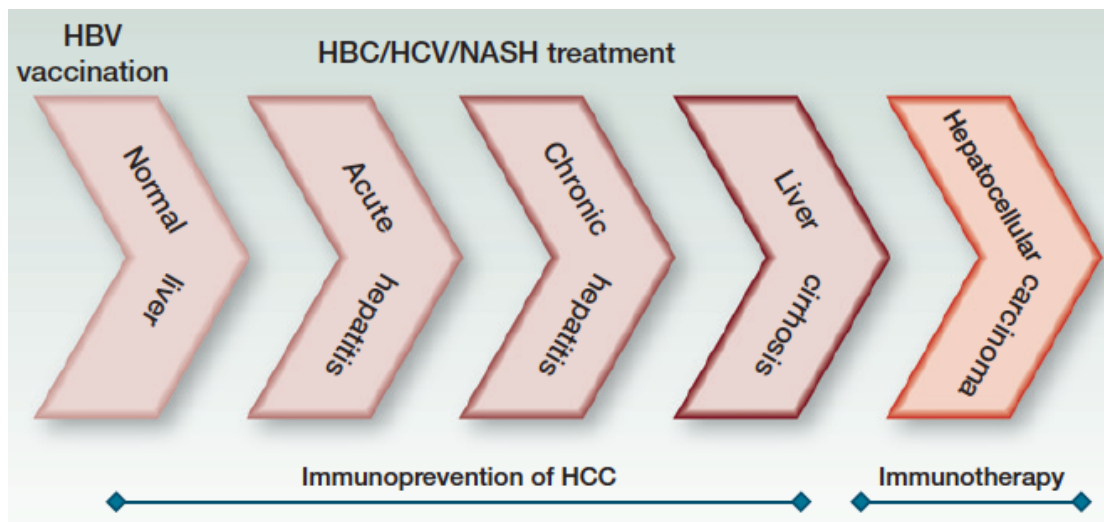


**Fig. 3.16: Development of Hepatocellular carcinoma(HCC).** Chronic viral infection or steatohepatitis can lead to the development of liver cirrhosis and hepatocellular carcinoma. The usage of immune-based therapies could prevent and treat HCC. Adapted from Greten *et al.*<sup>220</sup>

#### 3.5.1 Anatomy of the liver

The liver is the largest internal organ and represents approximately 2 – 3 % of the average body weight. Based on Couinaud's classification, the liver can be divided into eight segments, which are characterized by morphological and functional anatomy. The complex functions of the liver are carried out by a broad variety of cells. In general, they can be divided into parenchymal and non-parenchymal cells.

The parenchymal cells or hepatocytes represent 60 – 80 % of the entire liver cells and are involved in the metabolic, detoxifying and synthetic functions of the liver<sup>221</sup>.

The liver also displays an essential role as immunological filter, as it screens the blood for systemic and gut-derived pathogens<sup>222</sup>. Every minute approximately 30 % of the total blood passes the liver<sup>223</sup>. Blood enters the hepatic parenchyma mainly via the portal vein, which represents approximately 80 % of the blood supply, or the hepatic artery<sup>224</sup>. Afterwards it passes a complex structure of vascular channels and exits the liver via the central vein. The vascular channels, known as sinusoids, display an essential role for the immune functions within the liver (Fig. 3.17). The vascular structure of the sinusoids reduces the blood flow, thereby increasing the chance of a circulating pathogen to be in contact with the endothelium and recognized by the immune system is increased<sup>222</sup>.

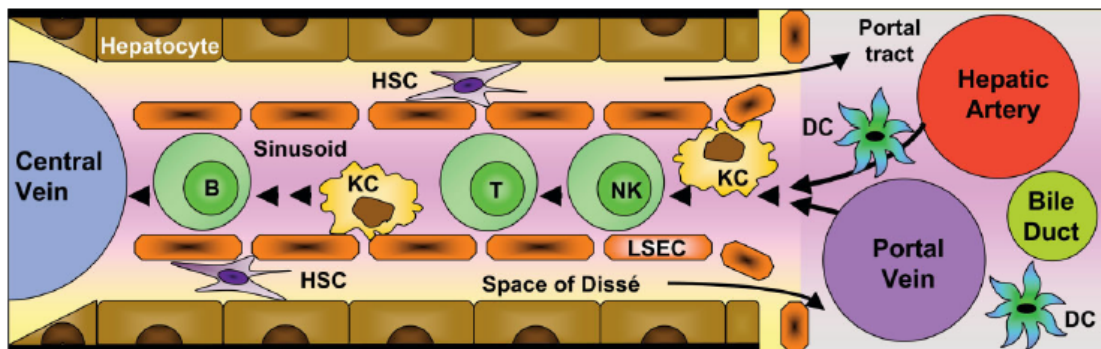


**Fig. 3.17: Structure of the liver sinusoids.** Liver sinusoids are sinusoidal blood vessels. A fenestrated monolayer of LSEC separates the hepatocytes from the sinusoids. The area between hepatocytes and LSECs is called space of Disse. HSEC are present in the space of Disse. Different immune cells pass the liver and screen the blood for pathogens. Arrows represent the direction of blood flow. B = B cell, KC = Kupffer cell, HSC = hepatic stellate cell, T = T cell, NK = natural killer cell, LSEC = liver sinusoidal endothelial cells, DC = dendritic cell. From Racanelli and Rehermann<sup>221</sup>

Sinusoids are lined by liver sinusoidal endothelial cells (LSEC) and flanked by hepatocytes. As the LSEC do not contain an organized basement layer, between hepatocytes and LSEC is a gap, called space of Dissé. LSECs contain fenestrae, which have a diameter of 100 nm and are organized into clusters, known as sieve plates<sup>225</sup>. These clusters allow the translocation of molecules from the sinusoidal lumen into the space of Dissé. Kempka *et. al* showed that the translocation is tightly regulated and sieve plates can exclude the passage of macromolecules as small as 12 nm<sup>226</sup>.

### 3.5.2 The etiologies of HCC

HCC is an inflammation-associated cancer. Chronic infections with hepatitis B or C virus (HBV/HCV) are known risk factors for the development of HCC. The majority of patients initially develops liver cirrhosis, which leads to HCC in a later stage of the disease. However, in other cases chronic HBV infection induced HCC in the absence of liver cirrhosis. Beside chronic viral infections, other risk factors have been linked with HCC development in the last years. Harmful alcohol consumption can lead to alcoholic steatohepatitis (ASH) and then to HCC. The escalating global epidemic of overweight and obesity led to an increased role of nonalcoholic steatohepatitis (NASH) as a risk factor for the development of HCC (Fig. 3.16)<sup>220</sup>.

### 3.5.3 T cells in HCC

High levels of CD8<sup>+</sup> T cells, but also CD4<sup>+</sup> within the tumor microenvironment have been described in patients with an superior survival in comparison to patients with low T cell counts<sup>227</sup>. In the case of HCC, studies indicated that CD8<sup>+</sup> T cells have the potential to kill malignant cells and the IFN- $\gamma$ , produced by a T<sub>H</sub>1 immune response, supports the anti-tumor immune response<sup>228</sup>. Attallah *et al.* reported lower levels of CD4<sup>+</sup> T cells and a reduced ratio helper T cells/suppressive T cells in the peripheral blood of liver cirrhosis and HCC patients<sup>229</sup>. The immunosuppressive functions of T cells in HCC have been studied extensively. One factor that has been linked with an increased disease severity is soluble CD25. HCC patients contained higher levels of soluble CD25 in their serum than healthy or patients with liver cirrhosis, suggesting that soluble CD25 could display a biomarker for the development of HCC. Moreover, depletion of soluble CD25 from the HCC serum improved the T cell response, indicated by higher levels of IFN- $\gamma$  production<sup>230</sup>. Another marker for T cell dysfunction in many types of cancer is the expression of PD-1 and its ligand PD-L1 on T cells and MDSCs, respectively. It has been shown that intratumoral Kupffer cells express high levels of PD-L1 and mediate T cell exhaustion<sup>231</sup>.

The function and importance of humoral immunity in HCC patients is poorly understood. However, reduced numbers of CXCR5<sup>+</sup> CD4<sup>+</sup> follicular T cells, which are important mediators of B cell differentiation and function, have been described

during HCC development. This was linked to a lower survival rate may resulting from a reduced secretion of IL-21 and an impaired B cell maturation<sup>232</sup>.

Tregs are important mediators of the immune suppressive environment in tumors<sup>107</sup>. The number of iTregs in the blood and tumors of HCC patients is increased and correlates with the severity of the disease<sup>233,234</sup>. Furthermore, increased numbers of CD4<sup>+</sup> CD25<sup>+</sup> Foxp3<sup>+</sup> Tregs correlated with a reduced tumor-infiltration of CD8<sup>+</sup> T cells compared with non-tumor regions. The effector function of tumor-infiltrating CD8<sup>+</sup> was impaired, as identified by a reduced expression of granzyme A, granzyme B and perforin, as well as inhibited proliferation and activation after *in vitro* activation with antibodies against CD3 and CD28 in the presence of Tregs<sup>235</sup>. Tregs not only affect the effector function of CD4<sup>+</sup> and CD8<sup>+</sup>, but also of NK cells. Ghiringhelli *et al.* discovered that the NK cell response is impaired by TGF- $\beta$  mediated down-regulation of the of NK group 2 member D<sup>236</sup>.

The presence of increased levels of IL-6 and TGF- $\beta$  was linked to an increased frequency of T<sub>H</sub>17 cells that could be detected in HCC tumors in comparison to non-tumor tissues. The increased abundance was associated with poor survival of HCC patients<sup>237</sup>. Especially the ratio of T<sub>H</sub>17/T<sub>H</sub>1 cells may serve as a potential prognostic marker for the overall survival of HCC patients. A study performed by Yan *et al.* indicates that an elevated T<sub>H</sub>17/T<sub>H</sub>1 ratio promotes tumor progression<sup>238</sup>. However, other studies suggest that T<sub>H</sub>17 cells promote anti-tumor responses of cytotoxic T cells<sup>239</sup>.

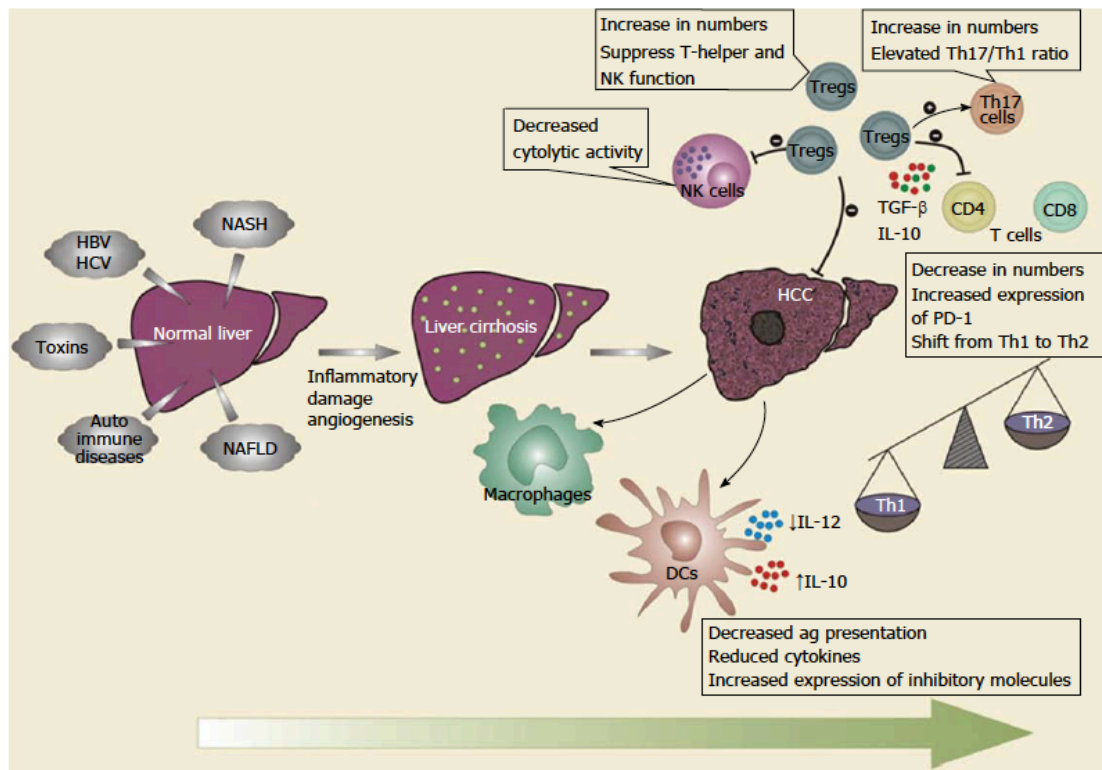


**Fig. 3.18: Influence of immune cells in HCC.** The function of many different cell types is impaired in HCC. DC fail to present antigens and show a reduced production of  $T_H1$ -associated cytokines. Macrophages have a M2 phenotype, which promotes the recruitment and differentiation of Tregs. These cells mediate immunosuppressive function and favor the differentiation of  $T_H17$  cells. The cytotoxic activity of NK cells is reduced. Higher frequencies of inhibitory receptors are detected on T cells. DC = dendritic cell;  $T_H$  = T helper cell; Treg = regulatory T cell; HBV = Hepatitis B virus; HCV = Hepatitis C virus. Adapted from Sachdeva *et al.*<sup>228</sup>

NK T cells, which represent characteristics of both, T cells and NK cells, display a considerable population in the liver. NK T cell function in HCC development and progression is poorly understood. On the one hand, NK T cells express the  $\alpha\beta$  TCR. On the other hand, they express several surface receptors of NK cells. Depending on their cytokine profile, they can contribute to anti-tumor responses or promote immune suppression. It has been shown that  $CD4^-$  NK T cells are beneficial for the patient and  $CD4^+$  NK T cells tend to induce tolerance<sup>240</sup>. Similar findings have been made also in the case of HCC. Higher frequencies of  $CD4^+$  NK T cells are present in the tumor microenvironment when compared to the blood and also non-tumorous liver tissue. These cells inhibited  $CD8^+$  T cells by the production of  $T_H2$  associated cytokines<sup>241</sup>. In contrast,  $CD4^-$  NK T cells seem to dampen the inflammatory response mediated by  $\beta$ -catenin-driven hepatocarcinogenesis<sup>242</sup>.

In addition, new techniques allow a better understanding and characterization of the different T cell populations in HCC patients. Recently, Zheng *et al.* published a study,

where they used single cell transcriptomics to analyze T cells from blood, liver and tumor and potentially identified new subsets of T cells that are associated with T cell dysfunction<sup>243</sup>. They identified that HCC-associated Tregs express CCR8 and LAYN, which was also expressed in tumor-infiltrating exhausted CD8<sup>+</sup> T cells and correlated with a poor prognosis. Moreover a study by Zheng *et al.* suggests that exhausted CD8<sup>+</sup> T cells within the tumor derive from other types of CD8<sup>+</sup> T cells inside the tumor, as they identified shared TCRs between different populations within the tumor. They supported other studies, which indicate that the clonal accumulation of CD8<sup>+</sup> T cells and Tregs was a result of local T cell proliferation and activation in the tumor microenvironment<sup>243-245</sup>.

### **3.5.4 Immunotherapeutic approaches to treat HCC**

HCC has a poor prognosis and liver transplantation is the best viable treatment option so far. Currently, more than 80 % of patients are diagnosed at an advanced stage of HCC, have liver dysfunction limiting treatment options or have recurrent disease. The median survival of this group of patients is only 1 year<sup>246</sup>. Even chemotherapy, which has been efficient for different types of cancers, is no therapeutic option for HCC, as it shows only very limited efficacies. The only treatment modality that has been proven efficiency in advanced stages of HCC is a combination of two multi-kinase inhibitors, sorafenib and regorafenib<sup>247-249</sup>. Therefore, novel treatment options are urgently needed. The development of immune-mediated therapies is a promising goal, as preclinical and clinical studies have shown potential benefits in patients with HCC. Tab. 3.1 gives an overview of the current strategies.

The design of vaccines against tumor-associated antigens displays a powerful tool to initiate a functional immune response and reduces the risk of recurrence. In the last years, several studies aimed to establish functional vaccines. A potential target is a member of the glypican family of heparin sulfate proteoglycans, GPC3, which is overexpressed in many HCC patients and correlates with a poor prognosis<sup>250</sup>. A phase I clinical study resulted in an increased infiltration of intratumoral CD8<sup>+</sup> T cells and in one out of 33 patients to a partial response<sup>251</sup>. These results were supported by a phase II clinical study with a GPC-3 vaccine, which resulted in an improved one-year recurrence rate<sup>252</sup>. Recent publications reported the design of an in situ cancer vaccine



(InCVAX) for the treatment of HCC<sup>253,254</sup>. InCVAX was designed to initiate a robust antitumor response, by a thermal treatment of tumors, such as with a laser, combined with the administration of *N*-dihydro-galacto-chitosan (NDGC). The migration of CD3<sup>+</sup>, CD4<sup>+</sup> and CD8<sup>+</sup> cells into the tumor upon administration of InCVAX has been described in a murine HCC model. Another potential target for vaccine design is  $\alpha$ -fetoprotein (AFP), which is expressed by up to 80 % of HCCs<sup>246</sup>. The activation of AFP-specific CD8<sup>+</sup> T cells and the reduction of tumors has been reported in mice following the application of a AFP/ heat shock protein 70 vaccine<sup>255</sup>. Although the first HCC vaccines were tested in clinical trials, further studies are required to optimize therapeutic efficiency.

**Tab. 3.1: Overview of the immunotherapeutic strategies used in HCC.** Details are described in the text. Adapted from Aravalli and Steer<sup>256</sup>

<b>Immunotherapeutic Strategy</b>	<b>Mode of Application</b>	<b>Mechanism of Action</b>
Vaccines	Antigenic peptides/proteins (GPC-3, AFD, NDGC) DC-based vaccines, APCs from tumor lysates, InCVAX	Targeting TAAs to overcome immune tolerance by expressing antigenic proteins/peptides or co-stimulatory molecules in DCs or tumor cells
Adoptive cell therapy	CIK infusion, CTL transfer, TCR T cells	Transfer of tumor-specific T cells from a healthy individual into the bloodstream of the patient to be treated after propagating them <i>ex vivo</i> to enhance immune responses
	CAR T cells, TCR T cells	Patient-derived T cells are modified to express artificial receptors, propagated <i>in vitro</i> and administered back into the patient
Immune checkpoint inhibitors	Antibody (pembrolizumab, Ipilimumab, Nivolumab, Tremelimumab, AMP-224, Lambrolizumab, CT-011 and others)	Targeting specific cellular receptors and their ligands (PD-1, PD-L1, CTLA-4, CD160, 2B4, LAG3, Tim-3, GP-2), and to enhance antigen presentation

The number of studies that described ACT for HCC are limited so far. Gao *et al.* designed CAR T cells against GPC-3, which successfully eliminated GPC-3 expressing cells *in vitro* and in a mouse model<sup>257</sup>. Beside the beneficial effect induced by CAR T cells, clinical studies indicated that CAR T cells can also target healthy tissue associated with severe complications<sup>188</sup>.

Another potential adoptive immunotherapy, which has already shown clinical benefits, is the transfer of cytokine-induced killer cells (CIK) namely activated T cells and NK cells<sup>258-260</sup>. In the case of HCC, an adjuvant immunotherapy with CIK performed by Hui *et al.* had no impact on the overall survival of the patients. Even though, the treatment may prevent recurrence and the development of metastasis<sup>261</sup>. Other studies showed decreased recurrence and improved recurrence-free survival upon lymphocyte infusion, as well as an improved over-all survival in HCC patients<sup>262,263</sup>. These results are supported by other studies and indicate the potential of CIK therapy especially for HCC patients with early stage HCC<sup>264-266</sup>.

A clinical study with an CTLA-4 blocking antibody (tremelimumab) in HCV-derived HCC patients induced a partial response in 17.5 % of the patients<sup>267</sup>. Tremelimumab treatments resulted in an improved TAA-specific CD8<sup>+</sup> T cell response and a reduced recurrence of HCC patients. Another randomized clinical trial used nivolumab in patients with chronic HCV. After a single dose treatment the viral load was reduced in one-third of the patients with no significant side effects<sup>268</sup>. Also other inhibitory receptors are targets for immunotherapy. The blockade of LAG3, as well as Tim-3, in chronic HCV patients and patients with HBV-derived HCC resulted in an improved T cell function<sup>269-271</sup>. Taken together, blockade of immune checkpoint inhibitors led to promising results for HCC patients and could support the beneficial effect of other treatment options.

## 4 Aims

T cell activation is a crucial checkpoint of adaptive immune responses to infections or cancers. Chronic T cell activation and/or changes in the environment of T cell activation can lead to T cell dysfunction and to an impaired clearance of the pathogen. While the molecular changes occurring following activation are well studied, little is known about the mechanisms leading to naïve T cell preparedness and the metabolic changes associated with T cell activation.

By using proteomics, metabolomics and functional assays, I aimed to

- Investigate the underlying mechanisms associated with naïve CD4<sup>+</sup> T cell preparedness
- Analyze the translational dynamics in naïve and activated CD4<sup>+</sup> T cells
- Dissect the metabolic changes associated with naïve CD4<sup>+</sup> T cell activation
- Investigate the dysfunctional state of tumor-infiltrating lymphocytes (TIL) in patients with hepatocellular carcinoma

Based on the knowledge gained from these initial studies, I aimed to develop approaches that have the potential to improve existing immunotherapies. In particular, the strategies were

- To improve the fitness and anti-tumor activity of adoptively transferred T cells by metabolic interventions
- To establish a high-throughput workflow (**Microfluidics-based grafting of T cell receptors**) that allows the characterization of the TCR repertoire of TILs regardless of their exhaustion state

The results of this study may contribute to an improved understanding of the translational and metabolic changes associated with T cell preparedness, activation and differentiation. Moreover, this study may lead to the identification of potential immunotherapeutic approaches to effectively treat cancer patients.

## 5 Individual contributions to the studies

The two publications “Translation profiling reveals regulations underlying T cell naiveté and preparedness” (in preparation) and “L-Arginine modulates T cell metabolism and enhances survival and anti-tumor activity”<sup>272</sup>, form the basis for the two initial results chapters. Within the first part, I performed western blot analysis and cell stimulations with CHX. Moreover, I performed pulsed SILAC experiments, prepared cells for MS analysis and performed data analysis. For the second part, I performed and analyzed withdrawal and proliferation assays, generated CRISPR/Cas9 knockout T cell clones and performed the follow up analysis. Furthermore, I processed the hepatocellular carcinoma samples and analyzed the cell suspensions by FACS, performed single cell cloning experiments and prepared cells for TCR sequencing. Together with Roger Geiger, I designed the cloning strategy for the microfluidic-based grafting of TCRs. Moreover, I generated the reporter Jurkat cell line, cloned the flu-specific TCR and performed stimulation experiments. Yun Ding and I performed microfluidic experiments.

Camilla Basso performed the animal experiments and Roger Geiger did the analysis of proteomics data and enrichment analysis. Marco Benevento, Jan Rieckmann, Felix Meissner and Roger Geiger performed the proteomic experiments and analyzed data. Yuehan Feng and Paula Picotti designed and performed limited proteolysis experiments. Tobias Fuhrer, Maria Kogadeeva and Nicola Zamboni designed and performed metabolome and flux experiments and analyzed data. Christopher Bleck and Dirk Bumann performed electron microscopy experiments. Robert Kimmerling and Scott Manalis performed measurements of single cell densities. Tim Beltraminelli analyzed electron microscopy data.

Giorgio Ercolani, Elisabetta Loggi and Pietro Andreone provided samples from HCC patients. Yun Ding and Andrew deMello designed the microfluidic device. Adaptive Biotechnologies performed TCR sequencing.

## 6 Results and discussion

### 6.1 Translation profiling reveals regulations underlying T cell naiveté and preparedness

#### 6.1.1 Results

Naïve T cells migrate quiescently through the body searching for their cognate antigen. The human body approximately contains  $2 \times 10^{11}$  naïve T cells<sup>273</sup>. These cells keep their size, metabolic activity and energy expenditure minimal for several years. However, upon encountering their cognate antigen naïve T cells are rapidly activated and aid in the clearance of pathogens. Therefore, the balance between minimal energy consumption and maximal preparedness for a rapid execution of the activation program is essential for naïve T cells. This chapter focuses on translational mechanisms that control naïve T cells quiescent and allow a rapid response towards antigenic stimulation.

Initially the aim was to analyze morphological differences between naïve and activated T cells. To do so, we compared human naïve CD4<sup>+</sup> T cells with 72 h activated CD4<sup>+</sup> T cells by serial block-free scanning electron microscopy and subsequent 3D reconstitution of images. The images show that naïve T cells contain a thin layer of cytoplasm (Fig. 6.1A-C). The volume of the cytoplasm was similar to the nucleoplasm (Fig. 6.1D). Moreover, mitochondria clustered on one side of the cell. Upon activation with antibodies to CD3 and CD28, the cells showed a 8-fold increase of the cytoplasm, which was significantly larger than the nucleoplasm of cells at the same time point (Fig. 6.1E). A similar 7.9-fold increase was observed for mitochondria. The mitochondria were still clustering on one side of the cell. The overall volume of T cells only increased 5.8-fold. Resting, naïve T cells had a volume of  $175 \text{ fl} \pm 34 \text{ fl}$ , whereas 72 h activated T cells had a volume of  $1'026 \text{ fl} \pm 294 \text{ fl}$ . These data were confirmed by using a microfluidic device that measures cell volumina<sup>274</sup> (Fig. 6.1F). In comparison, the protein concentration only increased 3-fold. Therefore, the protein density decreased from 125 mg/ml to 75 mg/ml following activation. The measurement of single cell density with a microfluidic mass sensor confirmed the calculations (Fig. 6.1G). In summary, naïve T cell are characterized by

a thin layer of cytoplasm and a high protein density. Once activated, they grow in size and become more fluid.

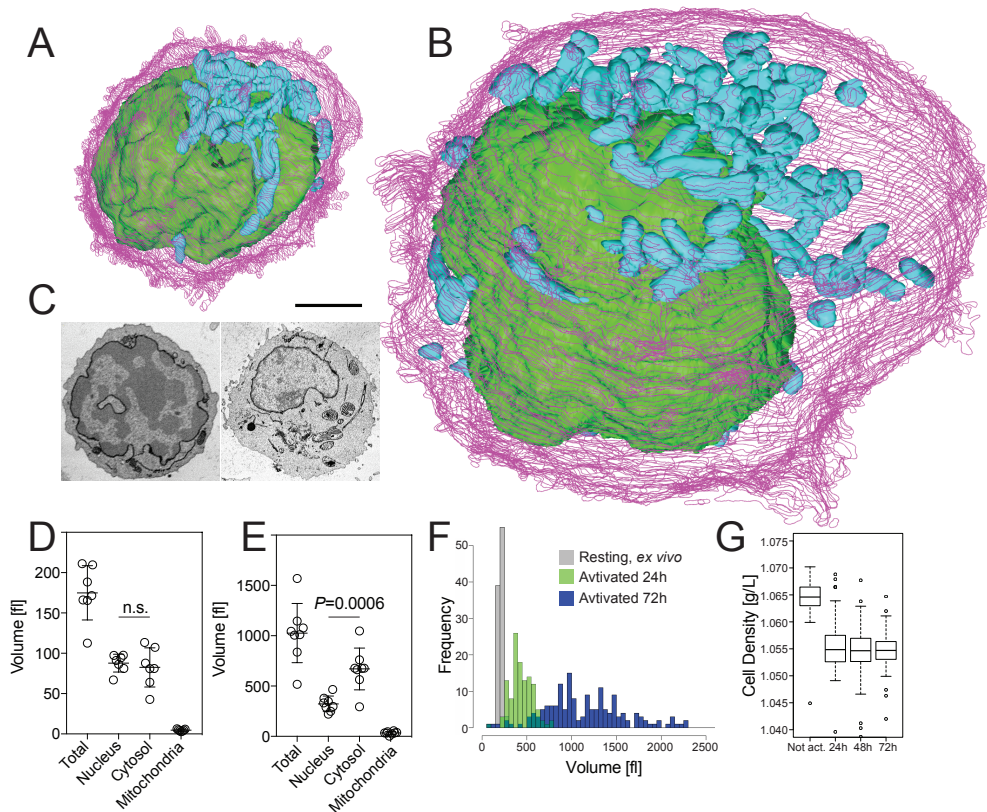


**Fig. 6.1: T cells enlarge their volume, but decrease their density upon activation.** A,B) 3D reconstitution of naïve (A) and 72 h activated CD4<sup>+</sup> T cells (B) based on electron micrographs. Both cells are drawn at the same scale (C) Examples for electron microscopy images of a naïve (left) and 72 h activated T cell (right). The 3D reconstitution was generated with 3Dmod. D) Naïve CD4<sup>+</sup> T cells analyzed by electron microscopy. The volume of the total cell or different cellular structures was analyzed with 3Dmod based on the 3D reconstitution. n = 7, error bars represent S.E.M. E) Same like in D, but for 72 h activated T cells. n = 8, error bars represent S.E.M. F) Distribution of total cell volume for naïve CD4<sup>+</sup> T cells or cells activated for 24 or 72 h determined by a microfluidic mass sensor. G) The cell density of naïve CD4<sup>+</sup> T cells was determined at different time points after activation. The cell density was calculated with a microfluidic based mass sensor.

Following activation naïve T cells not only change their morphology, but also their proteome. The relative expression of 2`824 out of 7`816 proteins changes significantly 72 h after activation (Fig. 6.13B). Subsequently the translational activity of naïve and activated T cells was investigated via a pulsed stable isotope labeling by amino acids in cell culture (SILAC) approach (Fig. 6.2). Naïve CD4<sup>+</sup> T cells were isolated from three healthy human donors and cultured with or without CD3/CD28 stimulation in medium containing heavy arginine (Arg10) and lysine (Lys8). This approach enables the discrimination of pre-existing proteins from newly synthesized proteins, as the incorporation of heavy amino acids will lead to a mass shift. Samples were collected at different time points (0, 6, 12, 24 and 48 h) and analyzed by liquid

chromatography-coupled high-resolution mass spectrometry (LC-MS/MS). 6'535 proteins were quantified and copy numbers of newly synthesized and total proteins were estimated.

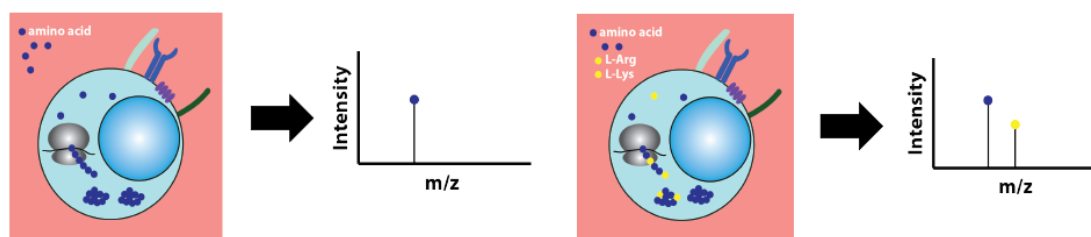


**Fig. 6.2: Schematic view of the pulsed SILAC principle.** T cells take up amino acids (blue dots) from the culture medium and incorporate them into their proteins (left). Under pulsed SILAC conditions, T cells are cultured in medium containing heavy isotope labeled amino acids (yellow dots). The incorporation of these amino acids leads to a mass shift, which can be detected via mass spectrometry (right).

In the naïve state T cells are thought to be quiescent and non-dividing leading to the hypothesis that the total proteome mass remains constant over time. This would mean that the rate of newly synthesized proteins reflects the degradation of their counterparts and represents a parameter for protein renewal. Our data indicated that the majority of proteins in naïve T cells were stable and only 1'578 proteins out of 6'535 were renewed within 48 h. The renewal rate greatly differed between protein species, e.g. the turnover rate of the ribosomal protein RPL12 was minimal while CD5 was more rapidly turned over and the transcription factor ETS-1 was even 90% renewed within only 6 hours (Fig. 6.3A). Within the group of renewed proteins, 67 proteins had a renewal rate higher than 80 % in this time. Interestingly, 10.6 % of these proteins were transcription factors associated with the maintenance of quiescence, CD4 lineage commitment, self-renewal and the expression of key surface receptors such as the TCR, IL-7 receptor, CCR7 and L-selectin (CD62L) (Fig. 6.3B).

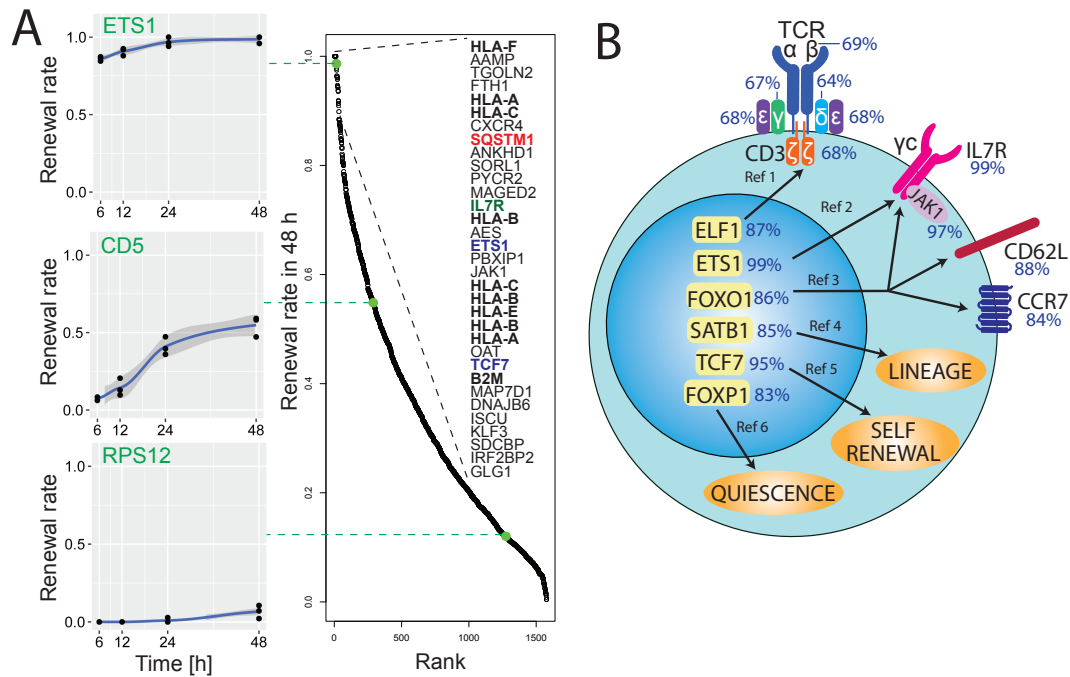


**Fig. 6.3: Naïve T cells have a stable proteome, but rapidly renew a small set of proteins.** A) Protein renewal in naïve CD4<sup>+</sup> T cells. Left: Fraction of selected proteins with incorporated <sup>13</sup>C-labeled amino acids. Right: Ranking of 1577 proteins according to their renewal rate at 48 h after labeling. Gene names of proteins with a renewal rate > 90% are listed. n = 3 from three donors. B) Illustration of transcription factors and some of their targets. The percentage next to the single proteins displays the renewal rate within 48 h. Ref 1 = Rellahan *et al.*<sup>275</sup>; Ref 2 = Grenningloh *et al.*<sup>276</sup>; Ref 3 = Kerdiles *et al.*<sup>277</sup>; Ref 4 = Kakugawa *et al.*<sup>278</sup>; Ref 5 = Lin *et al.*<sup>279</sup>; Ref 6 = Wei *et al.*<sup>280</sup>

To confirm that these transcription factors were indeed short-lived and needed to be constantly replenished, we inhibited protein synthesis in naïve T cells with cycloheximide (CHX) and found that within 24 h the relative abundance of the transcription factors decreased to less than 20% of the original amount (Fig. 6.4A). Furthermore, the treatment with CHX blocked translation completely, as no labeled transcription factors were detected when the cells were cultured under pulsed SILAC conditions. Following washout of CHX, the broad majority of transcription factors were labeled (Fig. 6.4B). Conclusively, the analysis of protein translation by a pulsed SILAC approach revealed that seven transcription factors are highly renewed in naïve T cells.



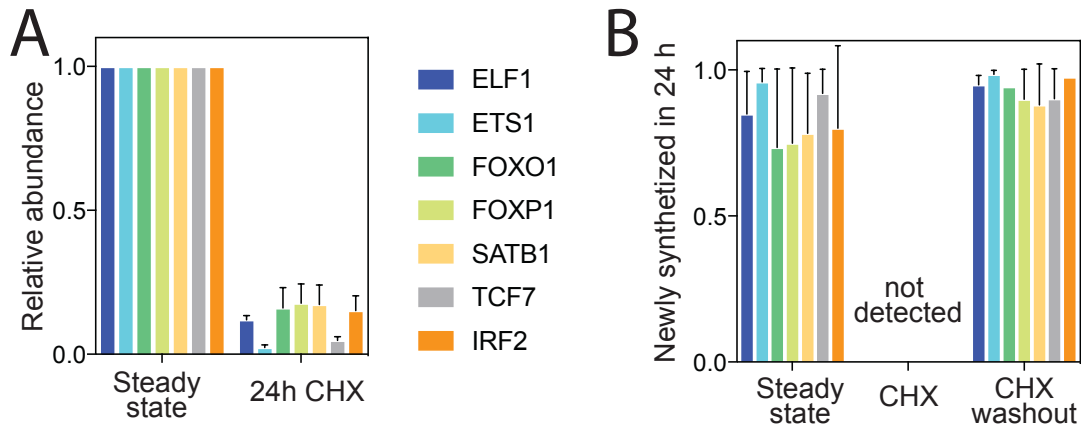


**Fig. 6.4: Translation controls abundance of rapidly renewed transcription factors.** A) Naïve CD4<sup>+</sup> T cells were incubated with isotope-labeled amino acids in the presence or absence of 50 µg/ml cycloheximide (CHX). Shown is the relative abundance as determined by mass spectrometry. n = 2 from two different donors. Bars indicate the S.E.M. B) Same as in A), but frequency of newly synthesized proteins is shown.

Continuous replenishment of unstable proteins requires large amounts of energy. However, it also displays a mechanism to rapidly tune down proteins. Indeed, the proteome analysis of naïve and activated T cells revealed that the T cell activation leads to the reduction of FOXO1 levels, which was a rapidly replenished transcription factor in naïve T cells. Interestingly, also proteins (IL-7R, CD62L and CCR7) that are controlled by FOXO1 showed a decreased expression following T cell activation (Fig. 6.5).

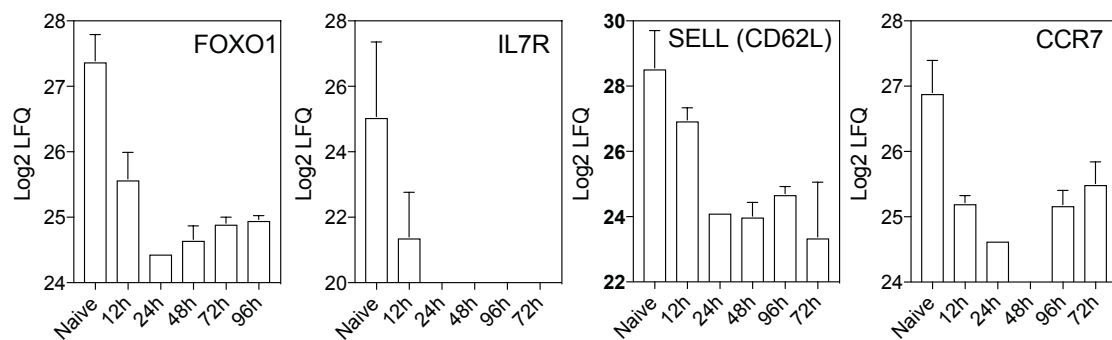


**Fig. 6.5: Rapidly renewed proteins decline upon T cell activation.** The proteome of naïve, resting T cells was analyzed by LC-MS/MS. Moreover, naïve CD4<sup>+</sup> T cells were activated with antibodies to CD3 and CD28 and the proteome was analyzed at different time points upon activation. The abundance (label free quantification, LFQ) for selected proteins is shown. Error bars represent S.E.M.

Sequestosome-1 (SQSTM1, also known as p62) is one of the proteins with the fastest renewal rate. It binds to polyubiquitinated proteins and links them to LC3 for degradation in autophagosomes<sup>281</sup>. The inhibition of translation reduced levels of SQSTM1, which indicates that the protein is rapidly degraded. Interestingly blockade of autophagic cargo degradation with bafilomycin A1 increased SQSTM1 levels four-

fold, suggesting that SQSTM1 was degraded through autophagy (Fig. 6.6A). In comparison, the treatments did not affect levels of the cytosolic enzyme GAPDH. At a global level, about half of the proteins that significantly accumulated in the presence of bafilomycin A1 were plasma membrane proteins that were likely endocytosed and degraded in endosomes/lysosomes while the other half were mitochondrial, ER, nuclear and cytosolic proteins that were most likely degraded by autophagy (Fig. 6.6B). Moreover, western blot analysis revealed changes in LC3 lipidation between naïve and activated T cells. While 60 % of LC3 was lipidated in naïve T cells, only 25 % of LC3 is lipidated in activated T cells. Interestingly, withdrawal of the IL-2 increased the lipidation of LC3 (Fig. 6.6C). These results were in line with a recent study by Xu *et al.* They showed that autophagy is decreased during the period of proliferation upon T cell activation and is then up-regulated when cells stop dividing just before the contraction phase<sup>282</sup>.

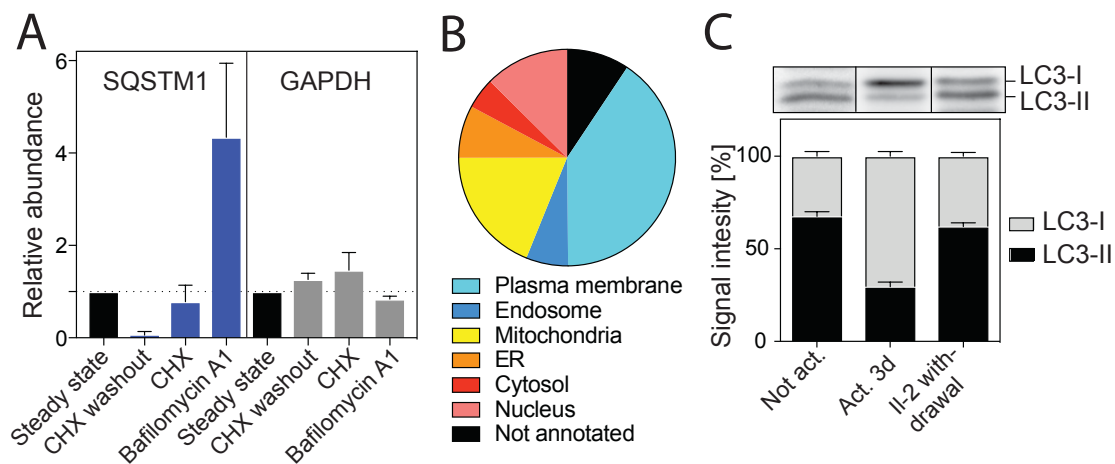


**Fig. 6.6: Autophagy is active in naïve T cells.** A) Naïve T cells were analyzed by mass spectrometry after a 24 h treatment with 100 nM bafilomycin A1, or 24 h with 50 µg/ml cycloheximide (CHX), or 24 h with CHX and then a further 24 h without CHX. Relative expression of SQSTM1 is shown in blue and of GAPDH in grey.  $n = 2$  from two different donors. Bars indicate the S.E.M. B) Subcellular distribution of proteins whose abundance increased >2 fold following bafilomycin A1 treatment. Pie chart shows the percentage of proteins according to subcellular localization based on GO annotation. C) Top: Western blot analysis of LC3 lipidation. Bottom: Quantification from 2 blots of 1 donor. Bars indicate the S.E.M.

A rapid turnover rate ( $t_{1/2} = 90$  min) could also be detected for three subunits of MHC-I (B2M, HLA-A and HLA-B). Our findings were confirmed when we blocked the translation in naïve T cells for 24 h with 50 µg/ml CHX. The expression of MHC-I on the surface was strongly reduced under these conditions and the washout of the inhibitor led to a restored surface expression of MHC-I within 6 h (Fig. 6.7A

and B). In conclusion, the majority of proteins in naïve T cells are stably expressed and the small renewed protein fraction is associated with important functions.

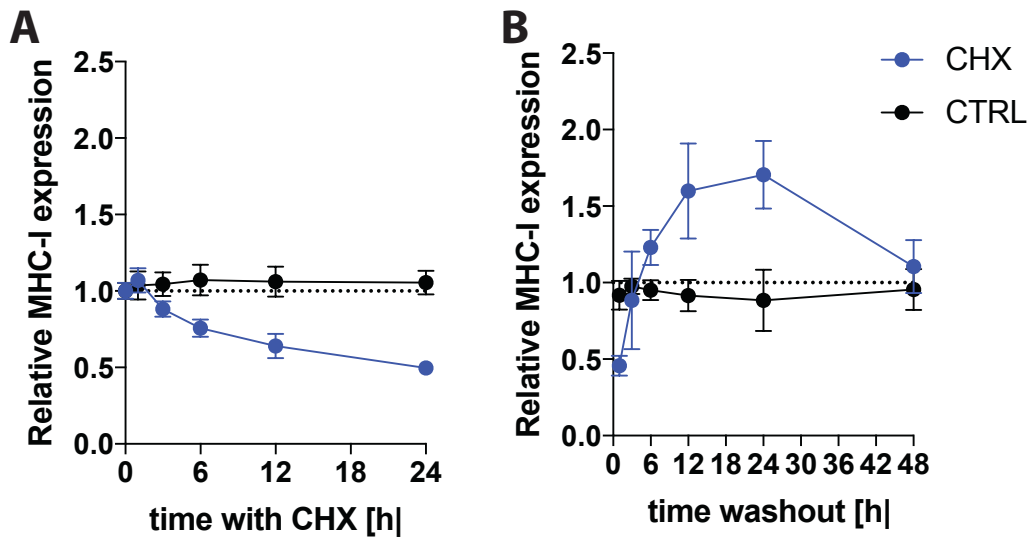


**Fig. 6.7: Blockade of translation results in reduced MHC-I levels on the surface of naïve T cells.** A) Primary CD4<sup>+</sup> naïve T cells were cultured with or without 50 µg/ml cycloheximide (CHX). DMSO was used as control. B) The cells were washed extensively with PBS after 48 h and cultured in control medium. The expression of MHC-I was determined by FACS-staining with an antibody binding to HLA-A/B/C at different time points. n = 12 replicates from four donors. Shown is mean +/- SD.

Based on the pulsed SILAC data, T cells synthesized about 20'000 proteins per minute in the quiescent state, but upon activation the translational activity increased 50-fold to 10<sup>6</sup> proteins per minute within 24 h (Fig. 6.8A), while the average number of ribosomal proteins only increased 5-fold over the same period. The expression of initiation and elongation factors increased 9-fold and 7-fold, respectively. Strikingly, 10 % of the proteome of naïve T cells were ribosomal proteins. Based on the absolute copy number estimation, it was assumed that naïve T cells have the material to assemble approximately 400'000 ribosomes. This estimation was used to calculate a translational rate per ribosome in naïve T cells, which was 0.3 amino acids per second and ribosome. T cell activation increased the translation rate 8-fold within 6 h of activation and plateaued at a rate of 2.6 amino acids per second and ribosome (Fig. 6.8B). These data suggest that naïve T cells contain a large number of ribosomes that are barely used in the quiescent state, but are immediately engaged to initiate the activation program when the T cell is activated.

We further investigated the influence of mRNA levels on protein translation and purified mRNA from naïve and activated T cells. On average naïve T cells contained 15.5 fg mRNA, but when activated for 24 h transcript levels were increased 6-fold.

This increase was similar to the level of ribosomal proteins (Fig. 6.8A). Next, we performed RNA-sequencing from mRNA of naïve and activated T cells (6 and 24 h). The copy number of each transcript was estimated by the assumption that the sum of all FPKM (frequency per kilobase of exon per million reads mapped) values is equivalent to the quantity of total purified mRNA. The proportion of every transcript represents the copy number. By using digital droplet PCR (ddPCR), we counted four selected transcripts. The ddPCR results were in line with the copy number estimation. Naïve T cells have 8'900 transcripts and every transcript was on average read off 14 times per minute. This was in strong contrast with the proteome of these cells, where we detected  $4 \times 10^8$  proteins. The mRNA of the ribosomal protein RPL27 (438 copies) was the most abundant transcript in naïve T cells.

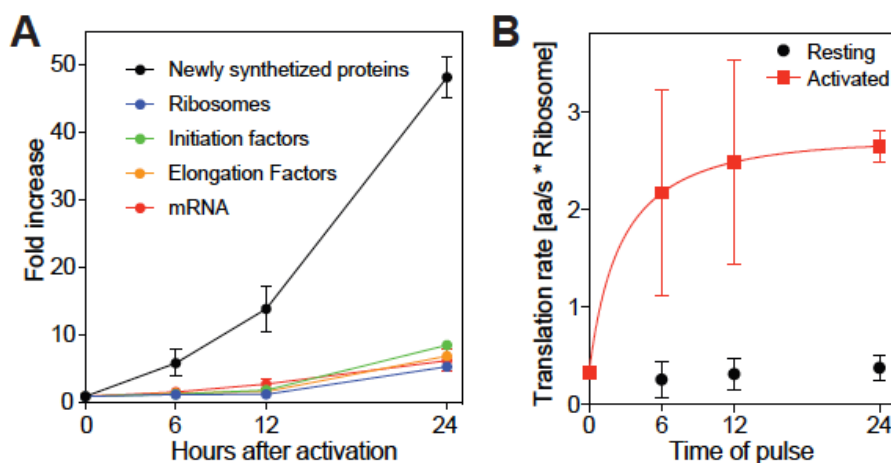


**Fig. 6.8: Translation rates increased dramatically in activated T cells.** A) Relative increase, as compared to naïve T cells, in the abundance of total newly synthesized proteins (black), ribosomes (blue), initiation factors (green), elongation factors (yellow) as detected by MS/MS, as well as mRNA (red). For proteins  $n = 3$  from three different donors. For mRNA  $n = 7$  from four different donors. B) Translation rate after pulse with heavy amino acids for naïve and activated T cells. T cells were pulsed with heavy amino acids at the time of activation.  $n = 3$  from three different donors. Bars represent the S.E.M.

Initially mRNA levels correlated minimally with protein synthesis rates ( $r = 0.2$ , Pearson correlation, only factors with mRNA and protein  $\geq 1$  were considered), but 6 h after activation, this correlation increased to  $r = 0.74$ . As the correlation was even stronger 24 h after activation ( $r = 0.77$ ), it suggests that transcript levels predominately controlled translation in activated T cells (Fig. 6.9). Among the most abundant transcripts, B2M (65 copies) showed the highest read off with 2'840 times per hour. Other high abundant transcripts, like EEF1A1 (137 copies), EIF1 (31 copies), PABPC1 (17 copies) and RPL15 (16 copies) were translated less than 60 times per hour. Whereas the read off of B2M was the same in naïve and 6 h activated

T cells (2'880 times/hour), the read off of the above mentioned transcripts increased more than 20-fold in the same time. Therefore, we hypothesize that the translation in naïve T cells is not generally suppressed, but as efficient as in activated T cells and the low translational output is likely attributable to idle or not fully assembled ribosomes.

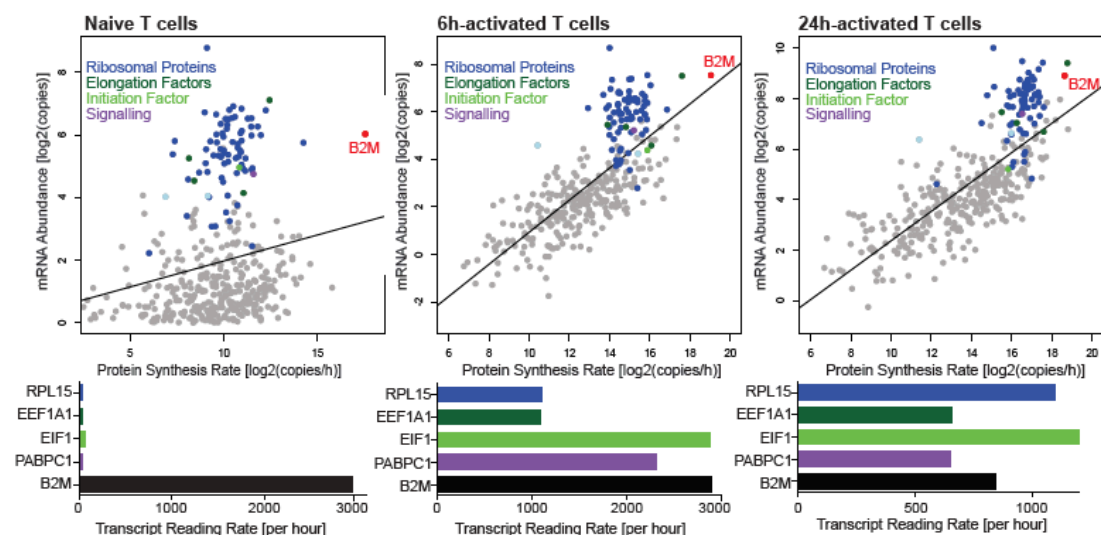


**Fig. 6.9: mRNA abundance correlates with protein synthesis only upon T cell activation.** The mRNA abundance in naïve CD4<sup>+</sup> T cells was directly analyzed (left) or after activation with antibodies to CD3 and CD28 for 6 (center) and 24 h (right). Dots representing signaling proteins, ribosomal proteins, transcription initiation and elongation factors are color-coded. The protein synthesis rate was determined by pulsed SILAC. The transcript-reading rate for selected proteins is shown below the dot plots.

We next addressed, why several highly abundant mRNAs are poorly translated in naïve T cells. When we analyzed these transcripts, we discovered that they encoded ribosomal proteins (Fig. 6.9, blue dots), transcription initiation and elongation factors (green dots), as well as signaling proteins (purple dots). Strikingly, all of them contained a 5'-terminal oligopyrimidin (TOP) motif. A study by Thoreen *et al.* indicated that the translation of TOP-mRNAs in mouse embryonic fibroblasts is strongly controlled by mTORC1<sup>283</sup>. They proposed that the phosphorylation of 4E-BP by mTORC1 leads to the release of eIF4E, which together with eIF4G1 initiates the translation of TOP-mRNAs. We next investigated if the mTOR pathway was also involved in the translation of TOP-mRNAs in activated T cells. Thus, the mTOR activity was measured by analyzing phosphorylation of the mTOR targets S6K1 and 4E-BP. Following activation, both targets were phosphorylated, which was prevented by the addition of the mTOR inhibitor rapamycin (Fig. 6.10). This suggests that mTOR could play a role in the regulation of the translation rate of TOP-mRNAs.

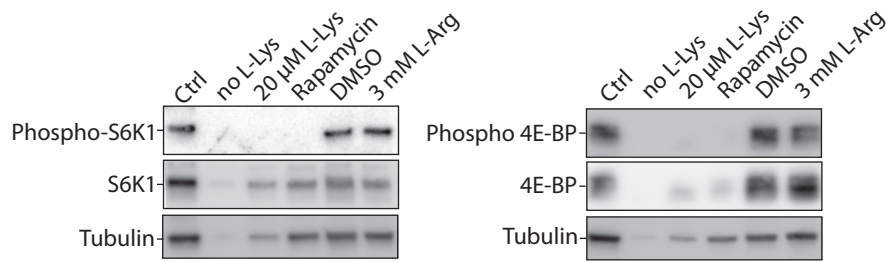


**Fig. 6.10: T cell activation leads to mTOR mediated phosphorylation of S6K1 and 4E-BP.** Naïve CD4<sup>+</sup> T cells were activated with antibodies to CD3 and CD28 and the indicated treatment. The cells were lysed 72 h after activation and the phosphorylation state of S6K1 (left) and 4E-BP (right) was analyzed via western blot. Experiment was done with cells from four healthy donors. Representative blots are shown.

To test the validity of the hypothesis naïve CD4<sup>+</sup> T cells were activated with or without the mTORC1 inhibitor torin-1 under pulsed SILAC conditions. The administration of torin-1 did not affect protein synthesis rates, upon analysis of the entire proteome of naïve or activated T cells (6 and 24 h). When we focused on proteins that derived from TOP-mRNAs in naïve T cells, we detected no difference between torin-1 stimulated and control cells. However, torin-1 stimulation dramatically inhibited the protein synthesis of TOP-mRNAs under activating conditions (Fig. 6.11). This indicates that mTOR plays an essential role in the translation of TOP-mRNAs, which could represent a mechanism of preparedness of naïve T cells.

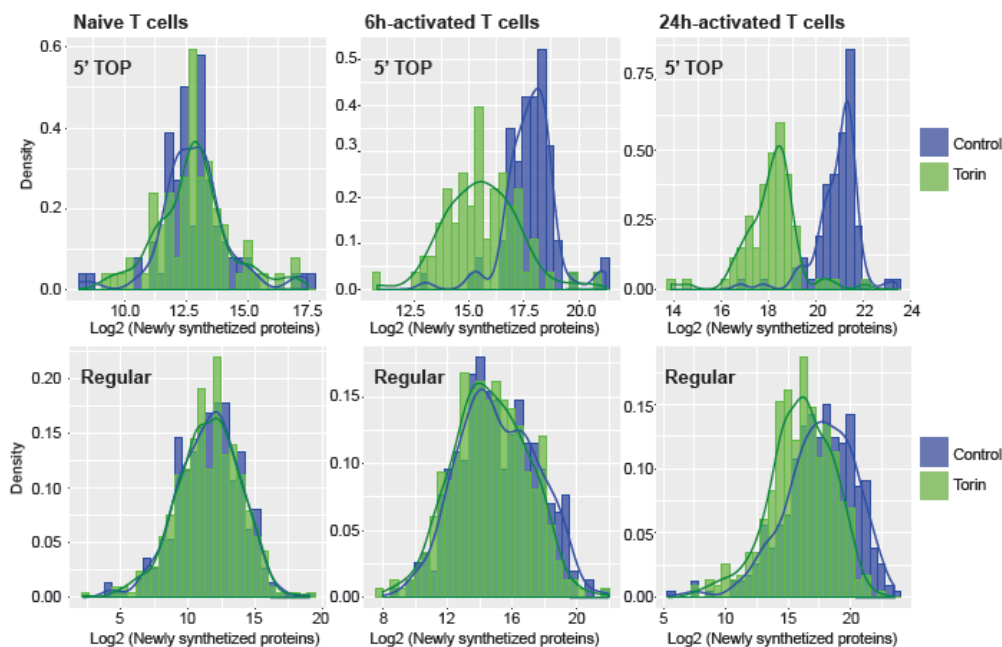


**Fig. 6.11: mTORC1 controls the expression of TOP-mRNAs upon T cell activation.** Histograms showing the distribution of the average protein synthesis rates of all detected protein groups from control T cells or T cells treated with 250 nM Torin 1. Proteins encoded by TOP-mRNAs are shown in the upper panel, proteins encoded by conventional mRNAs in the lower panel. n = 3 from three different donors.

Another important target of mTOR is the glycolytic pathway. It has been shown that mTORC1 promotes the uptake of glucose and the glycolytic flux<sup>284,285</sup>. Therefore, the abundance of glycolytic enzymes was analyzed upon T cell activation. Even though, naïve T cells are assumed to be metabolically quiescent and perform poorly glycolysis, the majority of glycolytic enzymes was highly abundant in naïve T cells ( $\text{Log}_2\text{LFQ} > 30$ ). The only enzymes present at lower frequencies were the glucose transporter SLC2A1 ( $\text{Log}_2\text{LFQ} = 24.2$ ) and SLC2A3 ( $\text{Log}_2\text{LFQ} = 25.5$ ), as well as hexokinase 2 (HK2) ( $\text{Log}_2\text{LFQ} = 25.6$ ) (Fig. 6.12A). Strikingly, the levels of the glucose transporter and HK2 increased significantly upon T cell activation, whereas the other glycolytic enzymes showed no significant changes (Fig. 6.12A and B). The rapid expression of HK2, SLC2A1 and SLC2A3 was rather controlled by translational mechanisms than transcriptional mechanisms, as transcript levels of all glycolytic enzymes increased upon activation, but only the three enzymes associated with the ignition of glycolysis showed significant changes in the proteome (Fig. 6.12C). In contrast, enzymes associated with gluconeogenesis (FBP1 and FBP2) were less abundant in activated T cells, which may be due to degradation of the mRNA, as the FBP1 transcript levels decreased upon activation (Fig. 6.12). In conclusion, all enzymes associated with glycolysis are highly abundant, but the glucose transporter (SLC2A1 and SLC2A3) and HK2. However, these enzymes are rapidly expressed upon T cell activation indicating another mechanisms of naïve T cell preparedness.

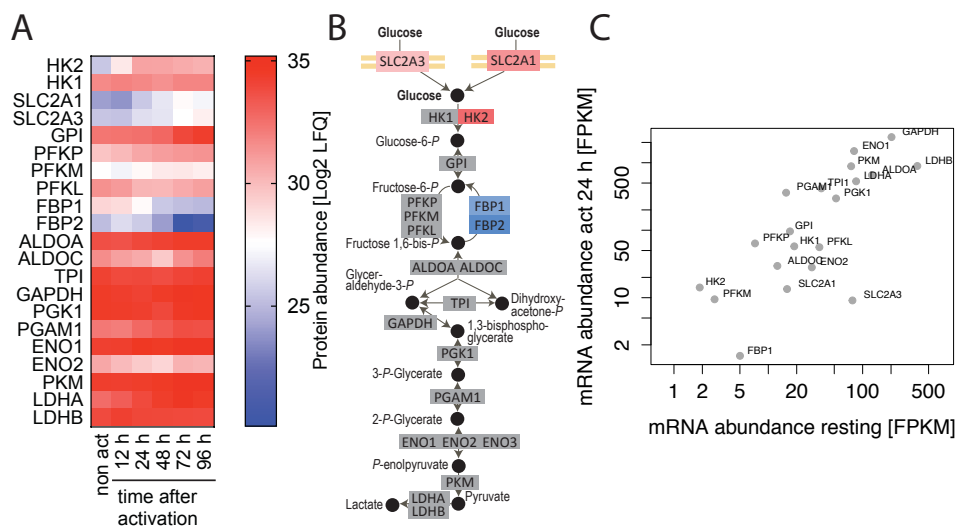


**Fig. 6.12: Naïve T cells contain large numbers of glycolytic enzymes.** A) Heatmap representing the abundance of glycolytic enzymes in naïve T cells (non-act) or at different time points following activation with antibodies to CD3 and CD28. B) Illustration of changes in the abundance of glycolytic enzyme 72 h after activation in comparison to naïve T cells. Significant changes are color-coded. Red = up-regulated in activated T cells. Blue = down-regulated. Grey = no significant changes. C) Abundance of mRNAs of glycolytic enzymes in naïve and 24 h activated T cells.

### 6.1.2 Discussion

In summary, naïve T cells circulate in a quiescent state through the body, but need to promptly engage a complex activation program in response to antigenic stimulation. We identified different mechanisms of naïve T cell preparedness. First, while the predominant part of the proteome of naïve T cells was stable, few proteins are rapidly renewed. These included transcription factors, which play important roles for the maintenance of quiescence and survival of naïve T cells. The high turnover of these transcription factors may allow the rapid replenishment upon activation. Second, we found that naïve T cells have a low translational activity even though they contain a large number of idle ribosomes and non-translated mRNAs, which had a TOP-motif. The translation of TOP-mRNAs upon activation is controlled by mTORC1. A better understanding of mechanisms that keep naïve T cells in a quiescent state, but at the same time allow them to respond rapidly towards antigenic stimulation, could lead to new therapeutic avenues to control the activation state of T cells.

Initially, we analyzed the morphology of naïve and activated T cells. We found that T cell activation is associated with a decrease in cell density. The high density within naïve T cells could display one mechanism of preparedness, as it has been shown that a reduced diffusion within the cytosol is associated with reduced cell growth<sup>286</sup>. In line, T cell activation is associated with an initial period of cell growths, which is followed by rapid proliferation<sup>287</sup>. Therefore, the decreased cell density upon activation could promote mechanisms that are associated with cell division.

When we analyzed the translational activity of naïve T cells, we found that 75 % of the proteome were not synthesized within 48 h. Among the proteins that were highly renewed in naïve T cells, we identified seven transcription factors that were associated with quiescence, self-renewal, lineage commitment and the identity of naïve T cells. For example, ETS-1 was shown to be a critical regulator of CD127, the binding unit of the IL-7R, which was also rapidly renewed in naïve T cells. Signaling mediated by IL-7 is an essential survival signal for T cells<sup>276</sup>. Another rapidly renewed transcription factor was FOXO1, which has been suggested to control the expression of the IL-7R, the adhesion molecule CD62L and the chemokine receptor CCR7, which is essential for the homing of naïve T cells to the lymph node<sup>277</sup>.



Moreover, FOXO1 promotes the expression of the transcription factor Kruppel-like factor 2 (KLF2), which mediates quiescence and survival in SP thymocytes<sup>288,289</sup>. Continuous replenishment of inherently unstable proteins could represent another mechanism of naïve T cell preparedness, as protein levels can be reduced rapidly when needed.

Another striking finding was that naïve T cells actively use autophagy for the degradation and recycling of cellular components. This was in contrast to findings from Li *et al.*, who could not detect autophagosomes in naïve T cells<sup>290</sup>. However, a more recent study from the group of Rafi Ahmed showed that autophagy is essential for the survival and memory formation of T cells<sup>282</sup>. Even though, autophagy has emerged as a crucial regulator of T cell homeostasis<sup>291</sup>, the role autophagy plays within naïve T cells remains elusive and needs further investigation.

Furthermore, we found that naïve T cells contain idle ribosomes and high abundant non-translated mRNAs, which are promptly translated upon activation and may represent another mechanism of naïve T cell preparedness. Further analysis of the non-translated mRNA revealed that all of them contained a TOP motif. Thoreen *et al.* showed that the translation of TOP-mRNAs is controlled by the mTOR pathway<sup>283</sup>. Interestingly, mTOR is inhibited in quiescent T cells and antigenic stimulation activates the mTOR pathway<sup>71</sup>. We found that the mTOR pathway controls the translation of TOP-mRNAs. Experiments in mouse embryonic fibroblasts suggested that 4E-BP, a downstream target of mTOR, inhibits the translation of TOP-mRNAs<sup>283</sup>. However, if this mechanism controls the translation of TOP-mRNAs also in naïve T cells is not clear.

Finally, we discovered that the broad majority of glycolytic enzymes are highly abundant in naïve T cells. This was surprising, as naïve T cells are described as metabolic quiescent cells that primarily rely on OXPHOS. Upon T cell activation the glucose transporter SLC2A1 and SLC2A3, as well as the initial enzyme of the glycolysis HK2 were significantly up-regulated. In contrast HK1 was highly abundant in naïve T cells and showed no significant changes upon T cell activation. The up-regulation of HK2 in human cancer patients has been considered a consequence of metabolic re-programming in cancer<sup>77,292,293</sup>. Furthermore, activated T cells only need

to up-regulate 3 out of 20 glycolytic enzymes. This may facilitates the switch from OXPHOS to aerobic glycolysis in activated T cells and could represent another mechanism of naïve T cell preparedness.

Taken together, we identified different mechanisms of preparedness, which allow naïve T cells to fulfill rapidly effector functions upon activation. The drop in cell density, the rapid renewal of factors required for survival and quiescence, as well as the TOP-mediated control of mRNA translation and high abundance of glycolytic enzymes represent promising targets for patients with abnormal T cell proliferation. The overexpression of mediators of T cell quiescence in patients with uncontrolled T cell proliferation, such as T cell leukemia/lymphoma, could induce quiescence in the malignant T cells.

## 6.2 L-Arginine modulates T cell metabolism and enhances survival and anti-tumor activity

### 6.2.1 Results

In addition to adapting their translational activity, activated T cells have also to arrange their metabolism to produce the required biomass and energy. Naïve T cells have low metabolic demands and use predominantly oxidative phosphorylation (OXPHOS) to generate ATP. Activated T cells no longer need nutrients for survival and homeostasis alone, but also to generate building blocks for clonal expansion and effector functions. Therefore, activated T cells adopt an anabolic metabolism and primarily rely on glycolysis<sup>215</sup>. This chapter focuses on the metabolic adaptations that are associated with T cell activation.

Initially, the metabolic adaptations underlying T cell activation were investigated by cellular proteome and metabolome analysis of naïve T cells immediately after sorting or at different time points after activation with antibodies to CD3 and CD28 (Fig. 6.13A). A total of 9'718 proteins were identified. We quantified the abundance of 7'816 at each time point and estimated their absolute copy number. Our non-targeted metabolome analysis led to the identification of 429 distinct species, which were putatively mapped to human metabolites.

We next performed a comparative analysis of 72 h activated and non-activated naïve T cells for both, the proteome and metabolome. The relative expression of 2'824 proteins changed significantly in this time period (Welch-test, false discovery rate [FDR] = 0.05,  $S_0 = 1$ ), supporting the fundamental changes in translational activity shown in the first chapter (Fig. 6.13B). Among the upregulated proteins, several were associated with metabolic pathways, like nucleotide synthesis, folate-mediated one-carbon metabolism, as well as arginine and proline metabolism. While one-third of the proteome showed significant changes following activation, only 15 % of metabolites changed significantly. 49 metabolites were more and only 14 were less abundant (Fig. 6.13C). Three (arginine, ornithine and N-acetyloronithine) out of these 14 metabolites belonged to the same metabolic pathway. Taken together, our metabolome and proteome data displays the dynamic changes associated with T cell activation.

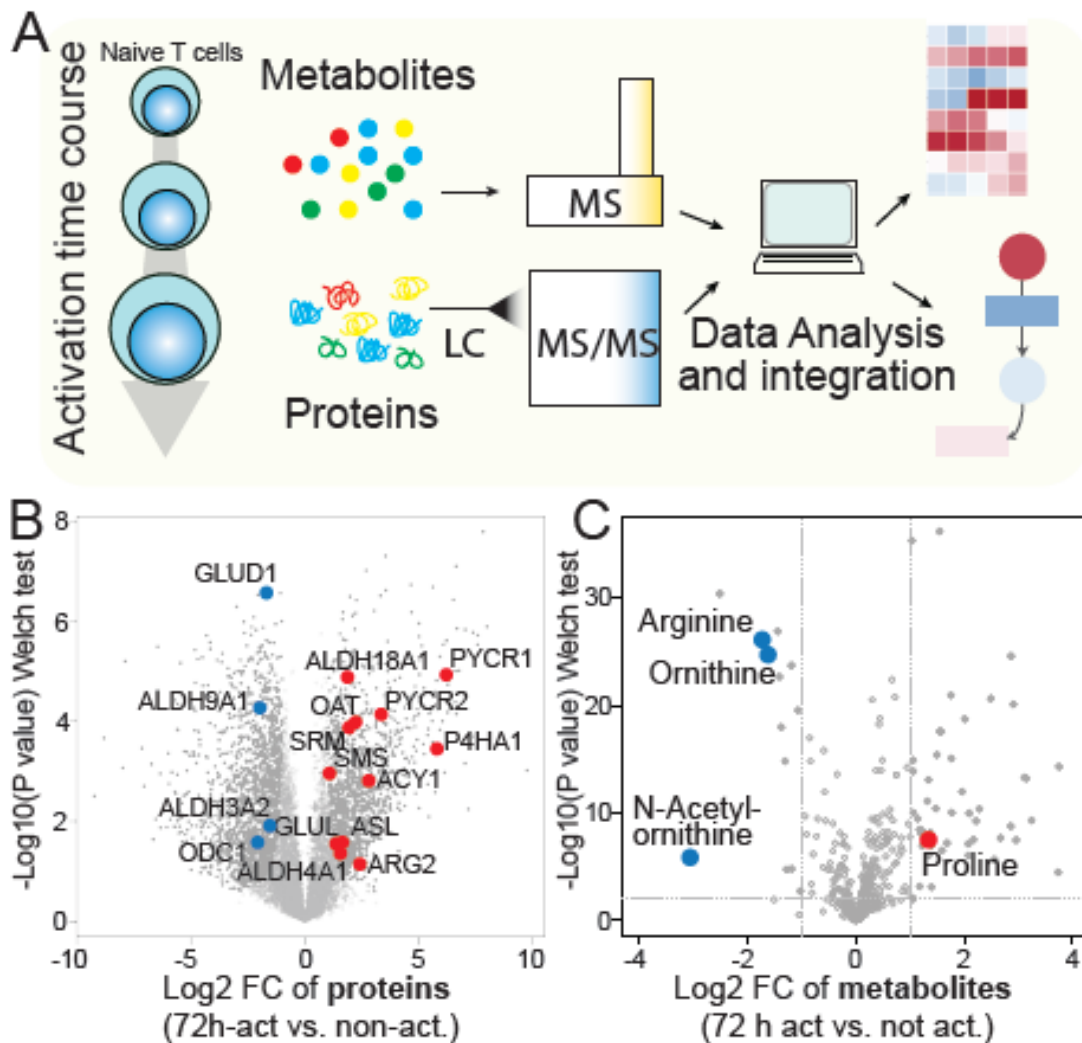


**Fig. 6.13: Metabolic and proteomic profiling reveals distinct changes in L-arginine metabolism in activated human T cells.** A) Overview of the experimental layout. B) The protein abundance of 72 h activated (CD3 and CD28 antibodies) human CD4<sup>+</sup> T cells were compared to non-activated cells. Closed circles indicate proteins that changed significantly (FDR = 0.05,  $S_0 = 1$ ). Colored dots are enzymes of the arginine and proline metabolism that changed significantly. C) Same analysis like B), but for metabolites. Closed circles indicate metabolites that changed significantly ( $|\text{Log}_2 \text{FC}| > 1$ ,  $p < 0.01$ ). Colored dots are metabolites linked to the arginine and proline metabolism that changed significantly.

Next the changes in arginine metabolism were analyzed more closely. Even though the cells were cultured in medium containing high concentrations of L-arginine (1 mM) and activated T cells showed a high uptake rate of <sup>3</sup>H-L-arginine (Fig. 6.14B), the intracellular arginine concentration declined abruptly between 24 and 48 h after activation (Fig. 6.14A). Interestingly, the required amount of L-arginine for protein synthesis exceeded the L-arginine uptake 2-fold (Fig. 6.14C).

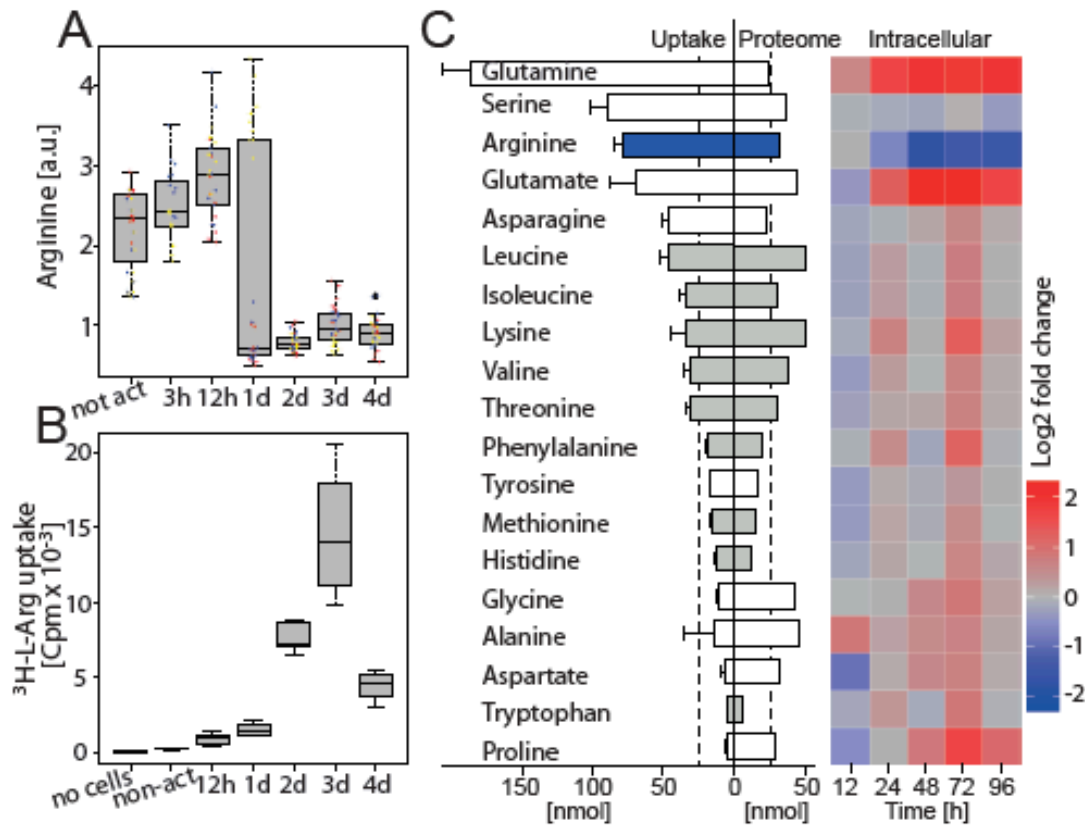


**Fig. 6.14: Arginine's uptake exceeds the requirements for protein synthesis in activated T cells.** A) Intracellular L-arginine levels in non-activated (non-act) and CD3/CD28-activated naïve CD4<sup>+</sup> T cells. Boxplot, n = 30 from three donors, each color represents a different donor. B) Uptake of <sup>3</sup>H-L-arginine during a 15 min pulse. Boxplot, n = 5 from three donors. C) Comparison of the uptake, proteome incorporation and intracellular abundance for the indicated amino acids. Barplot (left): Following the activation of 5 × 10<sup>4</sup> cells for four days, the consumption of amino acids from medium was analyzed. Grey bars represent essential amino acids. n = 4 from four donors, error bars represent S.E.M. Barplot (center): proteome incorporation of amino acids estimated from the copy numbers of each protein. Heat map (right): intracellular amino acid abundance in comparison to non-activated naïve T cells over time as determined by mass spectrometry. n = 30 from three donors. As leucine and isoleucine have the same mass, they could not be distinguished.

To address the influence of L-arginine on T cells, both CD4<sup>+</sup> and CD8<sup>+</sup> T cells were activated and expanded in L-arginine or control medium in the presence of IL-2. Subsequently, proliferation within the first days upon activation and viability of the cells were measured at different time points after cytokine withdrawal. Strikingly, L-arginine supplementation significantly increased CD4<sup>+</sup> and CD8<sup>+</sup> T cell survival upon withdrawal of the exogenous cytokine (Fig. 6.15A). Moreover, our data indicates that the L-arginine mediated prolonged survival of T cells was independent of mTOR, as L-arginine supplementation did not affect phosphorylation levels of the two mTOR targets S6K1 and 4E-BP (Fig. 6.10). When we activated T cells in L-arginine supplemented medium, the onset of proliferation was delayed, but, once initiated, doubling rates were similar to control cells (Fig. 6.15B). We next inhibited the conversion of L-arginine into L-ornithine with the arginase inhibitors norNOHA and

BEC, which has been shown to increase intracellular L-arginine levels<sup>294</sup>. The inhibition of arginase led to increased survival (Fig. 6.15 C). Interestingly, the inhibition of arginase did not affect the onset of proliferation (Fig. 6.15D). Taken together, these findings indicate that increased intracellular L-arginine levels can induce metabolic changes and a prolonged survival of human CD4<sup>+</sup> and CD8<sup>+</sup> T cells, independently on mTOR signaling or downstream metabolites.

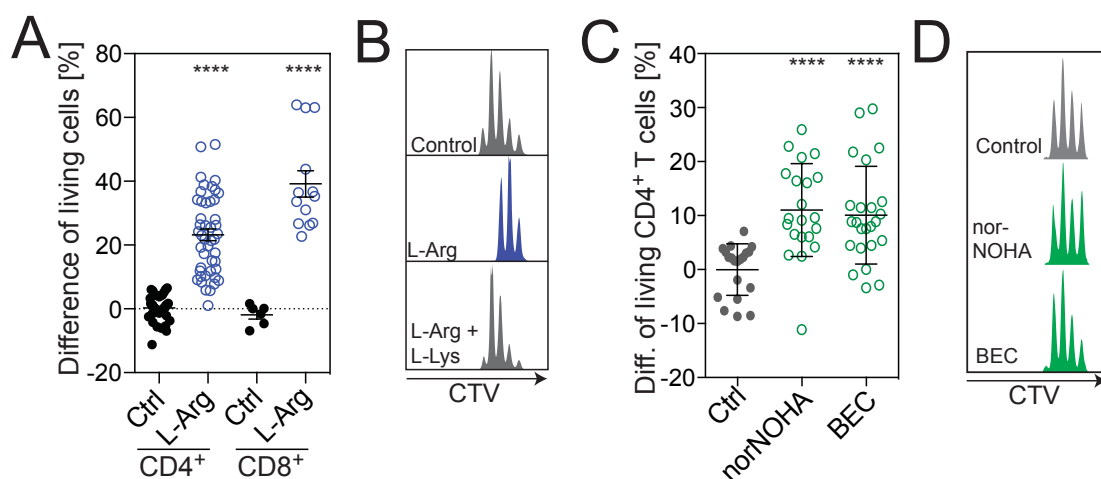


**Fig. 6.15: L-arginine endows cells with a high survival capacity *in vitro*.** A) After naïve CD4<sup>+</sup> and CD8<sup>+</sup> T cells were activated for 5 days in L-arginine or control medium in the presence of IL-2, the cells were extensively washed and cultured in control medium without IL-2. Annexin V staining 5 days after the IL-2 withdrawal determined the percentage of living cells. n = 46, from 16 donors (CD4<sup>+</sup> T cells) and n = 13 from four donors (CD8<sup>+</sup> T cells). B) Proliferation of 72 h activated T cells in the presence of L-Arg or L-Arg and L-Lys. C) Difference of living activated CD4<sup>+</sup> T cells 5 days after IL-2 withdrawal. Naïve CD4<sup>+</sup> T cells were activated in control medium or medium supplemented with the arginase inhibitor N<sup>ω</sup>-Hydroxy-nor-L-arginine (norNOHA, 0.3 mM) or S-(2-boronoethyl)-L-cysteine (BEC, 0.3 mM). n = 21 from seven donors. D) Proliferation of 72 h activated T cells in the presence of norNOHA or BEC. \*\*\*\* p < 0.0001 (Students t test). All error bars represent S.E.M.

As L-arginine directly promotes T cell survival, we hypothesized that direct interaction of L-arginine with a protein may induces conformational changes and initiates the pro-survival program. Using a recently developed workflow by Feng *et al.*, structural changes across the T cell proteome that occur in response to L-arginine were analyzed<sup>295</sup> (Fig. 6.16A). Homogenized T cells were incubated with 1 mM L-arginine, D-arginine or L-ornithine. Afterwards, the samples were subjected to limited proteolysis (LiP) with proteinase K, which preferentially cleaves flexible regions of a protein. Peptide mixtures, resulting from denaturation and trypsin digestion, were analyzed by LC-MS. This workflow resulted in half-tryptic peptides in flexible regions of a protein, since trypsin specifically cleaves polypeptides after arginine and lysine, while proteinase K cleaves after other amino acids. To analyze

structural changes induced by the addition of metabolites, we searched for changes in the abundance of half-tryptic peptides.

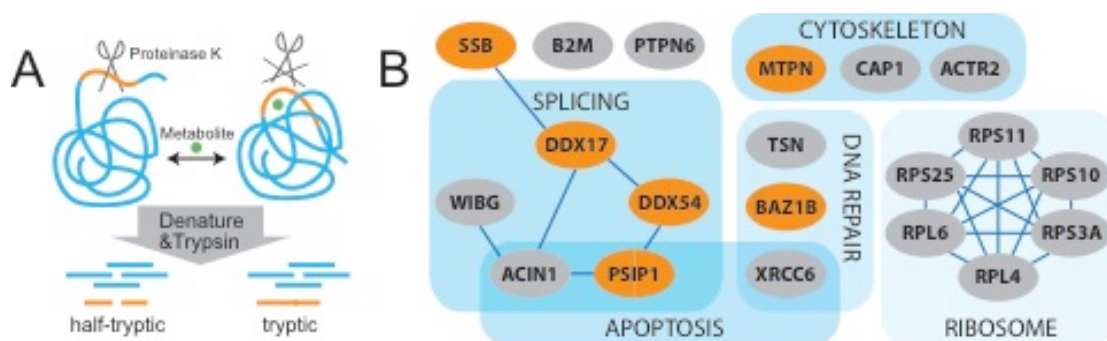


**Fig. 6.16: Limited proteolysis allows the identification of potential L-arginine sensors.** A) Overview of the limited proteolysis workflow. B) Proteins that specifically change their confirmation in the presence of L-arginine, but not D-arginine or L-ornithine. Transcriptional regulators are in orange, proteins are grouped according to their functions. Known interactions are indicated based on <http://string-db.org/> and <http://www.genemania.org/>.

Our data indicated that L-arginine, but not D-arginine or L-ornithine, promoted T cell survival. Therefore, we analyzed for changes in the abundance of half-tryptic peptides that were specifically affected by L-arginine and were cleaved by proteinase K at identical sites in all samples of six donors. These stringent criteria resulted in 20 potential candidates out of 5'856 identified proteins (Fig. 6.16B). We could exclude a bias toward large or abundant proteins, as the candidate proteins differed widely in molecular weight and abundance. The candidate proteins were associated with mRNA splicing, DNA-repair, regulation of the cytoskeleton and the ribosome. Seven of them were transcription factors (in orange in Fig. 6.16B).

Candidates identified through the structural analysis were depleted in primary human CD4<sup>+</sup> T cells by using the CRISPR/Cas9 system and analyzed for their influence on L-arginine-mediated longevity. While no viable clone could be detected that was deficient for XRCC6, ACIN1 or SSB, the depletion of PTPN6 or B2M did not alter the beneficial survival of L-arginine treated cells (Fig. 6.17A and B). However, the promoted survival mediated by L-arginine was impaired in clones that lacked the transcriptional regulators BAZ1B, PSIP1 and TSN (Fig. 6.17A and B), even though their proliferation and survival was not different from control cells when cultured in control medium (Fig. 6.17C). Taken together, these findings indicate that BAZ1B, PSIP1 and TSN interact with L-arginine and mediate the prolonged survival induced by L-arginine supplementation.

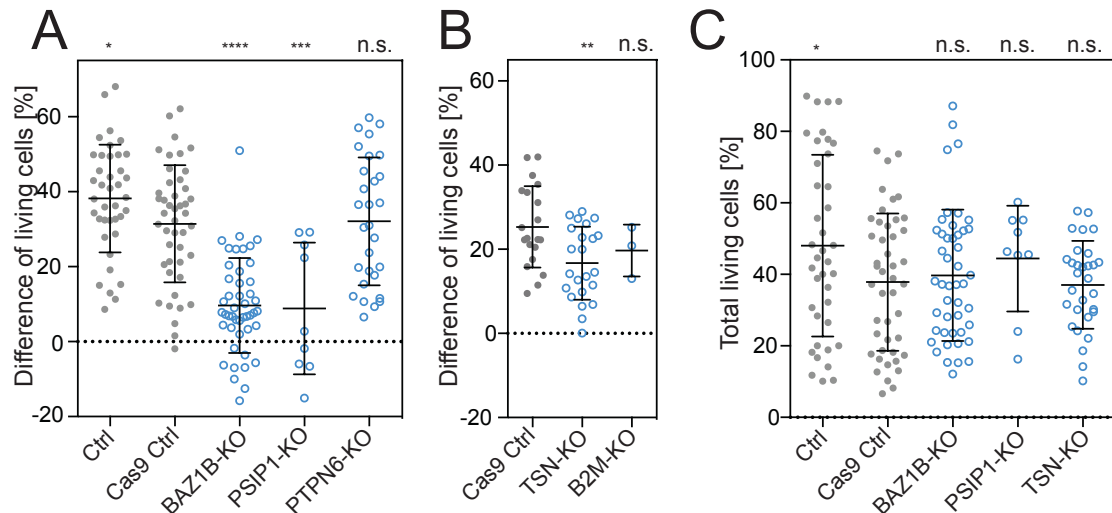


**Fig. 6.17: BAZ1B, PSIP1 and TSN mediate the L-arginine-dependent reprogramming of T cells toward increased survival capacity.** A) Survival upon IL-2 withdrawal with human CD4<sup>+</sup> T cells clones devoid of the indicated protein. Control (Ctrl) n = 39, Cas9-transduced control (Cas9 Ctrl) n = 45, BAZ1B-KO n = 46, PSIP1-KO n = 9, PTPN6-KO n = 29. Each T cell clone was analyzed in triplicates. B) Same as in A). Cas9 Ctrl n = 20, TSN-KO, n = 23, B2M-KO n = 3. C) Percentage of living cells after IL-2 withdrawal of T cells cultured in control medium. n are equal to A) and B). A-C) n.s. = non significant, \* p < 0.05, \*\* p < 0.01, \*\*\* p < 0.001, \* p < 0.0001 (Student's t test). Error bars represent S.E.M.

Finally, we investigated the influence of L-arginine supplementation on the anti-tumor response. Therefore, we adoptively transferred OT-I T cells into wild-type mice bearing B16 melanoma tumors expressing the OVA-antigen. When the transferred T cells were previously supplemented with L-arginine, the tumor size was reduced and the survival was increased (Fig. 6.18A and B). Similar results were obtained when mice were fed with L-arginine and primed OT-I T cells *in vivo* by OVA + Alum immunization of tumor-bearing mice. Mice that were fed with L-arginine showed a superior anti-tumor response compared to mice fed with PBS (Fig. 6.18C). In conclusion, the data indicate that increased levels of L-arginine have a beneficial effect on the survival of CD8<sup>+</sup> T cells and improve the anti-tumor response *in vivo*.



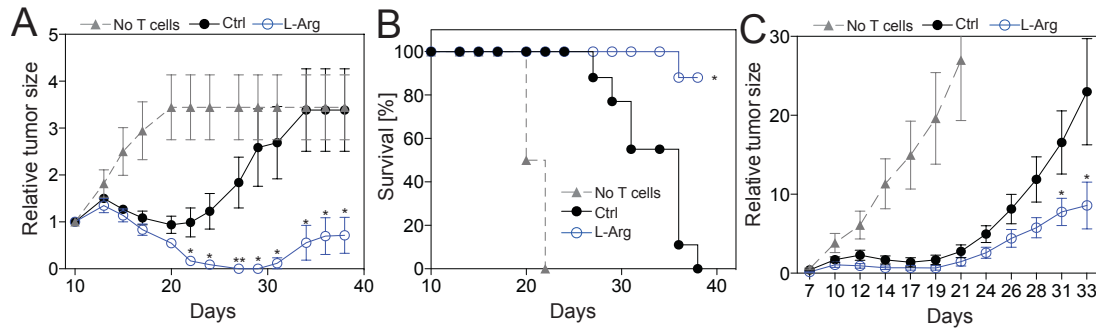


**Fig. 6.18: CD8<sup>+</sup> T cells with increased L-arginine levels display improved anti-tumor activity *in vivo*.** Tumor burden (A) and survival (B) were assessed over time. Data are representative of three independent experiments, each performed with seven to nine mice per group. C) B16.OVA melanoma cells were injected into C57BL/6 mice. Tumors were allowed to grow for six days. At this point, naïve CD8<sup>+</sup> T cells were transferred into tumor bearing mice and at day 7 mice were immunized with OVA peptide. Starting one day before the T cell transfer, PBS or L-Arg (1.5 mg/g body weight) was orally administrated daily. n = 19 from three independent experiments. \* p < 0.05 as determined by log-rank test comparison between curves. Error bars represent SEM. A-C) \* p < 0.05, \*\* p < 0.01, \*\*\* p < 0.001, \*\*\*\* p < 0.0001. Errors bars represent SEM.

### 6.2.2 Discussion

The combination of proteomics, metabolomics and functional approaches revealed that increased intracellular L-arginine levels directly impact the metabolic fitness and survival capacity of human and murine T cells. Structural analysis allowed the identification of sensors that induced L-arginine-mediated prolonged survival. Finally, L-arginine supplementation improved anti-tumor functionality in a mouse model.

Upon activation, T cells convert rapidly L-arginine into downstream metabolites, resulting in a decline of intracellular L-arginine levels. A 4-fold increase of L-arginine delayed the onset of proliferation and reduced effector functions in comparison to control T cells. However, L-arginine treated cells were able to differentiate into effector cells upon secondary stimulation. Interestingly, the inhibition or depletion of ARG2 in human or mouse cells did not affect proliferation of the cells suggesting that a downstream metabolite rather than the increased intracellular L-arginine levels induced the delayed onset of proliferation.

Intracellular L-arginine levels also controlled the survival of T cells. While reduced uptake was associated with poor survival, increased intracellular L-arginine levels were associated with prolonged survival. The combination of limited proteolysis and CRISPR/Cas9-mediated knockout experiments resulted in the identification of factors

involved in the beneficial effect of L-arginine on T cell survival. Two of the identified factors, BAZ1B and PSIP1, were linked to transcription. Arginine-induced changes in the PHD domain of BAZ1B, which seemingly binds to methylated histones, and the AT-hook DNA binding domain of PSIP1. Interestingly, PSIP1 has been linked to protection against stress-induced apoptosis<sup>296</sup>. A third factor linked to L-arginine-mediated longevity was TSN, a small DNA and RNA binding protein, which is involved in DNA repair, regulation of mRNA expression and RNAi<sup>297</sup>. As the depletion of each of the three different factors affected arginine-mediated longevity in a similar way, L-arginine has a potential impact on several mechanisms. Moreover, the variation between the different knockout clones for one sensor indicates that compensatory mechanisms exist. The underlying mechanisms by which L-arginine mediates longevity via the three identified sensors are elusive and need to be further investigated.

Finally, increased levels of L-arginine have a beneficial effect on the T cell-mediated anti-tumor response, which may be due to a combination of phenotypic changes. The improved survival capacity and the maintenance of a T<sub>CM</sub>-like phenotype may support the anti-tumor immune response, but metabolic adaptations mediated by increased arginine intake could be also advantageous. For instance, the switch from glycolysis to OXPHOS counteracts the Warburg effect, a common feature within the tumor microenvironment<sup>68</sup>. Even though further work is required to investigate the beneficial effect of L-arginine on anti-tumor immune responses, a recent publication by He *et al.* and recent data from our lab indicated that the combination of L-arginine supplementation with anti-PD-L1 therapy improves the immune response against osteosarcoma in a mice model in comparison to the single therapies<sup>298</sup>.

In conclusion, changes in metabolite levels can be generated without genetic intervention, making it easy to apply for therapeutic applications. The positive effect of L-arginine supplementation on T cell survival and anti-tumor functionality represents by itself a promising new therapeutic intervention. Moreover, the supplementation of L-arginine may improve existing strategies, such as checkpoint inhibitor therapy or adoptive T cell therapy.

## **6.3 High-throughput T cell receptor (TCR) grafting for adoptive T cell therapies to treat cancer**

### **6.3.1 Results**

In the previous chapter, we showed that metabolic intervention has a beneficial effect on the anti-tumor response. The liver plays an essential role for the body energy metabolism. Glucose and fatty acids are transported from the gastrointestinal tract to the liver, where they are stored as glycogen and triacylglycerol, respectively. Furthermore, amino acids are metabolized in the liver to provide energy or act as building blocks for protein synthesis or other bioactive molecules<sup>299</sup>. Chronic viral infections in the liver or metabolic disorders can cause the development of cancer within the liver. In this chapter, we aimed to investigate the anti-tumor T cell response in the context of a key metabolic organ, the liver.

We obtained tumor and non-tumorous liver tissues, as well as blood samples from patients, which gave their informed consent, from the university hospital in Bologna, Italy and the hospital G. B. Morgagni – L. Pierantoni in Forli, Italy. We received samples from 15 patients. Two-thirds of hepatocellular carcinomas (HCC) derived from chronic viral infections with HBV (4 out of 15) or HCV (6 out of 15). The other tumors derived from non-alcoholic steatohepatitis (NASH, 4 out of 15) and alcoholic steatohepatitis (ASH, 1 out of 15) (Fig. 6.19A). The male-female ratio was 2:1 (Fig. 6.19B). This was in line with the literature, as a male to female ratio of 2.17:1 was reported for the region of Romagna, where the hospitals of Bologna and Forli are located<sup>300</sup>. In conclusion, our patient cohort reflects the clinical situation and displays a good basis for the following investigations.

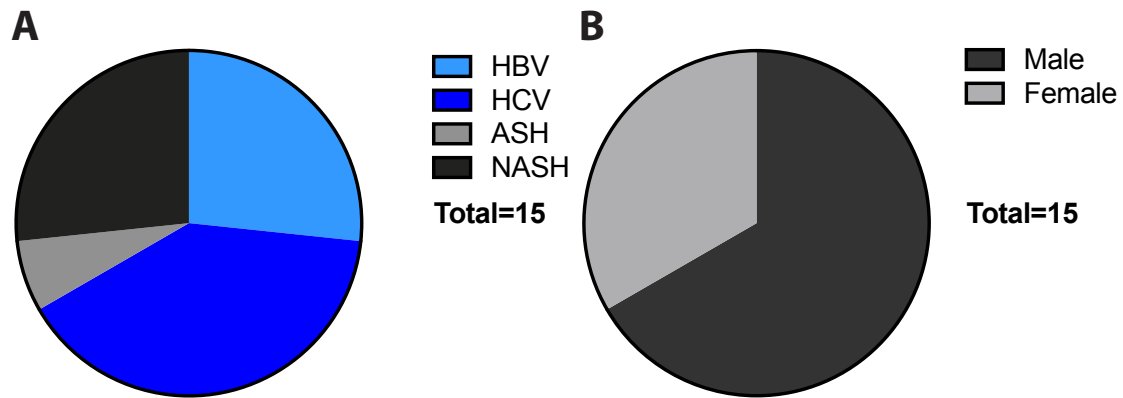


**Fig. 6.19: Chronic viral infections are the major cause of HCC in the cohort.** Distribution of etiologies (A) and sexes (B) are illustrated by pie charts. n = 15

To investigate the exhaustion state of T cells, we analysed the expression of the exhaustion marker PD-1 by flow cytometry. PD-1 levels showed a stepwise increase from blood to non-tumorous liver tissue to tumor tissue. This was true for both, viral- and non-viral-derived HCC. However, the highest levels of PD-1 were detected on CD8<sup>+</sup> T cells of viral-derived HCC patients (Fig. 6.20A and B).

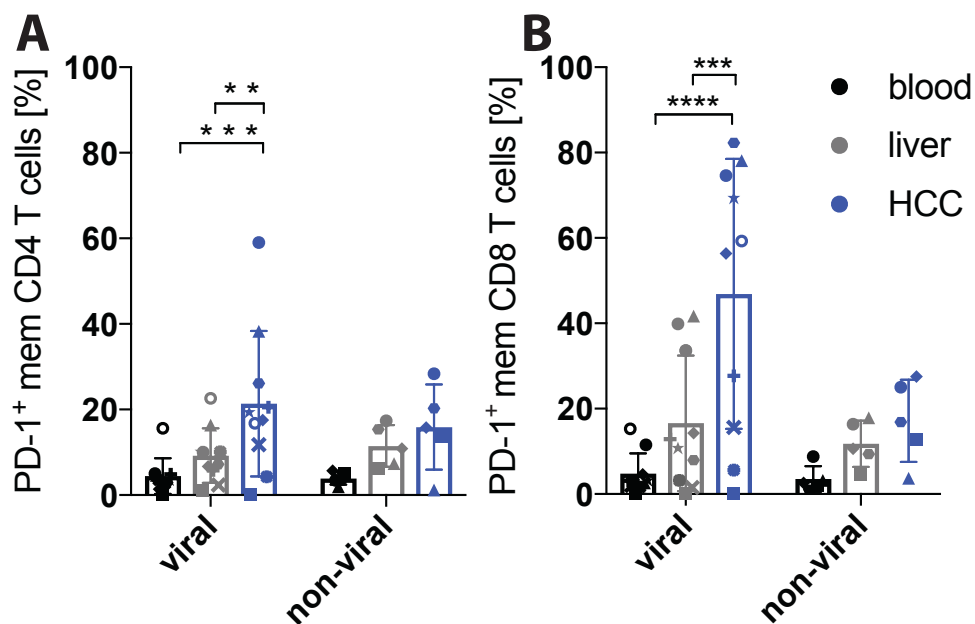


**Fig. 6.20: TILs express high levels of PD-1.** The PD-1 expression of memory CD4<sup>+</sup> (A) and CD8<sup>+</sup> (B) T cells is shown. All frequencies were determined by flow cytometry. The patients were divided into viral-derived (HBV and HCV) and non-viral-derived (ASH and NASH) HCC. The same symbol shape within the viral and non-viral group represents values from the same patient. Error bars represent SD. \*\* p < 0.01, \*\*\* p < 0.001, \*\*\*\* p < 0.0001 (Two-way ANOVA).

It has been shown that PD-1 plays a crucial role in establishing peripheral tolerance and in inhibiting the proliferation and function of T cells<sup>301</sup>. Therefore, we investigated the responsiveness of T cells from different compartments towards a polyclonal stimulation with phytohaemagglutinin A (PHA) and feeder cells. We

seeded the cells by limited dilution and calculated the cloning efficiency on the basis of wells, where T cell clones grew. CD4<sup>+</sup> and CD8<sup>+</sup> TILs had a significantly reduced cloning efficiency in comparison to T cells from the blood. This can be partially explained by the procedure to isolate the T cells from the tissue, as the cloning efficiency of T cells from non-tumorous liver tissue was lower than peripheral blood T cells. However, the cloning efficiency was higher for liver-resident T cells than for TILs. Strikingly, TILs from some patients resulted in no expanding clones, indicating that these cells were severely exhausted and could no longer respond to polyclonal stimulation (Fig. 6.21, left panel).

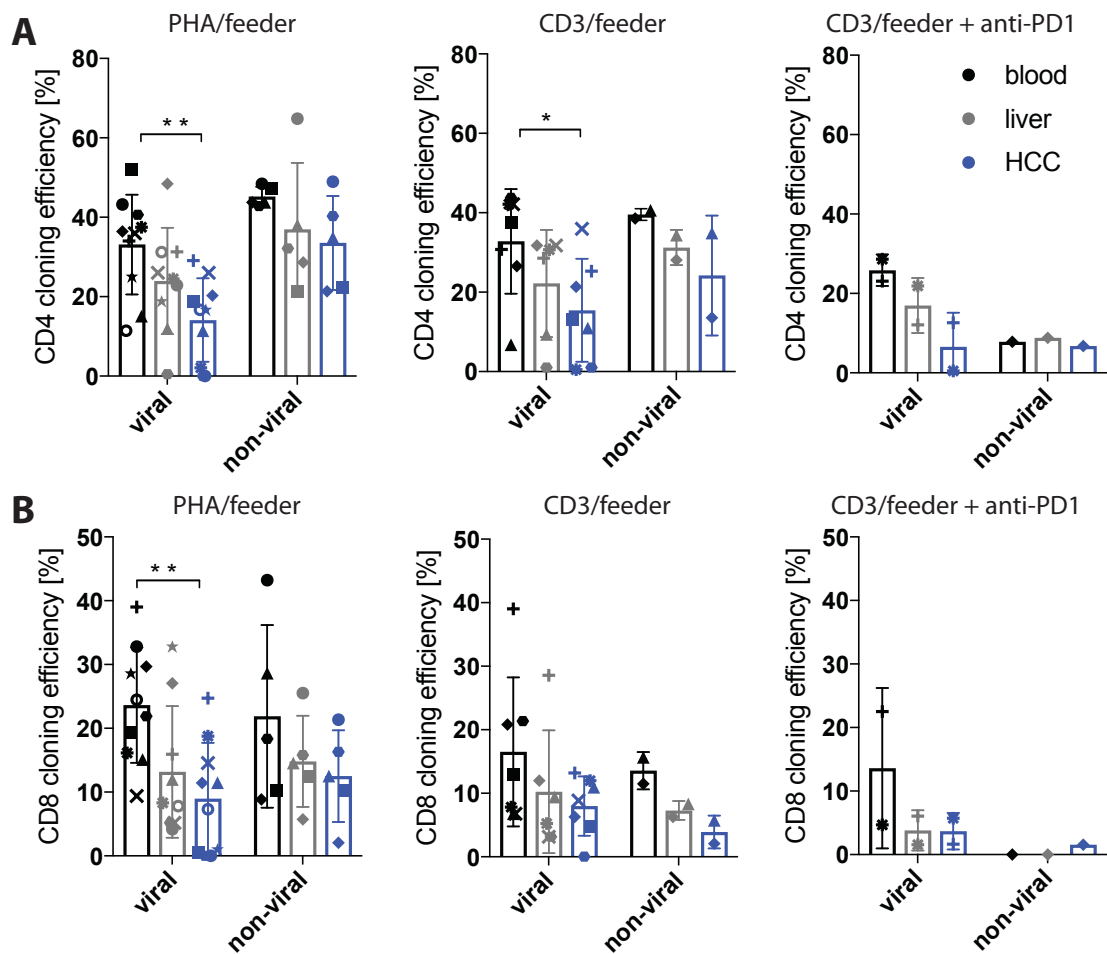


**Fig. 6.21: TILs display a reduced cloning efficiency.** Freshly isolated T cells were plated by limited dilution and stimulated with feeder and 6'000 Units/ml IL-2, as well as PHA (left), soluble anti CD3 antibody (30 ng/ml) (middle) or soluble anti-CD3 antibody plus anti-PD1 antibody (5µg/ml) (right). The wells containing a growing clone were counted 12 days after stimulation. The cloning efficiency for CD4<sup>+</sup> T cells (A) and CD8<sup>+</sup> T cells (B) is shown. The same symbol shape within the viral and non-viral group represents values from the same patient. Error bars represent SD. \* p < 0.05, \*\* p < 0.01 (Two-way ANOVA).

As PHA activates T cells by cross-linking surface molecules, it is possible that the reduced cloning efficiency is due to the stimulation of PD-1 on exhausted T cells. This would inhibit the proliferation of the cells. To test this hypothesis, we replaced

PHA with a soluble antibody against CD3. This treatment did not improve the cloning efficiency of TILs (Fig. 6.21, middle panel). PD-1 could still be triggered under these conditions, because PBMCs can also express the ligand of PD-1 (PD-L1). To block also this interaction, we stimulated single cells via the addition of soluble anti-CD3 antibody and feeder together with a PD-1 blocking antibody. Even this treatment could not restore the cloning efficiency of TILs (Fig. 6.21, right panel). Taken together, our data reveal that TILs, especially from viral-derived HCC patients, show signs of severe exhaustion and poorly respond to polyclonal stimulation.

The current protocols for ACT rely on the initial proliferation of TILs<sup>302</sup>. However, the reduced cloning efficiency of TILs may affect the expanded TIL populations, as few well growing clones could overgrow the exhausted, tumor-specific ones. To test this hypothesis, we analyzed the TCR-repertoire from one patient with HCV-derived HCC (hexagon shape in previous figures). The genomic DNA of CD4<sup>+</sup> TILs and memory CD4<sup>+</sup> peripheral blood T cells was isolated directly after sorting, 4 days after activation with antibodies against CD3 and CD28, and 14 days after activation with PHA and irradiated feeders. The genomic DNA was sent to Adaptive Biotechnologies and the  $\beta$ -chain of the TCR was sequenced. The chances to identify antigen-specific T cells not only depend on the origin of the T cells, but also on the clonality of the population. While the number of different clonotypes per 10<sup>5</sup> sequenced cells declined with time of expansion for peripheral blood T cells, a short expansion of 4 d with antibodies to CD3 and CD28 increased the frequency of different clonotypes 2.5-fold (Fig. 6.22A and B). Further expansion reduced the frequency 3.5-fold. Strikingly, the 10 most abundant TCRs within the expanded TIL population represented almost 70 % of all detected TCRs, whereas for the other conditions the top 10 clonotypes represented only 25 %. The percentage displayed by the 10 most abundant clones for peripheral blood T cells were under all conditions ~12 % (Fig. 6.22C). In conclusion, our data suggests that a short expansion of TILs improved the quality of TCR sequencing and could improve the chances to identify tumor-specific T cells. However, further expansion of TILs resulted in the outgrowth of well growing clones.

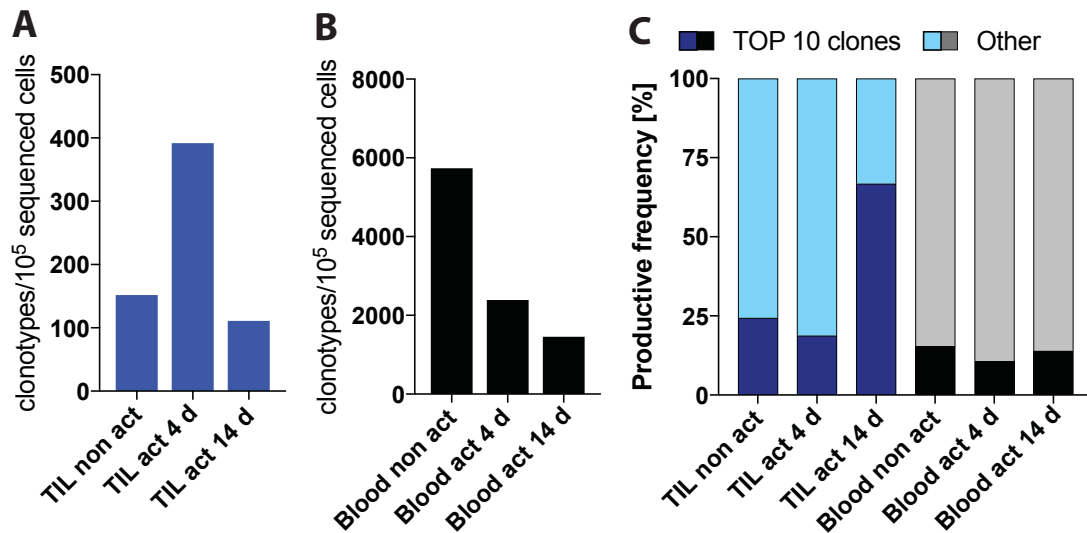


**Fig. 6.22: A short expansion of TILs improved the quality of TCR sequencing.** The genomic DNA of CD4<sup>+</sup> TILs and peripheral blood CD4<sup>+</sup> T cells from a patient with HCV-derived HCC (hexagon shape in previous figures) was purified directly after sorting (non act), 4 days after stimulation with CD3/28 (act 4 d) or 14 days after expansion with PHA and irradiated feeders (act 14 d). Adaptive Biotechnologies sequenced the genomic DNA for the  $\beta$  chain of the TCR. TCRs were distinguished via nucleotide sequence. A) The number of detected different clonotypes per 100'000 sequenced cells is displayed for TILs. B) Same as in A), but for memory T cells from the blood. C) Productive frequency of the ten most abundant TCRs within each population is shown in dark blue/black. Light blue and gray bars represent all other detected TCRs.

To avoid that few clones outgrowth the broad majority of TILs, we aimed to design a high-throughput workflow in order to graft the TCR from TILs at the point of lowest clonality on well expanding Jurkat cells. Microfluidic-based grafting of TCRs (MIGOT) will allow us to screen for tumor-specific TCRs regardless from the proliferative capacity of the initial cell population. By using a microfluidic device, TILs are coencapsulated together with mRNA capturing beads and lysis buffer. To ensure that a droplet does not contain more than one cell, we encapsulated the cells at a density that only one in twenty droplets contains a cell. The cells are lysed within the droplets and the beads captured the mRNA. After droplet breakage, the beads are rescued for reverse transcription *en bulk*, leading to cDNA-coated beads, which carry the information of only one cell per bead. Subsequently, the beads are encapsulated a second time. Within the droplets, the full-length sequences of TCR  $\alpha$  and  $\beta$  chain are amplified and linked via overlapping primers. The PCR product is isolated from the droplets and the linked PCR product is separated from the single chains by gel electrophoresis. After the PCR product of the linked TCR chains is purified, a nested PCR amplified specifically the linked PCR product, which was cloned *en bulk* into a lentiviral vector. Jurkat cells that lack their endogenous TCR are transduced with the lentiviral library and screened for tumor-specific T cells (Fig. 6.23).

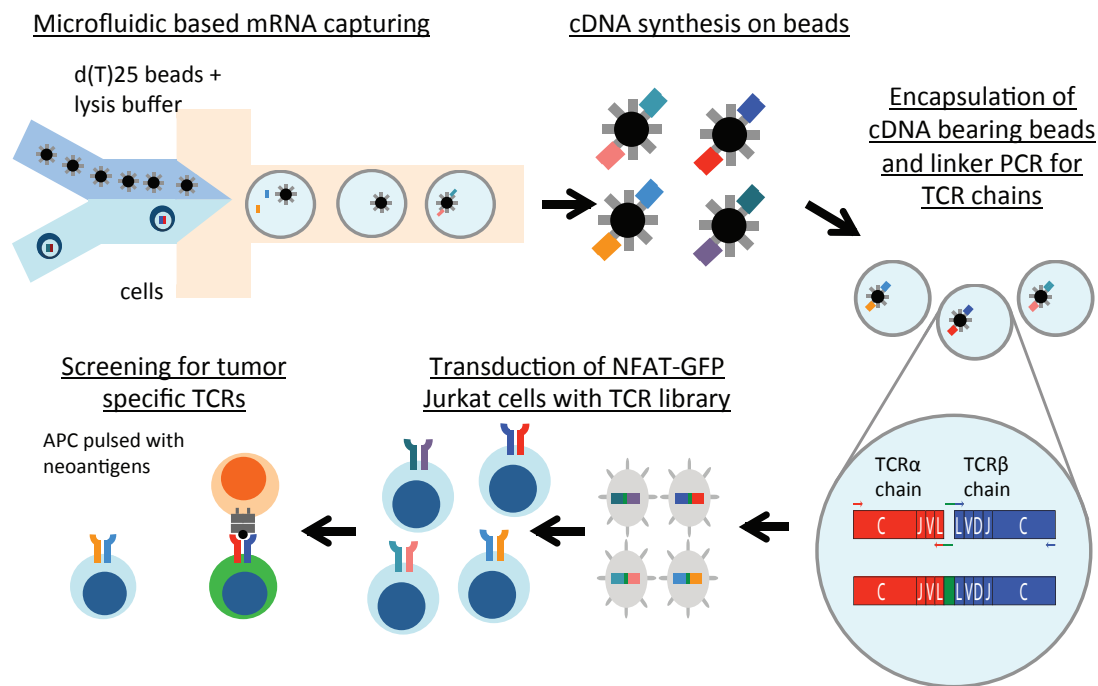


**Fig. 6.23: Microfluidic-based grafting of TCRs could result in the identification of tumor-specific TCRs.** A schematic overview of the procedure is shown. TILs are encapsulated in picoliter droplets together with mRNA capturing beads. After TILs are lysed, their mRNA is captured within the droplets. This is followed by cDNA synthesis, encapsulation of cDNA-coated beads and TCR linkage PCR within the droplets. The linked TCR product will be cloned into a lentiviral vector. TCR-deficient Jurkat cells will be transduced with the TIL-TCR library and screened for tumor-specificity.

To establish MIGOT, we collaborated with the lab of Andrew deMello, especially Yun Ding. The designed chip allowed us to coencapsulate cells together with mRNA-capturing beads and lysis buffer (Fig. 6.24A). Initially, we had to validate that the cells are lysed within the droplets and that the cellular content is equally distributed through the droplet. This would guarantee that the mRNA-capturing beads could efficiently capture mRNA. We labeled primary human T cells with CFSE and coencapsulated them with PBS or lysis buffer. Our microfluidic device did not affect the integrity of the cells, as the cells were still intact when encapsulated with PBS. Moreover, immediately after encapsulation with lysis buffer, the entire droplet was fluorescent (Fig. 6.24B). This indicated that cells are efficiently lysed within droplets and that the cellular content together with the mRNA is equally distributed within the droplet. We further examined whether the beads can capture mRNA within the droplets. Therefore, we coencapsulated beads with fluorochrome-labeled polyA. The Fig. 6.24C shows that the signal of the polyA co-localized with the fluorescent beads. Importantly, droplets that did not contain any beads had a higher background signal deriving from the polyA than droplets with beads. Moreover, even after droplet breakage the beads were labeled with the fluorescent polyA (Fig. 6.24D). This



indicated that mRNA can be captured within droplets and droplet breakage did not disrupt the capturing. We next wanted to confirm that we could capture not only artificial polyA, but also mRNA from a cell. Therefore, we coencapsulated primary human T cells together with mRNA-capturing beads and lysis buffer. After droplet breakage, cDNA was synthesized from the mRNA on the beads and the presence of TCR cDNA was validated by qPCR. A sarkosyl-based lysis buffer resulted in efficient cell lysis and mRNA capturing (Fig. 6.24E and F).

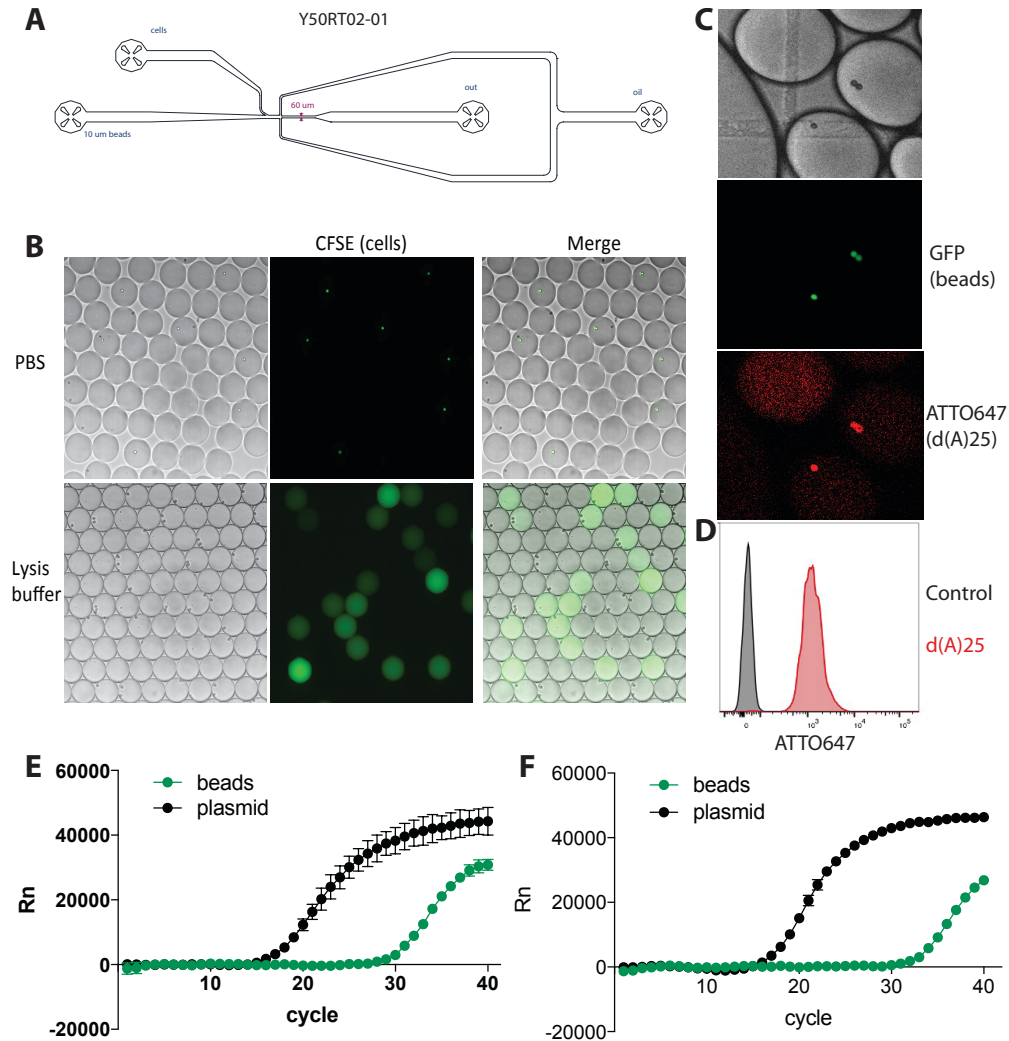


**Fig. 6.24: T cells are lysed and mRNA is captured within droplets.** A) Layout microfluidic chip. The purpose of inlets and outlets is indicated. B) CFSE-labeled cells were encapsulated with PBS or lysis buffer. The generated droplets were analyzed by microscopy. C) mRNA-capturing beads (green) were encapsulated together with fluorescent-labeled polyA (ATTO647 d(A)25). The generated droplets were analyzed by fluorescent microscopy. D) The beads from C) were isolated from the droplets and the frequency of poly A on the surface of the beads was determined by flow cytometry. Empty beads were used as control. E and F) Human primary CD4<sup>+</sup> T cells were encapsulated with mRNA capturing beads. The cells were lysed within the droplets and beads captured mRNA. Following droplet breakage, cDNA was synthesized and the beads were used to quantify the TCR  $\alpha$  (E) and  $\beta$  chain (F) via qPCR. A plasmid containing  $\alpha$  and  $\beta$  chain of a TCR was used as a control.

We next aimed to graft a TCR from a primary human T cell onto Jurkat cells, which were depleted for their endogenous TCR by CRISPR/Cas9. To this aim, we used a well characterized MHC-II associated TCR against the flu-antigen hemagglutinin (HA). After grafting the TCR, we sorted CD3<sup>+</sup> cells and expanded them. The expression levels of TCR-depleted Jurkat cells were similar to the unstained control, indicating that we successfully depleted the TCR on Jurkat cells. However, when we grafted a TCR onto the TCR-depleted Jurkat cells, the expression levels were comparable to wild-type Jurkat cells, but also to primary human CD4<sup>+</sup> T cells (Fig. 6.25A). We next addressed if the grafted TCR is functional. Therefore, we stimulated wild-type, TCR-depleted and TCR-grafted Jurkat cells with B cells pulsed with recombinant HA or the corresponding peptide pool. Non-pulsed B cells were used as a negative control. Based on the CD69 expression, the activation state of the cells was measured 24 h after activation. When wild-type or TCR-depleted Jurkat cells were stimulated with recombinant HA or the corresponding peptide pool pulsed B cells, we detected no difference in the activation marker in comparison to the cells stimulated with non-pulsed B cells. This indicates that we have a low frequency of false positive signals. Jurkat cells bearing the corresponding TCR for HA showed an increased expression of CD69 indicating that the grafted TCR is functional. In contrast, the stimulation with B cells, which were pulsed with the peptide pool, did not result in an increased expression of CD69 (Fig. 6.25B). These data suggest that the grafted TCR is functional, but the antigen-specific stimulation is not efficient.

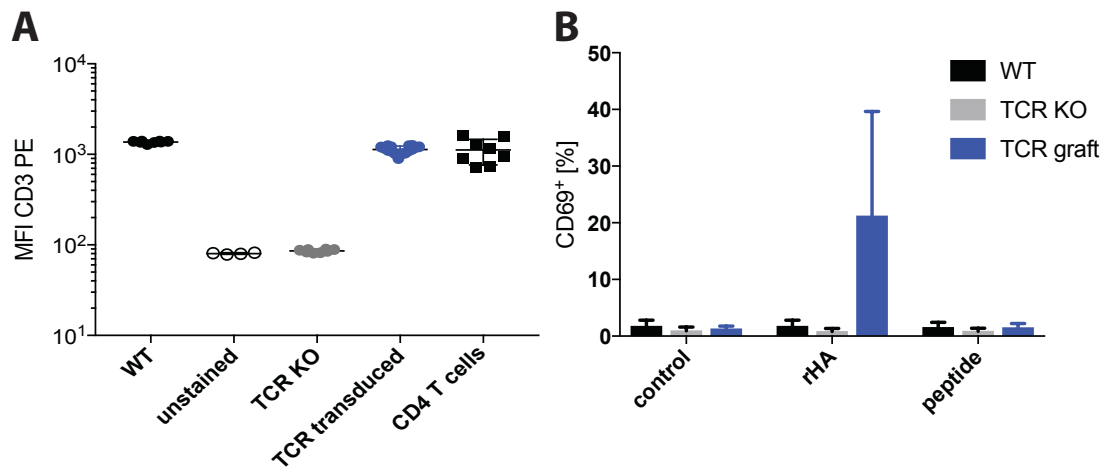


**Fig. 6.25: Grafted TCRs can induce T cell activation upon stimulation with the cognate antigen.** A) TCR-depleted Jurkat cells were transduced with a Haemagglutinin-specific TCR. The cells were positively sorted for the expression of CD3. Four days after sorting, the cells were stained for the expression of CD3. Primary human CD4<sup>+</sup> T cells were used as a positive control (CD4 T cells). WT n = 8, unstained n = 4, TCR KO n = 8, TCR transduced n = 16, CD4 from Buffy n = 8. B) Percentage of activated Jurkat upon stimulation. Irradiated B cells, which were autologous to the grafted TCR, were stimulated with recombinant Haemagglutinin (rHA), the corresponding peptide pool or were cultured only in medium (negative control) for 2 h. Afterwards, B cells and Jurkat cells were co-cultured in a ratio of 1:5. The activation of Jurkat cells was assessed 24 h after stimulation by staining of CD69. n = 4 - 8 from two independent experiments.

To optimize the antigen specific stimulation, we analyzed the reporter Jurkat cells for the expression of molecules involved in TCR signaling. Wild-type and TCR-depleted Jurkat did not express CD4. As CD4 plays an important role for the phosphorylation of the TCR after stimulation, we transduced Jurkat cells with a lentiviral construct encoding CD4. Following the transduction, the expression of CD4 was stable on wild-type, as well as TCR-depleted Jurkat cells (Fig. 6.26A). Afterwards, we repeated the stimulation from the previous experiment with CD4 expressing Jurkat cells. Wild-type and TCR-depleted Jurkat cells showed no increased expression of activation marker. When we stimulated CD4<sup>+</sup> Jurkat cells, bearing the HA specific TCR, the frequency of CD69<sup>+</sup> cells after stimulation with recombinant HA was similar to Jurkat cells not expressing CD4. Strikingly, the stimulation with B cells pulsed with peptides resulted in 25.1 % CD69<sup>+</sup> cells (Fig. 6.26B). Taken together, the expression of CD4<sup>+</sup> improved the TCR response to peptide indicating that the proposed screening method could lead to the identification of antigen-specific TCRs.

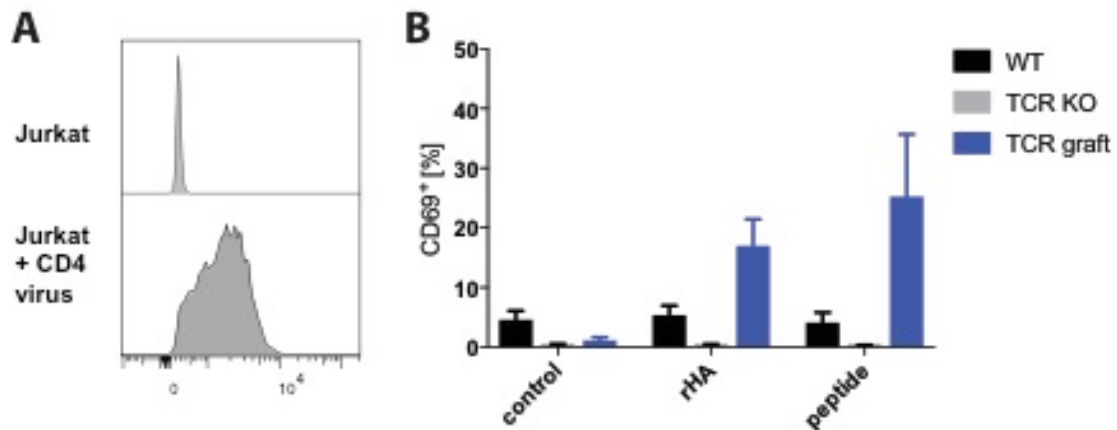


**Fig. 6.26: Expression of CD4 improved the response of Jurkat cells to stimulation.** A) Overexpression of CD4 in Jurkat cells. Jurkat cells were transduced with a lentiviral construct that contains the coding sequence of human CD4. Four days after transduction, the cells were positively sorted for the expression of CD4. Additional three days later, the expression of CD4 was analyzed by flow cytometry. Representative histograms are shown. B) Irradiated B cells, which were autologous to the grafted TCR, were stimulated with recombinant Haemagglutinin (rHA), the corresponding peptide pool or were cultured only in medium (negative control) for 2 h. Afterwards, B cells and CD4-expressing Jurkat cells were co-cultured in a ratio of 1:5. The activation of Jurkat cells was assessed 24 h after stimulation by staining of CD69. n = 4-8 from two independent experiments.

Finally, the sensitivity of TCR grafted Jurkat cells was compared to T cell clones with the same TCR. Therefore, B cells from the same donor like the T cell clones were pulsed with different concentrations of rHA. The frequency of activated Jurkat cells (CD69<sup>+</sup>) was lower than for T cell clones at every concentration. However, activated Jurkat cells were also detected at lower concentrations, such as 5 ng/ml (Fig. 6.27A). Similar results were obtained, when the cells were stimulated with different numbers of B cells, which were pulsed with 500 ng/ml rHA (Fig. 6.27B). In conclusion, the sensitivity of T cells towards their cognate antigen is roughly two log scales higher in comparison to the TCR-grafted Jurkat cells. However, the rapid and uniform expansion of Jurkat cells display an advantage of Jurkat cells over expanded primary T cell clones.

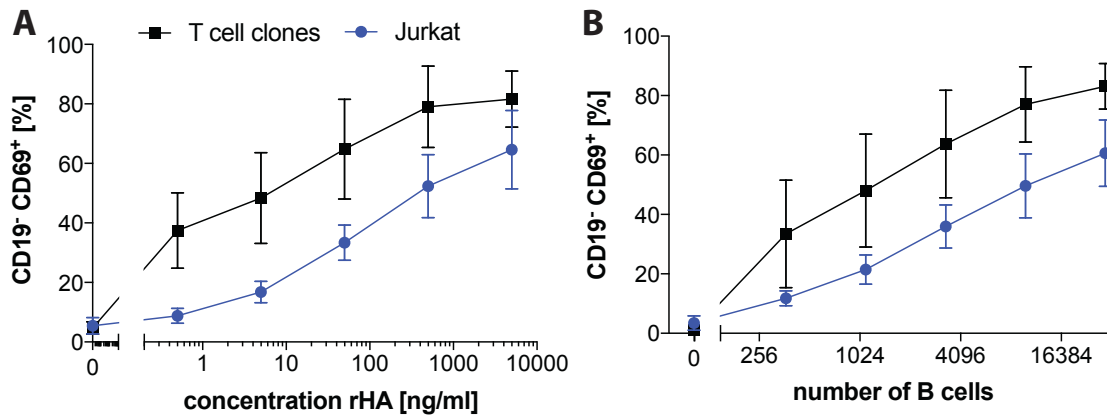


**Fig. 6.27: TCR grafted Jurkat cells are less sensitive to antigenic stimulation than T cell clones.** A)  $10^7$  autologous B cells/° were pulsed with the indicated concentration of rHA for 2 h at 37 °C.  $25^7$  flu-specific T cells (CDR3 $\alpha$ : CALGSGTYKYIF; CDR3 $\beta$ : CASSTASGRSSYEQYF) or Jurkat T cells expressing the same TCR were added. Four different T cell clones and two different TCR plasmids were used. B) Same as in A), but the concentration of B cells was diluted 1:3 from  $30^7$  cells/° to 370 cells/°. The concentration of rHA was 500 ng/ml. n = 8 from two independent experiments. Errors bars represent S.D.

### 6.3.2 Discussion

In summary, TILs, especially from viral-derived HCC patients, showed signs of severe exhaustion and responded poorly to polyclonal stimulation. The expansion of TILs resulted in strong proliferation of few clones potentially leading to the outgrowth of the majority of T cell clones in the tumor. Here, I described a workflow (MIGOT) that enables the analysis of the entire TCR repertoire from a TIL population independent of the proliferative capacity of the original cells. The usage of a microfluidic device allows several thousand single-cell PCRs in picoliter droplets to be conducted. After cloning the linked TCR from each cell into a lentiviral vector, the TCR library will be expressed in reporter Jurkat cells, which are screened for the specificity of the TCRs, potentially leading to the identification of tumor-specific TCRs. Thus ACT with T cells bearing TCRs, which had been lost by conventional methods, could improve the efficiency in liver cancers.

It has been shown that a higher number of intratumoral CD8<sup>+</sup> T cells are associated with reduced tumor cell proliferation and an increased number of apoptotic tumor cells<sup>303</sup>. However, another study showed that the location of CD8<sup>+</sup> T cells within the tumor microenvironment has a large impact on the survival of the patient. Patients with high numbers of CD8<sup>+</sup> T cells in the center of the tumor had a poor prognosis, whereas high numbers of CD8<sup>+</sup> T cells in the periphery of the tumor were associated with an increased overall survival<sup>304</sup>. In this context, it would be interesting to follow

our patients over time and link disease-free survival with the expression of exhaustion markers, such as PD-1. Apart from the number of TILs, the quality of the T cells has been shown to strongly influence outcome. A striking finding was that CD4<sup>+</sup> and CD8<sup>+</sup> TILs showed an increased expression of the exhaustion marker PD-1 indicating that TILs are dysfunctional. The highest levels of PD-1 expression were found on TILs from viral-derived HCC patients, which may be explained by findings that chronic viral infections can lead to T cell exhaustion and can induce the expression of PD-1<sup>305</sup>. Moreover, the analysis of the proteome of the cells from the different compartments could lead to the identification of new proteins that can be used as prognostic markers for HCC patients.

In line with the increased expression of PD-1, TILs responded poorly to polyclonal stimulation. This was expected, as it has been shown that severely exhausted T cells do not proliferate<sup>115</sup>. The cloning efficiency was not restored when the cells were stimulated with a CD3-specific antibody alone or in combination with blockade of PD-1. This may be due to the poor efficiency of PD-1 blockade in PD-1<sup>hi</sup> individuals<sup>306</sup>. However, the TILs of the patients used for this experiment showed an intermediate PD-1 expression and the cloning efficiency of cells from a patient with non-viral derived HCC was reduced after stimulation in the presence of a PD-1-blocking antibody. This was unexpected and could be caused by opsonization by the irradiated feeders. Further experiments with antibodies that do not bind to Fc receptors are required to investigate if the usage of immune checkpoint inhibitors improves the clonability of TILs. Another reason for the poor response of TILs towards polyclonal stimulation could be the different metabolic conditions the cells encounter during *in vitro* culture. As IL-2 promotes glycolysis, terminal differentiation may be promoted and the proliferation of exhausted T cells could be diminished<sup>169</sup>. Different culture conditions, such as low glucose levels, could improve the response of TILs towards polyclonal stimulation. Moreover, TIL expansion resulted in the rapid proliferation of few clones, which may lead to the outgrowth of other clones from the tumor. This may be a consequence of the exhausted state of TILs and highlights a problem of current protocols for ACT, as the initial expansion of TILs is an essential step in this process.

A recent study by Mognol *et al.* showed that T cell exhaustion requires antigen recognition by TILs<sup>307</sup>. These findings suggest that exhausted T cells are potentially tumor specific. As exhausted T cells are shown to have a poor proliferative capacity<sup>115</sup>, we developed an alternative workflow (MIGOT) to identify tumor-specific TCRs regardless of the proliferative capacity of the original cells. By using a microfluidic system, the single cell information is conserved during the engraftment of full-length TCRs from TILs onto a reporter cell line. Different studies describe microfluidic systems that link the two chains of the TCR<sup>308,309</sup> or BCR<sup>310</sup>. However, these studies use the linked PCR product only for sequencing, which resulted in information about the TCR diversity, but not specificity. MIGOT combines the information of the TCR diversity of a population with the possibility to screen for antigen specificity. Therefore, MIGOT may lead to the identification of tumor-reactive TCRs, which would be lost with other methods. These TCRs could be used for ACT, resulting in an increased efficiency of ACT therapies.

Finally, we found that CD69 was a reliable activation marker Jurkat cells that was up-regulated upon stimulation with antigen-pulsed B cells. Overexpression of CD4 on Jurkat cells further increased the expression of CD69, as CD4 is an important molecule to induce LCK-mediated phosphorylation of the cytosolic parts of the TCR. The analysis of the proteome of the reporter Jurkat cells could give hints if other proteins that are associated with the TCR are missing. The overexpression of the missing factors could further improve the sensitivity of the reporter cells.

In conclusion, TILs from HCC patients showed signs of severe exhaustion and responded poorly to polyclonal stimulation. Here, I postulate a workflow that allows the analysis of the entire TCR repertoire from non-proliferating CD4<sup>+</sup> and CD8<sup>+</sup> T cells. The TCR libraries of TILs can be used for screenings of tumor-antigen specific TCRs. Finally, the identification of highly tumor-specific TCRs could lead to improved ACT efficiency in liver cancer.

## 7 Outlook

T cell dysfunction is a dynamic process occurring during the development of tumors. Current immunotherapies aim to circumvent T cell dysfunction. Even though these therapies showed promising results in melanoma patients, many immunotherapies are rather inefficient for solid tumors, like hepatocellular carcinoma. Here, I described two potential therapies that display a new approach or could improve existing therapies for cancer patients.

In the first intervention we addressed cellular metabolism to improve the fitness and survival of adoptively transferred tumor-specific T cells. Strikingly, the oral administration of L-arginine supported an anti-tumor response. The oral application would be simply applicable to the clinic and displays a well-accepted treatment of patients. Moreover, it can be combined with other treatments, such as immune checkpoint blockade or ACT. Therefore, it would be promising to include arginine supplementation to clinical studies.

We discovered three sensors for intracellular L-arginine levels. The investigation of the mechanisms by which the different sensors can mediate arginine-mediated longevity could lead to a better understanding about the beneficial effects of arginine on the anti-tumor response. In line, the influence of the single sensors on the anti-tumor response would be needed to address *in vivo*. New insights into how the sensors contribute to the beneficial effects of L-arginine could lead to new therapeutic approaches for cancer patients or could support existing strategies.

The establishment of MIGOT would allow us to link information about TCR diversity with specificity in a high throughput scale. This would be of great benefit for screenings of tumor-specific T cells, as the procedure can be performed within one week and would lead to TCR-library engrafted Jurkat cells that can be easily screened for specificity. Beside TILs, also other T cell populations, such as  $T_{\text{regs}}$ , can be analyzed according to their diversity and specificity indicating the broad applicability of MIGOT.



Moreover, MIGOT is not restricted to the expression of full-length TCRs. It could also be adapted to analyze the B cell receptor (BCR) repertoire, as the efficiency of immortalization is only 30 %. Microfluidic-based grafting of BCRs would allow the analysis of thousands, in big scales even millions, of BCRs. This would represent a high-throughput sequencing of BCR diversity, which allows the linkage of sequencing results with specificity in a large scale. This could lead to the identification of rare antibodies and could improve the understanding of BCR diversity in healthy donors and patients.

Another promising adaptation of MIGOT would be the transformation of the TCR library into chimeric antigen receptors (CARs). Therefore, the transmembrane domain of CD28 replaces the transmembrane domain of the  $\alpha$  and  $\beta$  TCR. As CD28 builds dimers it would allow the formation of  $\alpha/\beta$  complexes. The intracellular part of the CAR-transformed TCR would consist of the signaling domains of CD28, 4-1BB and CD3 $\zeta$  (Fig. 7.1), similar to the third generation of CARs that are currently used in clinical trials<sup>311</sup>. This would combine advantages that CARs display over TCR, but would reduce the risk of non-target effects, as the identification of tumor antigens is MHC restricted.

Currently, we are collecting CD4<sup>+</sup> and CD8<sup>+</sup> T cells, as well as B cells and monocytes from the different compartments of HCC patients. The proteomic analysis could improve the current understanding of the changes in the TME of HCC patients leading to the identification of biomarkers to predict the response of T cells from patients to current therapies. The proteomic analysis of malignant cells and the soluble TME, which was collected during the tumor processing, could give hints for pathways that can be targeted with existing or new therapeutic strategies.

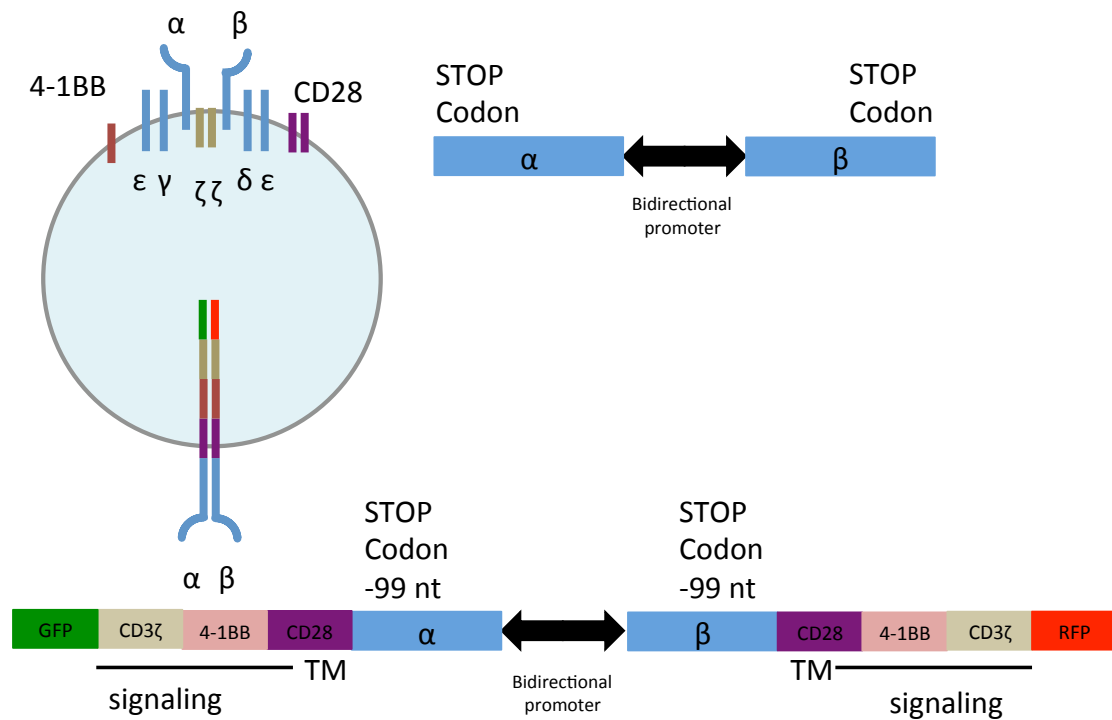


**Fig. 7.1: Design of CAR-transformed TCRs.** Up) Current strategy for MIGOT. The full length TCR sequence is cloned into a lentiviral vector and engrafted into TCR-depleted cells. The TCR signaling depends on the expression of costimulators of the host cell. Bottom) Design of CAR-transformed TCRs. The transmembrane domain of the two TCR chains will be removed by PCR amplification and replaced with the transmembrane domain (TM) of CD28, as well as the signaling domains of CD28, 4-1BB and CD3ζ. Fluorophores could be included to simplify the detection of CAR-transformed TCRs.

## 8 Experimental procedures

The experimental procedures involved in the part “L-Arginine modulates T cell metabolism and enhances survival and anti-tumor activity” derive from the corresponding manuscript<sup>272</sup>.

### 8.1 Isolation of primary cells from buffy coats

Blood from healthy donors was obtained from the Swiss Blood Donation Center of Basel and Lugano, and used in compliance with the Federal Office of Public Health. Peripheral blood mononuclear cells (PBMCs) were isolated by ficoll separation. CD4<sup>+</sup> T cells were enriched with magnetic microbeads (Miltenyi Biotec). Naïve T cells were sorted as CD4<sup>+</sup> CCR7<sup>+</sup> CD45RA<sup>+</sup> CD25<sup>-</sup> CD8<sup>-</sup> on a FACS Aria III cell sorter. For cell staining we used the following antibodies: anti-CD4-APC (allophycocyanin) clone 13B8.2; anti-CD8-APC clone B9.11; anti-CD8-FITC (fluorescein isothiocyanate) clone B9.11; anti-CD4-FITC clone 13B8.2; anti-CD45RA-PE (phycoerythrin) clone alb11; anti CD25-FITC clone B1.49.9 (all from Beckman coulter); anti-CCR7-Brilliant Violet 421 clone G043H7 from Biolegend.

### 8.2 Cell culture

Primary human T cells were cultured in RPMI-1640 medium supplemented with 2 mM glutamine, 1% (v/v) non-essential amino acids, 1% (v/v) sodium pyruvate, penicillin (50 U ml<sup>-1</sup>), streptomycin (50 µg ml<sup>-1</sup>; all from Invitrogen) and 5% (v/v) human serum (Swiss Blood Center). Jurkat cells were cultured in RPMI-1640 medium supplemented with 2 mM glutamine, penicillin (50 U ml<sup>-1</sup>), streptomycin (50 µg ml<sup>-1</sup>; all from Invitrogen) and 10% (v/v) fetal bovine serum. Cells were activated with plate bound anti-CD3 (5 µg ml<sup>-1</sup>, clone TR66) and anti-CD28 (1 µg ml<sup>-1</sup> CD28.2; BD Biosciences) for 48h. Then, only primary human T cells were cultured in IL-2 containing media (500 U ml<sup>-1</sup>). T cells were labeled with CFSE (Invitrogen) according to standard protocols.

In order to stimulate TCR transduced Jurkat cells, B cells were pre-incubated for 2 hours with recombinant HA (5 µg/ml) or the peptide pool (5 µg/ml) and irradiated (45 Gy) prior to T cell co-culture. Single cell clones were generated by limiting

dilution as described by Messi *et al.*<sup>312</sup>. In indicated experiments, 30 ng/ml OKT3 and 5 µg/ml anti-PD1 was used.

### **8.3 Flow cytometry**

The following antibodies were used for FACS analysis: CD3-APC (Biolegend, 300412), CD3-PE (Beckman Coulter, IM1282U), CD4-APC (Beckman Coulter, IM2468), CD4-FITC (Beckman Coulter, #A07750), CD8-APC (Beckman Coulter, #IM2469), CD45RA-QD655 (Life Technologies, #Q10069), CCR7-BV421 (Biolegend, #335208), CD19-PE-TR (Life Technologies, #MHCD1917), PD-1-BV785 (Biolegend, #329929), CD56-PE-Cy5 (Beckman Coulter, #A07789), CD14-V500 (BD, #561391).

### **8.4 Withdrawal assay**

Naïve CD4<sup>+</sup> T cells were activated with plate-bound CD3 and CD28 antibodies. 48 h after activation IL-2 was added to culture media (500 U ml<sup>-1</sup>). After a further 3 days of culturing, cells were washed, counted and equal cell numbers were plated in medium devoid of IL-2. The withdrawal medium was no longer supplemented with e.g. L-arginine. Cell viability was assessed with annexin V.

### **8.5 ATP measurement**

Naïve CD4<sup>+</sup> T cells were activated for four days in the presence or absence of L-arginine. Cells were washed, counted and 200'000 cells per sample were frozen in liquid nitrogen. ATP was extracted with distilled water by three freeze-thaw cycles and ATP content was determined using an ATP Determination Kit (Molecular Probes).

### **8.6 Metabolomics**

Naïve CD4<sup>+</sup> T cells were either analyzed directly after isolation or after different times of activation with CD3 and CD28 antibodies. Then, cells were washed twice in 96-well plates with 75 mM ammonium carbonate at pH 7.4 and snap frozen in liquid nitrogen. Metabolites were extracted three times with hot (>70°C) 70% ethanol. Extracts were analyzed by flow injection – time of flight mass spectrometry on an Agilent 6550 QTOF instrument operated in the negative mode as described

previously<sup>313</sup>. Typically 5'000-12'000 ions with distinct mass-to-charge (m/z) ratio could be identified in each batch of samples. Ions were putatively annotated by matching their measured mass to that of the compounds listed by the KEGG database for *homo sapiens* allowing a tolerance of 0.001 Da. Only deprotonated ions (without adducts) were considered in the analysis. In case of multiple matching such as in the case of structural isomers, all candidates were retained.

### **8.7 Metabolic flux experiments**

Naïve CD4<sup>+</sup> T cells were activated and four days later extensively washed and pulsed with L-arginine free RPMI medium containing 1 mM [U-<sup>13</sup>C]-L-Arginine hydrochloride (Sigma). After increasing pulse-times, cells were washed and snap frozen in liquid nitrogen. Metabolites were extracted and analyzed by HILIC LC-MS/MS.

### **8.8 Detection of amino acids and polyamines by HILIC LC-MS/MS**

Supernatants from extraction were dried at 0.12 mbar to complete dryness in a rotational vacuum concentrator setup (Christ, Osterode am Harz, Germany) and dried metabolite extracts were stored at -80°C. Dry metabolite extracts were resuspended in 100 µl water and 5 µl were injected on an Agilent HILIC Plus RRHD column (100 x 2.1 mm x 1.8 µm; Agilent, Santa Clara, CA, U.S.A.). A gradient of mobile phase A (10 mM ammonium formate and 0.1% formic acid) and mobile phase B (acetonitrile with 0.1% formic acid) was used as described previously<sup>314</sup>. Flow rate was held constant at 400 µl/min and metabolites were detected on a 5500 QTRAP triple quadrupole mass spectrometer in positive MRM scan mode (SCIEX, Framingham, MA, U.S.A.).

### **8.9 Sample preparation for proteome MS analysis**

Samples were processed as described by Hornburg et al.<sup>315</sup>. In brief, cell pellets were washed with PBS and lysed in 4% SDS, 10 mM HEPES (pH 8), 10 mM DTT. Cell pellets were heat-treated at 95°C for 10 min and sonicated at 4°C for 15 min (level 5, Bioruptor, Diagenode). Alkylation was performed in the dark for 30 min by adding 55 mM iodoacetamide (IAA). Proteins were precipitated overnight with acetone at -20°C and resuspended the next day in 8 M Urea, 10 mM Hepes (pH 8). A two-step

proteolytic digestion was performed. First, samples were digested at room temperature (RT) with LysC (1:50, w/w) for 3h. Then, they were diluted 1:5 with 50 mM ammoniumbicarbonate (pH 8) and digested with trypsin (1:50, w/w) at RT overnight. The resulting peptide mixtures were acidified and loaded on C18 StageTips<sup>316</sup>. Peptides were eluted with 80% acetonitrile (ACN), dried using a SpeedVac centrifuge (Eppendorf, Concentrator plus, 5305 000.304), and resuspended in 2% ACN, 0.1% trifluoroacetic acid (TFA), and 0.5% acetic acid. For deeper proteome analysis a peptide library was built. For this, peptides from naive and activated T cells were separated according to their isoelectric point on dried gel strips with an immobilized pH gradient (SERVA IPG BlueStrips, 3-10 / 11 cm) into 12 fractions as described by Hubner et al.<sup>317</sup>.

### **8.10 LC-MS/MS for analysis of proteome**

Peptides were separated on an EASY-nLC 1000 HPLC system (Thermo Fisher Scientific, Odense, Denmark) coupled online to a Q Exactive mass spectrometer via a nanoelectrospray source (Thermo Fisher Scientific)<sup>318</sup>. Peptides were loaded in buffer A (0.5% formic acid) on in house packed columns (75  $\mu$ m inner diameter, 50 cm length, and 1.9  $\mu$ m C18 particles from Dr. Maisch GmbH, Germany). Peptides were eluted with a non-linear 270 min gradient of 5-60% buffer B (80% ACN, 0.5% acetic acid) at a flow rate of 250 nl/min and a column temperature of 50°C. Operational parameters were real-time monitored by the SprayQC software<sup>319</sup>. The Q Exactive was operated in a data dependent mode with a survey scan range of 300-1750 m/z and a resolution of 70'000 at m/z 200. Up to 5 most abundant isotope patterns with a charge  $\geq 2$  were isolated with a 2.2 Th wide isolation window and subjected to higher-energy C-trap dissociation (HCD) fragmentation at a normalized collision energy of 25<sup>320</sup>. Fragmentation spectra were acquired with a resolution of 17,500 at 200 m/z. Dynamic exclusion of sequenced peptides was set to 45 s to reduce the number of repeated sequences. Thresholds for the ion injection time and ion target values were set to 20 ms and 3E6 for the survey scans and 120 ms and 1E5 for the MS/MS scans, respectively. Data was acquired using the Xcalibur software (Thermo Scientific).

### 8.11 Pulsed SILAC

Primary human CD4<sup>+</sup> T cells were cultured with control medium or “heavy” medium. The “heavy” medium contained <sup>15</sup>N<sub>2</sub><sup>13</sup>C<sub>6</sub>-lysine (Lys8) and <sup>15</sup>N<sub>4</sub><sup>13</sup>C<sub>6</sub>-arginine (Arg10) in SILAC medium (PAA) with 5 % dialyzed serum, penicillin, 2 mM glutamine, 1% (v/v) sodium pyruvate, penicillin (50 U ml<sup>-1</sup>), 50 μM β-mercaptoethanol and streptomycin (50 μg ml<sup>-1</sup>; all from Invitrogen). The cells were cultured for the indicated time in the medium. Afterwards the cells were processed for proteome analysis.

### 8.12 Tumor processing

The tumor samples were digested with the tumor dissociation kit from Miltenyi according to the user manual. In brief, the samples were cut in small pieces and transferred into a C-tube with the digestion solution. The tubes were attached to the gentle MACS and the program h\_tumor\_01 was started. Afterwards, the tubes were incubated for 30 minutes at 37 °C under continuous rotation. After a second run of the program h\_tumor\_01, the tubes were incubated for additional 30 minutes. The program h\_tumor\_01 was started a third time and the solution was filtered through a 70 μm strainer into a 50 ml tube. Bigger pieces stay in the C-tube and further digested by the program m\_imptumor\_01. The solution was passed through the same filter and the tube and filter was washed with 5 ml wash buffer (RPMI1640 + 10 % complete medium). The cells were pelleted by centrifugation and mononuclear cells were isolated by ficoll-gradient.

### 8.13 <sup>3</sup>H-arginine uptake assay

Arginine uptake was measured as previously described for glutamine uptake<sup>321</sup>. Briefly, resting or activated T cells were resuspended at a concentration of  $1.5 \times 10^7$  cells per milliliter in serum-free RPMI 1640 lacking L-arginine. 50 μl 8% sucrose/20% perchloric acid were layered to the bottom of a 0.5 ml eppendorf tube and 200 μl 1-bromododecane on top of it (middle layer), followed by 50 μl L-Arg free medium containing 1.5 mCi L-[2,3,4-<sup>3</sup>H]-arginine-monohydrochloride (Perkin Elmer). Then, 100 μl cell suspension was added to the top layer and cells were allowed to take up radiolabeled L-arginine for 15 min at room temperature. Then cells

were spun through the bromododecane into the acid/sucrose. This stops the reaction and separates cells from unincorporated  $^3\text{H}$ -arginine. The bottom layer containing the cells was carefully removed and analyzed by liquid scintillation. As controls cell-free media were used.

#### **8.14 Quantitative determination of amino acid uptake and calculation of proteome incorporation**

150'000 freshly isolated naïve  $\text{CD4}^+$  T cells were activated with plate bound CD3 and CD28 antibodies and cultured in the same medium for four days. As a control, medium without cells was co-cultured. Then cell supernatants and control media were analyzed by quantitative amino acid analysis (MassTrak, Waters) at the functional genomics center in Zurich. Amino acid uptake was calculated as the difference between control media and cell supernatants. At the time of the measurement, we counted on average 850'000 cells. We then calculated how much of each amino acid is incorporated into the proteome of 850'000 cells based on the amino acid sequences and copy numbers of each protein. Average copy numbers from the time point 72h were used.

#### **8.15 OCR measurement**

Measurements were performed using a Seahorse XF-24 extracellular flux analyzer (Seahorse Bioscience). Naïve  $\text{CD4}^+$  T cells were sorted and activated with plate-bound CD3 and CD28 antibodies in complete medium or medium supplemented with 3 mM L-Arg. Four days later, cells were pooled, carefully count and plated ( $7 \times 10^5$  cells/well) in serum-free unbuffered RPMI-1640 medium (Sigma) onto Seahorse cell plates coated with Cell-Tak (BD Bioscience). The serum-free unbuffered medium was not supplemented with L-Arg. Oligomycin (1.4  $\mu\text{M}$ , Sigma), Carbonyl cyanide-4-(trifluoromethoxy)phenylhydrazone (FCCP, 0.6  $\mu\text{M}$ , Sigma) and antimycin (1.4  $\mu\text{M}$ , Sigma) were injected.

#### **8.16 Nitric oxide detection assay**

To detect nitric oxide in primary human T cells DAF-FM diacetate (Thermo Fischer) was used. The procedure was in agreement with the standard protocol.



### 8.17 Limited proteolysis and mass spectrometry

Naïve CD4<sup>+</sup> T cells were washed twice with PBS and homogenized on ice under non-denaturing conditions (20 mM Hepes, 150 mM KCl and 10 mM MgCl<sub>2</sub>, pH 7.5,) using a tissue grinder (Wheaton, Millville, NJ, NSA). Homogenates were further passed several times through a syringe (0.45x12mm) on ice. Next, cell debris was removed by centrifugation and protein concentration of supernatants was determined by BCA assay (BCA Protein Assay Kit, Thermo Scientific, Rockford, IL, USA). L-arginine (L-arg) or D-arginine (D-arg) was added to homogenates to a final concentration of 1 nmol per µg total protein, and incubated for 5 minutes at room temperature. As a control, samples without added metabolites were processed in parallel. Then, proteinase K from *Tritirachium album* (Sigma) was added at an enzyme to substrate ratio of 1:100, followed by an incubation of 5 minutes at room temperature. The digestion was stopped by boiling the reaction mixture for 3 minutes. Proteins were denatured by adding 10% sodium deoxycholate (DOC) solution (1:1, v/v) to the reaction mixture, followed by a second boiling step of 3 minutes. Disulfide bridges were reduced with 5 mM Tris(2-carboxyethyl)phosphine hydrochloride (Thermo Scientific) at 37°C for 30 minutes and subsequently free cysteines were alkylated with 40 mM IAA at 25 °C for 30 minutes in the dark. DOC concentration of the mixture was diluted to 1% with 0.1 M ammonium bicarbonate (AmBiC) prior to a stepwise protein digestion with LysC (1:100, w/w) for 4 hours at 37°C and trypsin (1:100, w/w) overnight at 37°C. The resulting peptide mixture was acidified to pH < 2, loaded onto Sep-Pak tC18 cartridges (Waters, Milford, MA, USA), desalted and eluted with 80% acetonitrile. Peptide samples were dried using a vacuum centrifuge and resuspended in 0.1% formic acid for analysis by mass spectrometry.

Peptides were separated using an online EASY-nLC 1000 HPLC system (Thermo Fisher Scientific) operated with a 50 cm long in house packed reversed-phase analytical column (Reprosil Pur C18 Aq, Dr. Maisch, 1.9 µm) (Reprosil Pur C18 Aq, Dr. Maisch, 1.9 µm) before being measured on a Q-Exactive Plus (QE+) mass spectrometer. A linear gradient from 5-25% acetonitrile in 240 min at a flowrate of 300 nl/min was used to elute the peptides from the column. Precursor ion scans were measured at a resolution of 70,000 at 200 m/z and 20 MS/MS spectra were acquired after higher-energy collision induced dissociation (HCD) in the Orbitrap at a

resolution of 17,500 at 200 m/z per scan. The ion count threshold was set at 1,000 to trigger MS/MS, with a dynamic exclusion of 25 s. Raw data were searched against the *H. sapiens* Uniprot database using SEQUEST embedded in the Proteome Discoverer software (both Thermo Fisher Scientific). Digestion enzyme was set to trypsin, allowing up to two missed cleavages, one non-tryptic terminus and no cleavages at KP (lysine-proline) and RP (arginine-proline) sites. Precursor and fragment mass tolerance was set at 10 ppm and 0.02 Da, respectively. Carbamidomethylation of cysteines (+57.021 Da) was set as static modification whereas oxidation (+15.995 Da) of methionine was set as dynamic modification. False discovery rate (FDR) was estimated by the Percolator (embedded in Proteome Discoverer) and the filtering threshold was set to 1%.

Label-free quantitation was performed using the Progenesis-QI Software (Nonlinear Dynamics, Waters). Raw data files were imported directly into Progenesis for analysis. MS1 feature identification was achieved by importing the filtered search results (as described above) from Proteome Discoverer into Progenesis to map the corresponding peptides based on their m/z and retention times. Annotated peptides were then quantified using the areas under their extracted ion chromatograms. Pairwise comparisons were performed with the untreated (no metabolite added) sample as a reference and peptide fold changes were calculated using three biological replicates per condition where the statistical significance was assessed with a two-tailed heteroscedastic Student's t-Test. A fold change was considered significant with an absolute change > 5 and a corresponding p-value < 0.05. Only proteins with two or more peptides changing significantly (according to the aforementioned criteria) were taken into consideration. To reduce false discoveries only proteins with a molecular mass of less than 200 kDa and an abundance of less than 1 Mio copies per cell were considered. Protein candidates, which were also identified as D-arginine interactors, were removed from the list of potential L-arginine interactors.

### **8.18 CRISPR/Cas9-mediated gene disruption**

Two to four short guide RNAs (sgRNAs) per gene (Tab. 8.1) were designed using the online tool provided by the Zhang laboratory (<http://tools.genome-engineering.org>). Oligonucleotide pairs with BsmBI-compatible overhangs were annealed and cloned

into the lentiviral vector lentiCRISPR v2 (Addgene plasmid # 52961)<sup>322</sup>. For virus production, HEK293FT cells were transfected with lentiCRISPR v2, psPAX2 (Addgene # 12260) and pMD2.G (Addgene plasmid # 12259) at a 8:4:1 ratio using polyethylenimine and cultured in Dulbecco's modified Eagle medium supplemented with 10 % fetal bovine serum (FBS), 1% sodium pyruvate, 1 % non-essential amino acids, 1 % Kanamycin, 50 Units/ml Peniciline/Streptomycine and 50  $\mu$ M  $\beta$ -mercaptoethanol. The medium was replaced 12 h after transfection and after a further 48 h virus was harvested from supernatant. Cell debris was removed by centrifugation (10 min at 2000 rpm) followed by ultra-centrifugation (2.5 hours at 24'000 rpm) through a sucrose cushion.

Freshly isolated naïve CD4<sup>+</sup> T cells were lentivirally transduced and activated with plate-bound CD3 and CD28 antibodies. 48 h after activation IL-2 was added to culture media (500 U/ml<sup>-1</sup>). 6 days after activation, cells were cultured for 2 days in medium supplemented with 1  $\mu$ g/ml puromycin to select for cells expressing the lentiCRISPR v2 vector. Subsequently, cells were cultured in normal medium followed by additional two days in medium containing puromycin for a second selection step. Then, single cell clones were generated by limiting dilution as described by Messi *et al.*<sup>312</sup>.

The sg for the TCR  $\alpha$  and  $\beta$  chain were cloned into pSpCas9(BB)-2A-GFP (PX458), which was a gift from Feng Zhang (Addgene plasmid # 48138). Jurkat cells and primary human T cells were transfected with the Human T cell Nucleofector kit (Lonza) based on the optimized protocol recommended by the company.

To screen for clones with disrupted target genes, individual clones were lysed with sample buffer containing 80 mM Tris pH 6.8, 10.5 % glycerol, 2 % SDS and 0.00004 % Bromophenol blue. Lysate of 100'000 cells was separated by SDS-PAGE followed, blotted onto PVDF membranes and analyzed with antibodies to target proteins, Baz1B (Abcam, ab50850), PSIP1 (Bethyl, A300-848A), DDX17 (Abcam, ab180190), PTPN6 (Santa Cruz, sc-287) or TSN (Sigma, HPA059561). As loading control membranes were reprobated with an antibody to beta-tubulin (Sigma, T6074). To screen for clones with disrupted *B2M*, single cell clones were stained with an

antibody to MHC-I (eBioscience, HLA-ABC-FITC) and analyzed by flow cytometry. TCR depleted Jurkat cells were screened via the surface of expression of CD3.

**Tab. 8.1: Overview of designed sgRNAs.**

Target	sg	Target sequence
ACIN1	1	GAG TTC TGA GTG GTA ATC GA
	2	GGT ACT CGG GTC CGT CCC GA
ACTR	1	TGG TGT GCG ACA ACG GCA CC
	2	ACT GGT GTA GTG GTA GAC TC
B2M	1	GAG TAG CGC GAG CAC AGC TA
	2	CCT GAA TCT TTG GAG TAC GC
Baz1B	1	AGT ATG AAG CCC GCT TGG AA
	2	ATT TGG ACG TGC AAG AGT AC
	3	AAC GGC TTC ACC AGC GGG AA
	4	AAA GGT ACA GTG AGC GCA TT
CAP1	1	AAG GAC TGT CTG CAT ACC CA
	2	AGG AGC AGC TCC ATA TGT GC
DDX17	1	GCC GCC TCT CTC GTC GGA GA
	2	TCC GGT CTG GTG ACG ACC GA
MTPN	1	GTG CGA CAA GGA GTT CAT GT
	2	GAT GTC AAC CGG ACA CTA GA
PTPN6	1	GGT TTC ACC GAG ACC TCA GT
	2	GGA CAC CTC GGC CCT TGA GC
PSIP	1	ATG ACT CGC GAT TTC AAA CC
	2	AAA AGA GCC GGA TAA AAA AG
SSB	1	TCC TTT AGA AAC TTG TCC CG
	2	GGA TGA AGG CTG GGT ACC TT
TCRA	1	TGT GCT AGA CAT GAG GTC TA
	2	AAA GTC AGA TTT GTT GCT CC
TCRB	1	TCT CCG AGA GCC CGT AGA AC
	2	GGC TCT CGG AGA ATG ACG AG
TSN	1	TGA AAT CCT TTC TCC CGA TC
	2	AAC CTG TAA TAC TGT TCA GC
XRCC	1	CTC TGC TTC TTC ATC GCC CT
	2	ATC CGT GGC CCA TCA TGT CT

### 8.19 Analysis of phosphorylation level of 4E-BP and S6K1

Naïve CD4<sup>+</sup> T cells were activated with plate-bound antibodies to CD3 and CD28. Four days after activation, cells were lysed and analyzed by Western blot with the following antibodies obtained from Cell Signaling Technology. Phospho-p70

S6K(Thr389) #9205; p70 S6 Kinase #9202; Phospho-4E-BP1 (Thr37/46) #2855; 4E-BP1 #9644. Rapamycin (Sigma) was used at 100 nM.

### **8.20 Cytokine assay**

$10^5$  naïve CD4<sup>+</sup> T cells were stimulated with plate bound anti-CD3 ( $5 \mu\text{g ml}^{-1}$ ) and anti-CD28 ( $1 \mu\text{g ml}^{-1}$ ) in the presence of IL-12 (10 ng/ml, R&D Systems) to polarize cells towards a Th1 phenotype. After 48 h, cells were transferred into U-bottom plates and IL-2 (10 ng/ml, R&D Systems) was added. Three days later, supernatants were collected and interferon- $\gamma$  was quantified using FlowCytomix assays (eBioscience). Samples were analyzed on a BD LSR Fortessa FACS instrument and quantification was performed with the FlowCytomix Pro 3.0 software. For re-stimulation, cells were cultured for 5 h in the presence of  $0.2 \mu\text{M}$  phorbol 12-myristate 13-acetate (PMA) and  $1 \mu\text{g/ml}$  ionomycin (both from Sigma).

### **8.21 Glucose consumption assay**

The amount of glucose in media was determined using the Glucose (GO) Assay Kit from Sigma. Consumption was calculated as the difference between glucose content in reference medium (co-incubated medium without cells) and cell supernatants.

### **8.22 Serial block-face scanning electron microscopy and 3D reconstruction of single layers**

The analysis of resting and activated cells via electron microscopy was performed at the Biozentrum of the university of Basel, Switzerland. The experiments were performed according to established protocols. The 3D reconstruction was generated with 3Dmod.

### **8.23 Measuring single cell densities**

A microfluidic device was used to measure single cell densities. The experimental procedure was adapted to the protocol of Grover *et al.*<sup>274</sup>

### **8.24 Estimation of transcript copy numbers**

Total RNA was isolated from flow sorted naïve CD4<sup>+</sup> T cells using the RNeasy Plus Mini Kit from Qiagen. RNA samples from two healthy donors were pooled and sent to IGA technology services. The TruSeq Stranded mRNA Sample Prep kit

(Illumina, San Diego, CA) was used for library preparation starting with 1-2 µg of RNA (R.I.N. >7) as input. The poly-A mRNA was fragmented 3 minutes at 94°C and every purification step was performed by using 1X (or 0.6X if paired end reads) Agencourt AMPure XP beads. Both RNA samples and final libraries were quantified using the Qubit 2.0 Fluorometer (Invitrogen, Carlsbad, CA) and quality tested by Agilent 2100 Bioanalyzer RNA Nano assay (Agilent technologies, Santa Clara, CA). Libraries were then processed with Illumina cBot for cluster generation on the flowcell and sequenced on single-end (or paired-end if required) mode at the multiplexing level requested on HiSeq2500 (Illumina, San Diego, CA). The CASAVA 1.8.2 version of the Illumina pipeline was used to process raw data for format conversion and de-multiplexing.

### 8.25 qPCR

cDNA-coated beads were analyzed for the TCR abundants via qPCR. The Sso Advanced universal SYBR Green Supermix from BioRAD (#172-5271) was used according to the recommended protocol. The plates were analyzed with QunatStudio 3 from Thermo Fisher Scientific.

**Tab. 8.2: Primers used for qPCR.**

Name	Sequence
TRBC for	CACTTCCGCTGTCAAGTCCAGTTCTAC
TRBC rev	CCTAGCAGGATTCATAGAGGATGGT
TRAC for	GCTGAGAGACTCTAAATCCAGTGAC
TRAC rev	GGTGTCTTCTGGAATAATGCTG

### 8.26 Microfluidic device handling and droplet PCR

The microfluidic chip used in this study was designed and produced by Yun Ding in the lab of Andre deMello (ETH Zurich) (Fig. 6.24A). The same chip was used for the encapsulation of cells together with lysis buffer and mRNA capturing beads, as well as the droplet PCR. The oligo d(T)<sub>25</sub> coated polystyrene beads were produced by Spherotech and had an average diameter of 10 µm. QX200™ Droplet Generation Oil for EvaGreen (BioRAD, #1864006) was used.

For the mRNA capturing within droplets, cells were used at a concentration of 500'000 cells/ml. The cells were washed with PBS and resuspended in PBS containing 0.1 % BSA and 16 % Opti-Prep. The beads were washed with 0.2 M tris pH 8.0 and centrifugated for 2 min at 4'000 x g. The supernatant was removed and the beads were resuspended in lysis buffer (6 % Ficoll 400, 2 % Sarkosyl, 20 mM EDTA, 0.2 M Tris pH 8.0, 50 mM DTT) at a concentration of  $10^7$  beads/ml. The cells and beads were stored on ice until usage. A 5 ml syringe (BD, #309649) was loaded with the mineral oil. For the beads and cells, 1 ml syringes (0.33 mm (29 G) x 12.7 mm, BD, #324927) were flushed once with the corresponding buffer before loading the cells or beads. All syringes were connected via Tygon tubing to the microfluidic chip. The syringes were placed in a low-pressure syringe pump neMESYS 290N and the flow rates were adjusted to 25  $\mu$ l/min for oil and 2.5  $\mu$ l/min for beads or cells. The generated droplets were collected in a 50 ml falcon tube.

After the entire solution passed the microfluidic device, the outlet tubing was removed from the 50 ml falcon tube and the tube was centrifuged for 1 min at 100 x g. Additional oil was removed and 20 ml TE/TW (10 mM Tris pH 8.0, 1 mM EDTA, 1 % Tween-20) was added. The droplets were broken by the addition of 1 ml PicoBreak (Sphere Fluidics, # 3200229). After the tube was inverted 3 times, it was centrifuged for 1 min at 1'000 x g. The supernatant was removed and the beads were kicked up three times with 6 ml TE/TW. The beads were transferred to a new 50 ml falcon tube and centrifuged for 5 min at 3'200 x g. The supernatant was removed but 1 ml, which was used to resuspend the beads and transfer them into a 1.5 ml DNA low binding tube. After a centrifugation of 4'000 x g for 2 min, the beads were washed for two times with 1 x reverse transcription buffer. The washed beads were stored in 1 x reverse transcription buffer for short terms or directly resuspended in reverse transcription mix (1 x First strand buffer, 0.9 mM each dNTP, 10 mM DTT, 0.85 units/ $\mu$ l RNasin, 2 units/ $\mu$ l SuperScript III reverse transcriptase). The tubes were incubated for 90 min at 50 °C with soft resuspension every 30 mins. Afterwards, the beads were washed once with 1 x polymerase buffer and short term stored at 4 °C or directly used for droplet PCR. The PCR-mix contained 1 x polymerase buffer, 0.625 mM of each dNTP, 0.25 mM TRC primer mix (Tab. 8.3), 0.25 mM TRAL primer mix (Tab. 8.4), 0.25 mM TRBL primer mix (Tab. 8.5), 0.1 units/ $\mu$ l PfuUltra, 0.1 % BSA.

**Tab. 8.3: Overview of T cell receptor constant region primer.** Primers called link were used for the linker PCR and primer called nested were used for nested PCR. The overhangs were used to clone the linked PCR product into the lentiviral vector. Link and nested primers were mixed equally.

name	overhang	sequence
TRAC link		AGCACAGGCTGTCTTACAATCTTGC
TRAC nested	CAACTAGAAGGCACAGTCGC	TACAATCTTGCAGATCTCAGCTGG
TRBC1 link		CTCCTAACTCCACTTCCAGGGCTGC
TRBC1 nested	CAGAGGTTGATTGTCGACGC	GGGCTGCCTTCAGAAATCC
TRBC2 link		GAATGACCTGGGATGGTTTTGGAGC
TRBC2 nested	CAGAGGTTGATTGTCGACGC	GAGCTAGCCTCTGGAATCC

**Tab. 8.4: Overview of TRAL primers.** All primers contained the sequence GATTGAGCGGCCGCTAGGTATGAGCCACC on the 5' site and were mixed equally.

name	sequence	reactivity
A1	ATGTGGGGAGYTTTCCTTCTYTATG	1.1, 1.2
A2	ATGGCTTTCAGAGCACTCTGGGGGC	2
A3	ATGGCCTCTGCACCCATCTCGATGC	3
A4	ATGAGGCAAGTGGCGAGAGTGATCGTG	4
A5	ATGAAGACATTTGCTGGATTTTCGTTT	5
A6	ATGGAGTCATTCCTGGGAGGTGTTTTG	6
A7	ATGCTCCTGTTGCTCATACCACTGC	8.1
A8	ATGCTCCTGCTGCTCGTCCCAGYGYTC	8.2, 8.4, 8.6
A9	ATGCTCCTGGWGCTYATCCCCTGCTG	8.3, 8.5
A10	ATGAACTATTCTCCAGGCTTAGTATC	9.2
A11	ATGAAAAAGCATCTGACGACCTTCTTG	10
A12	ATGAWATCCTTGAGAGTTTACTRGTG	12.1, 12.2, 12.3
A13	ATGATGAAATCCTTGAGAGTTTACTG	12.3
A14	ATGACATCCATTCGAGCTGTATTTATATTC	13.1
A15	ATGGCAGGCATTCGAGCTTTATTTATG	13.2
A16	ATGTCACTTTCTAGCCTGCTGAAGG	14/DV4
A17	ATGAAGCCCACCCTCATCTCAGTGC	16
A18	ATGGAACTCTCCTGGGAGTGTCTTTG	17
A19	ATGCTGACTGCCAGCCTGTTGAGGGC	19
A20	ATGGAGAAAATGTTGGAGTGTGCATTC	20
A21	ATGGAGACCCTCTGGGCCTGCTTATCC	21
A22	ATGAAGAGGATATTGGGAGCTCTGCTG	22
A23	ATGGACAAGATCTTAGGAGCATC	23/DV6
A24	ATGGAGAAGAATCCTTTGGCAGCCCCATTAC	24
A25	ATGCTACTCATCACATCAATGTTGGTC	25
A26	ATGAAGTTGGTGACAAGCATTACTG	26.2
A27	ATGGTCCTGAAATTCTCCGTGTCCATTC	27
A28	ATGGCCATGCTCCTGGGGGCATCAGTG	29/DV5
A29	ATGGAGACTGTTCTGCAAGTACTCCTAGG	34
A30	ATGCTCCTTGAACATTTATTAATAATC	35
A31	ATGATGAAGTGTCCACAGGCTTACTAGC	36
A32	ATGACACGAGTTAGCTTGCTGTGGGC	38.1
A33	ATGGCATGCCCTGGCTTCTGTGGGC	38.2/DV8
A34	ATGAAGAAGCTACTAGCAATGATTCTGTGG	39
A35	ATGAACTCCTCTCTGGACTTTCTAATTCTG	40



**Tab. 8.5: Overview of TRBL primers.** All primers contained the sequence TACCTAGCGGCCGCTCAATCGTTGCCGCC on the 5' site and were mixed equally.

name	sequence	reactivity
B1	ATGGATAYCTGGCTCSTMTGCTGGG	2, 17
B2	ATGGGCTGCAGGCTGCTCTGCTGTGCG	4.1, 4.2, 4.3
B3	ATGGGCTCCAGGCTGCTCTGTTGG	5.1
B4	ATGGGCCCYGGGCTCCTCTGCTGGG	5.3, 5.4, 5.5, 5.6, 5.7
B5	ATGGGACCCAGGCTCCTCTTCTGGGC	5.8
B6	ATGAGMATCRGSCTCCTGTGCTGTG	6.1, 6.4, 6.5, 6.6, 6.7
B7	ATGAGCCTCGGGCTCCTGTGCTGTG	6.1, 6.2, 6.3, 6.7, 6.8, 6.9
B8	ATGGGCACMAGGCTCCTCTKCTGGG	7.1, 7.2, 7.3, 7.4, 7.5, 7.8, 11.2
B9	ATGGGYACCAGTCTCCTATGCTGGGTG	7.6, 7.7
B10	ATGRGCACCAGSCTYCTCTGCTGGATG	7.9, 11.1
B11	ATGGGCTKCAGGCTCCTCTGCTRTGTG	3.1, 3.2, 9
B12	ATGGGCACMAGGSTSTTCTTCTATG	10.1, 10.2, 10.3
B13	ATGGSYACCAGGCTCCTCTGCTGKGTG	7.4, 7.5, 7.8, 11.3, 12.5
B14	ATGGACTCCTGGACCTTCTGCTGTG	12.3
B15	ATGGACTCCTGGACCCTCTGCTGTG	12.4
B16	ATGCTTAGTCCTGACCTGCCTGAC	13
B17	ATGGTTTCCAGGCTTCTCAGTTTAG	14
B18	ATGGGTCCTGGGCTTCTCCACTGG	15
B19	ATGAGCCCAATATTCACCTGCATC	16
B20	ATGGACACCAGAGTACTCTGCTGTGC	18
B21	ATGAGCAACCAGGTGCTCTGCTGTG	19
B22	ATGCTGCTGCTTCTGCTGCTTCTG	20.1
B23	ATGGCCTCCCTGCTCTTCTTCTGTGG	24.1
B24	ATGACTATCAGGCTCCTCTGCTACATGG	23.1
B25	ATGGGCCCCCAGCTCCTTGGCTATG	27
B26	ATGGGAATCAGGCTCCTCTGTCTGTG	28
B27	ATGCTGAGTCTTCTGCTCCTTCTCC	29.1

The procedure for the encapsulation of cDNA-coated beads for droplet PCR was similar to the one described above, but a bigger outlet tube was used to slow down the speed of outlet droplets. The inlet for cells was blocked and the flow rate for the bead/PCR mix was 5 µl/min. The general setup is shown in Fig. 8.1.

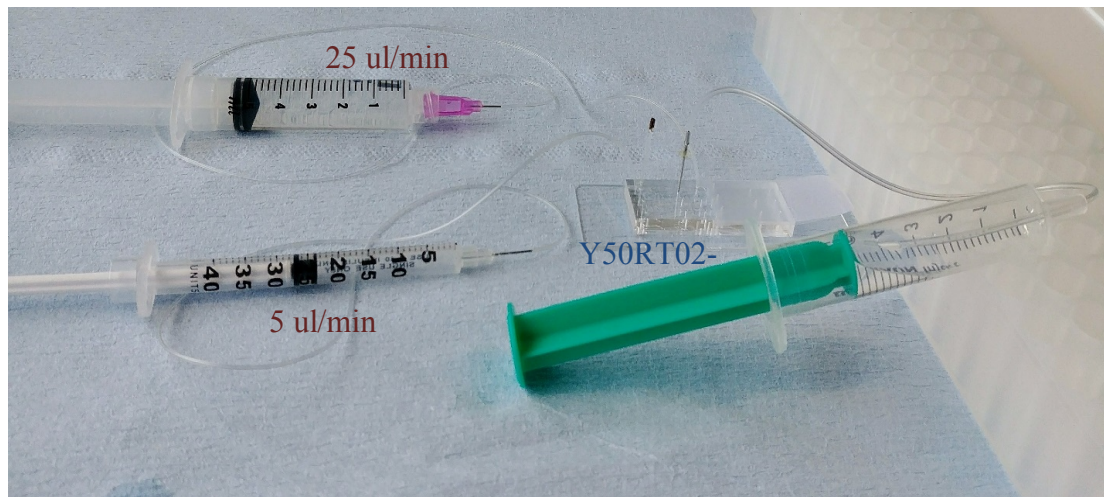


**Fig. 8.1:** Overview of the setup of microfluidic device to generate droplets for the droplet PCR.

### **8.27 Design of CD4 and NFAT-GFP construct**

The coding sequence of CD4 was PCR-amplified from the cDNA of activated CD4<sup>+</sup> T cells from a human donor and cloned into a lentiviral vector. The NFAT-binding sequence was PCR-amplified from the NFAT luciferase reporter, which was a gift from Toren Finkel<sup>323</sup> (Addgene plasmid #10959) and cloned into a lentiviral vector in front of GFP.

### **8.28 Droplet generation with vortex mixer**

To test the linker PCR within droplets, we adapted a protocol from Schütze *et al.*<sup>324</sup>. In brief, we added 600 µl of oil (mineral oil or fluorinated oil) to 200 µl PCR mix and fixed the tube to a vortex mixer. We vortexed the samples for 5 min at full or half speed at 4 °C. Afterwards, the droplets were transferred to a PCR tube and placed into a thermal cycler for PCR amplification.

### **8.29 MinION sequencing**

Oxford Nanopore Technology (ONT) was used to sequence the PCR product of the linked TCR chains. Different PCR conditions could be separated based on barcodes introduced during the nested PCR. The Nanopore 2D sequencing kit SQK-LSK207 was used to generate the sequencing library, which was loaded onto the Nanopore flow cells FLO-MIN106. We sequenced for 20 h with the MinION Mk1B for 6 h.

## 8.30 Animal experiments

Camilla Basso performed the mice experiments.

### 8.30.1 Mice

C57BL/6J and BALB/c mice were obtained from Envigo (Italy). CD3 $\epsilon^{-/-}$  mice, which lack all T cells but exhibit organized lymphoid organ structures and normal B cell development, have been described previously<sup>325</sup>. All OT-I (JAX 003831) mice were bred and maintained on a Rag1 $^{-/-}$  (JAX 002216) background. ARG2 KO C57BL/6 mice were kindly provided by W. Reith (JAX 020286). HA TCR-transgenic BALB/c mice were kindly provided by J. Kirberg and bred in our facility. All mice were bred and maintained under specific pathogen-free conditions. Animals were treated in accordance with guidelines of the Swiss Federal Veterinary Office or the Institutional Animal Care and Use Committee guidelines of the University of California, San Francisco, and experiments were approved by the Dipartimento della Sanita` e Socialita` of Canton Ticino.

### 8.30.2 Isolating and culturing of mouse CD8<sup>+</sup> T cells

Naïve OT-I CD8<sup>+</sup> cells were isolated from Rag1 $^{-/-}$  OT-I transgenic mice. Lymph nodes and spleens were harvested and homogenized using the rubber end of a syringe and cell suspensions were filtered through a fine mesh. Cells were first enriched with anti-CD8 magnetic beads (CD8a, Ly-2 MicroBeads, mouse, Miltenyi Biotec) and then sorted on a FACSAria III Cell Sorter (BD Biosciences) to obtain cells with a CD8<sup>+</sup>CD44<sup>low</sup>CD62L<sup>high</sup> phenotype. OT-I cells CD90.1<sup>+</sup> were cultured for 2 days in  $\alpha$ CD3/ $\alpha$ CD28 (2ug/ml) bound to NUNC 96 well MicroWell™ MaxiSorp™ plates, (Sigma-Aldrich M9410) in the presence or absence of 3 mM L-arginine in the culture medium. On day 2 cells were transferred to U-bottom plates and cultured for 2 additional days in the presence of IL-2 (500 U/ml).

### 8.30.3 Adoptive T cell transfer and survival experiments

OT-I CD90.1<sup>+</sup> CD45.1/2<sup>+</sup> cells were activated with plate-bound CD3 and CD28 antibodies in complete medium. OT-I cells with a different congenic marker (CD90.1<sup>+</sup> CD45.1<sup>+</sup>) were activated in medium supplemented with 3 mM L-arginine.

At day four, equal cell numbers were injected into the tail vein of CD3 $\epsilon$ <sup>-/-</sup> host mice. To study the expansion of OT-I effector cells, host mice were sacrificed after 1, 3, 6, and 10 days post transfer and CD90.1<sup>+</sup> OT-I T cells from lymphoid organs (spleen and lymph nodes) were enriched with anti-CD90.1 micro beads (Miltenyi Biotec), stained and analysed by FACS. The following monoclonal antibodies were used  $\alpha$ -CD8 $\alpha$  (53-6.7),  $\alpha$ -CD44 (IM7),  $\alpha$ -CD62L (MEL-14),  $\alpha$ -CD90.1 (OX-7),  $\alpha$ -CD90.2 (30-H12),  $\alpha$ -CD45.1 (A20),  $\alpha$ -CD45.2 (104).

#### **8.30.4 Tumor experiments: *in vitro* activation of T cells**

B16-OVA cells were cultured in RPMI 1640 plus 10% FCS, 1% penicillin/streptomycin and 2 mM glutamine. Before injection into mice, cells were trypsinized and washed twice in PBS. Then, 5x10<sup>5</sup> cells were subcutaneously injected in the dorsal region of C57BL/6 mice. Ten days post injection, 5\*10<sup>6</sup> OT-I cells that have been activated *in vitro* (as described above) were injected into the tail vein of the mice. The size of tumors was measured in a blinded fashion using calipers.

#### **8.30.5 Tumor experiments: *in vivo* priming of T cells**

B16-OVA melanoma cells were cultured and injected into wild type C57BL/6 mice as described above. Five days post injection, tumor-bearing mice were  $\gamma$ -irradiated (5 Gy) and 24 hours later they received 4 to 8\*10<sup>5</sup> OT-I cells intravenously (i.v.). The day after mice were immunized intraperitoneally (i.p.) with SIINFEKL peptide (OVA<sub>257-264</sub>) in Imject Alum Adjuvant (Thermo Fisher Scientific). L-Arg (1.5 g/Kg body weight) or PBS, as control, was daily orally administered, starting one day before T cell transfer and until the end of the experiment. The size of tumors was measured in a blinded fashion using calipers.

#### **8.30.6 Experiments with Arg2<sup>-/-</sup> mouse T cells**

For *in vitro* experiments, 5x10<sup>4</sup> FACS-sorted naïve T cells were activated with plate-bound antibodies to CD28 (2  $\mu$ g/ml) and CD3 (2  $\mu$ g/ml). Two days after activation, T cells were transferred into U-bottom plates and IL-2 was added to culture media. Four days after activation, cells were washed and plated in medium devoid of IL-2. Cell viability was measured two days after IL-2 withdrawal using annexin V. For *in vivo* experiments 10<sup>6</sup> FACS-sorted wild type CD8<sup>+</sup> naïve T cells (CD45.1<sup>+</sup>) were

transferred together with  $10^6$  FACS-sorted Arg2 KO CD8<sup>+</sup> naïve T cells (CD45.2<sup>+</sup>, CD90.2<sup>+</sup>), into slightly  $\gamma$ -irradiated (3 Gy) WT mice (CD45.2<sup>+</sup>, CD90.1<sup>+</sup>). The day after, host mice were immunized subcutaneously (s.c.) with MHC class-I binding peptide SIINFEKL (Chicken Ovalbumin, OVA, amino acids 257-264, 15  $\mu$ g/mouse) emulsified in Complete Freund's Adjuvant, CFA. CFA was prepared by adding 4 mg/ml of *M. tuberculosis* H37RA, from Difco, to Incomplete Freund's Adjuvant, IFA, from BD. SIINFEKL peptide (OVA<sub>257-264</sub>) was obtained from Servei de Proteòmica, Pompeu Fabra University, Barcelona, Spain. On day 15 post immunization mice were euthanized and draining lymph nodes (dLNs) were collected and analyzed by flow cytometry. Cells were counted according to the expression of congenic markers and by gating on live CD8<sup>+</sup>, CD44<sup>+</sup>, H-2kb OVA<sub>257-264</sub> multimer<sup>+</sup> cells. The H-2kb OVA<sub>257-264</sub> multimer was purchased from TCMetrix.

### **8.30.7 Mouse experiments with dietary L-arginine**

$2 \times 10^5$  CD4<sup>+</sup> CD90.1<sup>+</sup> hemagglutinin (HA) TCR-transgenic T cells, on a BALB/c background, were adoptively transferred in WT CD90.2<sup>+</sup> BALB/c mice. The day after host mice were immunized s.c. with influenza HA<sub>110-120</sub> peptide emulsified in CFA. L-Arg (1.5 g/kg body weight) or PBS, as control, was daily orally administrated, starting 1 day before T cell transfer and until the end of the experiment. dLNs were analysed on day 15 p.i. for the presence of transferred transgenic memory CD4<sup>+</sup> CD44<sup>+</sup> CD90.1<sup>+</sup> T cells.

### **8.31 Quantification and statistical analysis**

Roger Geiger did the analysis of proteomics data and enrichment analysis.

#### **8.31.1 Analysis of proteomics data**

MaxQuant software (version 1.3.10.18) was used to analyze MS raw files<sup>326</sup>. MS/MS spectra were searched against the human Uniprot FASTA database (Version May 2013, 88'847 entries) and a common contaminants database (247 entries) by the Andromeda search engine<sup>327</sup>. Cysteine carbamidomethylation was applied as fixed and N-terminal acetylation and methionine oxidation as variable modification. Enzyme specificity was set to trypsin with a maximum of 2 missed cleavages and a

minimum peptide length of 7 amino acids. A false discovery rate (FDR) of 1% was required for peptides and proteins. Peptide identification was performed with an allowed initial precursor mass deviation of up to 7 ppm and an allowed fragment mass deviation of 20 ppm. Nonlinear retention time alignment of all measured samples was performed in MaxQuant. Peptide identifications were matched across different replicates within a time window of 1 min of the aligned retention times. A library for 'match between runs' in MaxQuant was built from additional single shot analysis at various time points as well as from OFF gel fractionated peptides of naïve and memory CD4<sup>+</sup> T cells. Protein identification required at least 1 razor peptide. A minimum ratio count of 1 was required for valid quantification events via MaxQuant's Label Free Quantification algorithm (MaxLFQ)<sup>326,328</sup>. Data were filtered for common contaminants and peptides only identified by side modification were excluded from further analysis. In addition, it was required to have a minimum of two valid quantifications values in at least one group of replicates. Copy numbers were estimated based on the protein mass of cells<sup>329</sup>. We found the protein mass of a naïve T cells to be 25 pg and of activated T cells 75 pg.

### 8.31.2 Enrichment analysis

Univariate test was performed on either all proteins or metabolites by t-test with unequal variance (Welch Test). The resulting p-values were adjusted using the Benjamini-Hochberg procedure. Enrichment analysis was performed as suggested by Subramanian *et al.*<sup>330</sup>. Both for metabolomics and proteomics data, we applied a permissive filtering with adj. p-value less or equal than 0.1 and absolute log<sub>2</sub>(fold-change) larger or equal than 0.5. Enrichment p-values were calculated by the Fisher's exact test for all incremental subsets of filtered features ranked by the p-value. For the 261 pathways defined by KEGG, the lowest p-value was retained as a reflection of the best possible enrichment given by the data independently of hard cut-offs. Eventually, enrichment p-values were corrected for multiple testing by the Benjamini-Hochberg method. In general, enrichments with an adjusted p-value < 0.05 were considered significant. Pathway enrichments were calculated independently for proteomics and metabolomics data. For metabolome-based enrichments, structural isomers in pathway were condensed and counted only once to account for the fact that the employed technology cannot distinguish between metabolite with identical molecular weight.

## 9 References

1. Abbas, A. K., Lichtman, A. H. & Pillai, S. *Cellular and Molecular Immunology E-Book*. (Elsevier Health Sciences, 2014).
2. Girardi, M. Immunosurveillance and immunoregulation by  $\gamma\delta$  T cells. *Journal of Investigative Dermatology* **126**, 25–31 (2006).
3. Arstila, T. P. *et al.* A direct estimate of the human  $\alpha\beta$  T cell receptor diversity. *Science* **286**, 958–961 (1999).
4. Turner, S. J., Doherty, P. C., McCluskey, J. & Rossjohn, J. Structural determinants of T-cell receptor bias in immunity. *Nature reviews. Immunology* **6**, 883 (2006).
5. Kondo, M., Weissman, I. L. & Akashi, K. Identification of clonogenic common lymphoid progenitors in mouse bone marrow. *Cell* **91**, 661–672 (1997).
6. Akashi, K., Traver, D., Miyamoto, T. & Weissman, I. L. A clonogenic common myeloid progenitor that gives rise to all myeloid lineages. *Nature* **404**, 193 (2000).
7. Blom, B. & Spits, H. Development of human lymphoid cells. *Annu. Rev. Immunol.* **24**, 287–320 (2006).
8. Weerkamp, F. *et al.* Human thymus contains multipotent progenitors with T/B lymphoid, myeloid, and erythroid lineage potential. *Blood* **107**, 3131–3137 (2006).
9. Corces, M. R. *et al.* Lineage-specific and single-cell chromatin accessibility charts human hematopoiesis and leukemia evolution. *Nature genetics* **48**, 1193–1203 (2016).
10. Koch, U. & Radtke, F. Mechanisms of T cell development and transformation. *Annual review of cell and developmental biology* **27**, 539–562 (2011).
11. Rothenberg, E. V., Moore, J. E. & Yui, M. A. Launching the T-Lineage Developmental Programme. *Nature reviews. Immunology* **8**, 9 (2008).
12. Porritt, H. E., Gordon, K. & Petrie, H. T. Kinetics of steady-state differentiation and mapping of intrathymic-signaling environments by stem cell transplantation in nonirradiated mice. *J Exp Med* **198**, 957–962 (2003).
13. Radtke, F. *et al.* Deficient T cell fate specification in mice with an induced inactivation of Notch1. *Immunity* **10**, 547–558 (1999).
14. Tan, J. B., Visan, I., Yuan, J. S. & Guidos, C. J. Requirement for Notch1 signals at sequential early stages of intrathymic T cell development. *Nat Immunol* **6**, 671 (2005).
15. Petrie, H. T. & Zúñiga-Pflücker, J. C. Zoned out: functional mapping of stromal signaling microenvironments in the thymus. *Annu. Rev. Immunol.* **25**, 649–679 (2007).
16. Takahama, Y. Journey through the thymus: stromal guides for T-cell development and selection. *Nature reviews. Immunology* **6**, 127–135 (2006).
17. Masuda, K. *et al.* T cell lineage determination precedes the initiation of TCR $\beta$  gene rearrangement. *The Journal of Immunology* **179**, 3699–3706 (2007).
18. Kang, J., Volkman, A. & Raulet, D. H. Evidence that  $\gamma\delta$  versus  $\alpha\beta$  T cell fate determination is initiated independently of T cell receptor signaling. *J Exp Med* **193**, 689–698 (2001).

19. Ciofani, M., Knowles, G. C., Wiest, D. L., Boehmer, von, H. & Zúñiga-Pflücker, J. C. Stage-specific and differential notch dependency at the  $\alpha\beta$  and  $\gamma\delta$  T lineage bifurcation. *Immunity* **25**, 105–116 (2006).
20. Lauritsen, J. P. H. *et al.* Marked induction of the helix-loop-helix protein Id3 promotes the  $\gamma\delta$  T cell fate and renders their functional maturation Notch independent. *Immunity* **31**, 565–575 (2009).
21. Boehmer, Von, H. Opinion: Unique features of the pre-T-cell receptor [alpha]-chain: not just a surrogate. *Nature reviews. Immunology* **5**, 571 (2005).
22. Brugnera, E. *et al.* Coreceptor reversal in the thymus: signaled CD4+ 8+ thymocytes initially terminate CD8 transcription even when differentiating into CD8+ T cells. *Immunity* **13**, 59–71 (2000).
23. Sarafova, S. D. *et al.* Modulation of coreceptor transcription during positive selection dictates lineage fate independently of TCR/coreceptor specificity. *Immunity* **23**, 75–87 (2005).
24. Liu, X. & Bosselut, R. Duration of TCR signaling controls CD4-CD8 lineage differentiation in vivo. *Nat Immunol* **5**, 280 (2004).
25. Wang, L. & Bosselut, R. CD4-CD8 lineage differentiation: Thpok-ing into the nucleus. *The Journal of Immunology* **183**, 2903–2910 (2009).
26. Wang, L. *et al.* Distinct functions for the transcription factors GATA-3 and ThPOK during intrathymic differentiation of CD4+ T cells. *Nat Immunol* **9**, 1122–1130 (2008).
27. Hernández-Hoyos, G., Anderson, M. K., Wang, C., Rothenberg, E. V. & Alberola-Ila, J. GATA-3 expression is controlled by TCR signals and regulates CD4/CD8 differentiation. *Immunity* **19**, 83–94 (2003).
28. Collins, A., Littman, D. R. & Taniuchi, I. RUNX proteins in transcription factor networks that regulate T-cell lineage choice. *Nature reviews. Immunology* **9**, 106 (2009).
29. Carpenter, A. C. & Bosselut, R. Decision checkpoints in the thymus. *Nat Immunol* **11**, 666–673 (2010).
30. Shioh, L. R. *et al.* CD69 acts downstream of interferon-[alpha]/[beta] to inhibit S1P1 and lymphocyte egress from lymphoid organs. *Nature* **440**, 540 (2006).
31. Ngoenkam, J., Schamel, W. & Pongcharoen, S. Selected signalling proteins recruited to the T cell receptor-CD3 complex. *Immunology* (2017).
32. Brownlie, R. J. & Zamoyska, R. T cell receptor signalling networks: branched, diversified and bounded. *Nature reviews. Immunology* **13**, 257 (2013).
33. Hermiston, M. L., Xu, Z. & Weiss, A. CD45: a critical regulator of signaling thresholds in immune cells. *Annu. Rev. Immunol.* **21**, 107–137 (2003).
34. Schmedt, C., Saijo, K., Nildome, T. & Kuhn, R. Csk controls antigen receptor-mediated development and selection of T-lineage cells. *Nature* **394**, 901 (1998).
35. Li, M. O. & Rudensky, A. Y. T cell receptor signalling in the control of regulatory T cell differentiation and function. *Nature reviews. Immunology* **16**, 220–233 (2016).
36. Bousso, P. T-cell activation by dendritic cells in the lymph node: lessons from the movies. *Nature reviews. Immunology* **8**, 675 (2008).
37. Anderson, A. O. & Anderson, N. D. Studies on the structure and permeability of the microvasculature in normal rat lymph nodes. *The American journal of*



- pathology* **80**, 387 (1975).
38. Ruddle, N. H. & Akirav, E. M. Secondary lymphoid organs: responding to genetic and environmental cues in ontogeny and the immune response. *The Journal of Immunology* **183**, 2205–2212 (2009).
  39. Masopust, D. & Schenkel, J. M. The integration of T cell migration, differentiation and function. *Nature reviews. Immunology* **13**, 309 (2013).
  40. Bousso, P. & Robey, E. Dynamics of CD8<sup>+</sup> T cell priming by dendritic cells in intact lymph nodes. *Nat Immunol* **4**, 579 (2003).
  41. Yokosuka, T. & Saito, T. in *Immunological Synapse* 81–107 (Springer, 2010).
  42. Lanzavecchia, A. Three signals and a master switch in the regulation of T-cell immunity. in **64**, 253–258 (Cold Spring Harbor Laboratory Press, 1999).
  43. Irvine, D. J., Purbhoo, M. A., Krogsgaard, M. & Davis, M. M. Direct observation of ligand recognition by T cells. *Nature* **419**, 845 (2002).
  44. Chen, L. & Flies, D. B. Molecular mechanisms of T cell co-stimulation and co-inhibition. *Nature reviews. Immunology* **13**, 227 (2013).
  45. Sharpe, A. H. & Abbas, A. K. T-cell costimulation—biology, therapeutic potential, and challenges. *New England Journal of Medicine* **355**, 973–975 (2006).
  46. Hutloff, A., Dittrich, A. M., Beier, K. C. & Eljaschewitsch, B. ICOS is an inducible T-cell co-stimulator structurally and functionally related to CD28. *Nature* **397**, 263 (1999).
  47. McAdam, A. J. *et al.* Mouse inducible costimulatory molecule (ICOS) expression is enhanced by CD28 costimulation and regulates differentiation of CD4<sup>+</sup> T cells. *The Journal of Immunology* **165**, 5035–5040 (2000).
  48. Yong, P. F., Salzer, U. & Grimbacher, B. The role of costimulation in antibody deficiencies: ICOS and common variable immunodeficiency. *Immunological reviews* **229**, 101–113 (2009).
  49. Walker, L. S. & Sansom, D. M. The emerging role of CTLA4 as a cell-extrinsic regulator of T cell responses. *Nature reviews. Immunology* **11**, 852–863 (2011).
  50. Kim, H. *et al.* Direct interaction of CD40 on tumor cells with CD40L on T cells increases the proliferation of tumor cells by enhancing TGF- $\beta$  production and Th17 differentiation. *PLoS One* **10**, e0125742 (2015).
  51. Lanzavecchia, A. Immunology: licence to kill. *Nature* **393**, 413–414 (1998).
  52. Parish, C. R. & Liew, F. Y. Immune response to chemically modified flagellin. *J Exp Med* **135**, 298–311 (1972).
  53. Szabo, S. J., Dighe, A. S., Gubler, U. & Murphy, K. M. Regulation of the interleukin (IL)-12R  $\beta$ 2 subunit expression in developing T helper 1 (Th1) and Th2 cells. *J Exp Med* **185**, 817–824 (1997).
  54. Owyang, A. M. *et al.* Interleukin 25 regulates type 2 cytokine-dependent immunity and limits chronic inflammation in the gastrointestinal tract. *J Exp Med* **203**, 843–849 (2006).
  55. Annunziato, F. & Romagnani, S. Heterogeneity of human effector CD4<sup>+</sup> T cells. *Arthritis research & therapy* **11**, 257 (2009).
  56. Muranski, P. & Restifo, N. P. Essentials of Th17 cell commitment and plasticity. *Blood* **121**, 2402–2414 (2013).
  57. O’Shea, J. J. & Paul, W. E. Mechanisms underlying lineage commitment and plasticity of helper CD4<sup>+</sup> T cells. *Science* **327**, 1098–1102 (2010).
  58. Becattini, S. *et al.* Functional heterogeneity of human memory CD4<sup>+</sup> T cell

- clones primed by pathogens or vaccines. *Science* **347**, 400–406 (2015).
59. Sallusto, F., Cassotta, A., Hoces, D., Foglierini, M. & Lanzavecchia, A. Do Memory CD4 T Cells Keep Their Cell-Type Programming: Plasticity versus Fate Commitment? T-Cell Heterogeneity, Plasticity, and Selection in Humans. *Cold Spring Harbor Perspectives in Biology* a029421 (2017).
  60. Lanzavecchia, A. & Sallusto, F. Dynamics of T lymphocyte responses: intermediates, effectors, and memory cells. *Science* **290**, 92–97 (2000).
  61. Almeida, L., Lochner, M., Berod, L. & Sparwasser, T. Metabolic pathways in T cell activation and lineage differentiation. *Seminars in Immunology* **28**, 514–524 (2016).
  62. GUPPY, M., GREINER, E. & BRAND, K. The role of the Crabtree effect and an endogenous fuel in the energy metabolism of resting and proliferating thymocytes. *The FEBS Journal* **212**, 95–99 (1993).
  63. Bradley, L. M., Haynes, L. & Swain, S. L. IL-7: maintaining T-cell memory and achieving homeostasis. *Trends in Immunology* **26**, 172–176 (2005).
  64. Cekic, C., Sag, D., Day, Y.-J. & Linden, J. Extracellular adenosine regulates naive T cell development and peripheral maintenance. *J Exp Med* jem–20130249 (2013).
  65. Wang, R. *et al.* The transcription factor Myc controls metabolic reprogramming upon T lymphocyte activation. *Immunity* **35**, 871–882 (2011).
  66. Sinclair, L. V. *et al.* Control of amino-acid transport by antigen receptors coordinates the metabolic reprogramming essential for T cell differentiation. *Nat Immunol* **14**, 500–508 (2013).
  67. Macintyre, A. N. *et al.* The glucose transporter Glut1 is selectively essential for CD4 T cell activation and effector function. *Cell metabolism* **20**, 61–72 (2014).
  68. Vander Heiden, M. G., Cantley, L. C. & Thompson, C. B. Understanding the Warburg effect: the metabolic requirements of cell proliferation. *Science* **324**, 1029–1033 (2009).
  69. MacIver, N. J., Michalek, R. D. & Rathmell, J. C. Metabolic regulation of T lymphocytes. *Annu. Rev. Immunol.* **31**, 259–283 (2013).
  70. Anastasiou, D. *et al.* Inhibition of pyruvate kinase M2 by reactive oxygen species contributes to cellular antioxidant responses. *Science* **334**, 1278–1283 (2011).
  71. Chi, H. Regulation and function of mTOR signalling in T cell fate decisions. *Nature reviews. Immunology* **12**, 325–338 (2012).
  72. Delgoffe, G. M. *et al.* The kinase mTOR regulates the differentiation of helper T cells through the selective activation of signaling by mTORC1 and mTORC2. *Nat Immunol* **12**, 295–303 (2011).
  73. Pollizzi, K. N. *et al.* mTORC1 and mTORC2 selectively regulate CD8+ T cell differentiation. *J Clin Invest* **125**, 2090 (2015).
  74. Laplante, M. & Sabatini, D. M. mTOR signaling in growth control and disease. *Cell* **149**, 274–293 (2012).
  75. Porstmann, T. *et al.* SREBP activity is regulated by mTORC1 and contributes to Akt-dependent cell growth. *Cell metabolism* **8**, 224–236 (2008).
  76. Miyamoto, S., Murphy, A. N. & Brown, J. H. Akt mediates mitochondrial protection in cardiomyocytes through phosphorylation of mitochondrial hexokinase-II. *Cell Death & Differentiation* **15**, 521–529 (2008).
  77. John, S., Weiss, J. N. & Ribalet, B. Subcellular localization of hexokinases I and II directs the metabolic fate of glucose. *PLoS One* **6**, e17674 (2011).

78. Buck, M. D., O'Sullivan, D. & Pearce, E. L. T cell metabolism drives immunity. *J Exp Med* **212**, 1345–1360 (2015).
79. Chou, C. *et al.* c-Myc-induced transcription factor AP4 is required for host protection mediated by CD8<sup>+</sup> T cells. *Nat Immunol* **15**, 884–893 (2014).
80. Kim, J.-W., Tchernyshyov, I., Semenza, G. L. & Dang, C. V. HIF-1-mediated expression of pyruvate dehydrogenase kinase: a metabolic switch required for cellular adaptation to hypoxia. *Cell metabolism* **3**, 177–185 (2006).
81. Finlay, D. K. *et al.* PDK1 regulation of mTOR and hypoxia-inducible factor 1 integrate metabolism and migration of CD8<sup>+</sup> T cells. *J Exp Med* *jem*–20112607 (2012).
82. Doedens, A. L. *et al.* Hypoxia-inducible factors enhance the effector responses of CD8<sup>+</sup> T cells to persistent antigen. *Nat Immunol* **14**, 1173–1182 (2013).
83. Kopf, H., Gonzalo, M., Howard, O. Z. & Chen, X. Rapamycin inhibits differentiation of Th17 cells and promotes generation of FoxP3<sup>+</sup> T regulatory cells. *International immunopharmacology* **7**, 1819–1824 (2007).
84. Delgoffe, G. M. *et al.* The mTOR kinase differentially regulates effector and regulatory T cell lineage commitment. *Immunity* **30**, 832–844 (2009).
85. Michalek, R. D. *et al.* Cutting edge: distinct glycolytic and lipid oxidative metabolic programs are essential for effector and regulatory CD4<sup>+</sup> T cell subsets. *The Journal of Immunology* **186**, 3299–3303 (2011).
86. Shi, L. Z. *et al.* HIF1 $\alpha$ -dependent glycolytic pathway orchestrates a metabolic checkpoint for the differentiation of TH17 and Treg cells. *J Exp Med* **208**, 1367–1376 (2011).
87. Dang, E. V. *et al.* Control of T H 17/T reg balance by hypoxia-inducible factor 1. *Cell* **146**, 772–784 (2011).
88. Lee, K. *et al.* Mammalian target of rapamycin protein complex 2 regulates differentiation of Th1 and Th2 cell subsets via distinct signaling pathways. *Immunity* **32**, 743–753 (2010).
89. Yang, K. *et al.* T cell exit from quiescence and differentiation into Th2 cells depend on Raptor-mTORC1-mediated metabolic reprogramming. *Immunity* **39**, 1043–1056 (2013).
90. Inoki, K., Zhu, T. & Guan, K.-L. TSC2 mediates cellular energy response to control cell growth and survival. *Cell* **115**, 577–590 (2003).
91. Haxhinasto, S., Mathis, D. & Benoist, C. The AKT–mTOR axis regulates de novo differentiation of CD4<sup>+</sup> Foxp3<sup>+</sup> cells. *J Exp Med* **205**, 565–574 (2008).
92. Gerriets, V. A. & Rathmell, J. C. Metabolic pathways in T cell fate and function. *Trends in Immunology* **33**, 168–173 (2012).
93. Weng, N.-P., Araki, Y. & Subedi, K. The molecular basis of the memory T cell response: differential gene expression and its epigenetic regulation. *Nature Publishing Group* **12**, 306–315 (2012).
94. Intlekofer, A. M. *et al.* Effector and memory CD8<sup>+</sup> T cell fate coupled by T-bet and eomesodermin. *Nat Immunol* **6**, 1236–1244 (2005).
95. van der Windt, G. J. *et al.* Mitochondrial respiratory capacity is a critical regulator of CD8<sup>+</sup> T cell memory development. *Immunity* **36**, 68–78 (2012).
96. Araki, K. *et al.* mTOR regulates memory CD8 T cell differentiation. *Nature* **460**, 108 (2009).
97. Gallegos, A. M. & Bevan, M. J. Central tolerance to tissue-specific antigens mediated by direct and indirect antigen presentation. *J Exp Med* **200**, 1039–1049 (2004).

98. Koble, C. & Kyewski, B. The thymic medulla: a unique microenvironment for intercellular self-antigen transfer. *J Exp Med* **206**, 1505–1513 (2009).
99. Rattay, K., Meyer, H. V., Herrmann, C., Brors, B. & Kyewski, B. Evolutionary conserved gene co-expression drives generation of self-antigen diversity in medullary thymic epithelial cells. *Journal of autoimmunity* **67**, 65–75 (2016).
100. Takaba, H. & Takayanagi, H. The Mechanisms of T Cell Selection in the Thymus. *Trends in Immunology* (2017).
101. Koonpaew, S., Shen, S., Flowers, L. & Zhang, W. LAT-mediated signaling in CD4<sup>+</sup> CD25<sup>+</sup> regulatory T cell development. *J Exp Med* **203**, 119–129 (2006).
102. Akiyama, T. *et al.* Dependence of self-tolerance on TRAF6-directed development of thymic stroma. *Science* **308**, 248–251 (2005).
103. Kajiura, F. *et al.* NF- $\kappa$ B-inducing kinase establishes self-tolerance in a thymic stroma-dependent manner. *The Journal of Immunology* **172**, 2067–2075 (2004).
104. Watanabe, N., Yi-Hong, W., Lee, H. K. & Ito, T. Hassall's corpuscles instruct dendritic cells to induce CD4<sup>+</sup> CD25<sup>+</sup> regulatory T cells in human thymus. *Nature* **436**, 1181 (2005).
105. Lin, W. *et al.* Regulatory T cell development in the absence of functional Foxp3. *Nat Immunol* **8**, 359 (2007).
106. Gavin, M. A. *et al.* Foxp3-dependent programme of regulatory T-cell differentiation. *Nature* **445**, 771 (2007).
107. Sakaguchi, S., Yamaguchi, T., Nomura, T. & Ono, M. Regulatory T cells and immune tolerance. *Cell* **133**, 775–787 (2008).
108. Chen, W. *et al.* Conversion of peripheral CD4<sup>+</sup> CD25<sup>–</sup> naive T cells to CD4<sup>+</sup> CD25<sup>+</sup> regulatory T cells by TGF- $\beta$  induction of transcription factor Foxp3. *J Exp Med* **198**, 1875–1886 (2003).
109. Kretschmer, K. *et al.* Inducing and expanding regulatory T cell populations by foreign antigen. *Nat Immunol* **6**, 1219 (2005).
110. Chen, Q., Kim, Y. C., Laurence, A., Punkosdy, G. A. & Shevach, E. M. IL-2 controls the stability of Foxp3 expression in TGF- $\beta$ -induced Foxp3<sup>+</sup> T cells in vivo. *The Journal of Immunology* **186**, 6329–6337 (2011).
111. Benson, M. J., Pino-Lagos, K., Roseblatt, M. & Noelle, R. J. All-trans retinoic acid mediates enhanced T reg cell growth, differentiation, and gut homing in the face of high levels of co-stimulation. *J Exp Med* **204**, 1765–1774 (2007).
112. Gallimore, A. *et al.* Induction and exhaustion of lymphocytic choriomeningitis virus-specific cytotoxic T lymphocytes visualized using soluble tetrameric major histocompatibility complex class I-peptide complexes. *J Exp Med* **187**, 1383–1393 (1998).
113. Zajac, A. J. *et al.* Viral immune evasion due to persistence of activated T cells without effector function. *J Exp Med* **188**, 2205–2213 (1998).
114. Wherry, E. J. T cell exhaustion. *Nature Publishing Group* **131**, 492–499 (2011).
115. Wherry, E. J. & Kurachi, M. Molecular and cellular insights into T cell exhaustion. *Nature Publishing Group* **15**, 486–499 (2015).
116. Doering, T. A. *et al.* Network analysis reveals centrally connected genes and pathways involved in CD8<sup>+</sup> T cell exhaustion versus memory. *Immunity* **37**, 1130–1144 (2012).

117. Schietinger, A. & Greenberg, P. D. Tolerance and exhaustion: defining mechanisms of T cell dysfunction. *Trends in Immunology* **35**, 51–60 (2014).
118. Wherry, E. J., Blattman, J. N., Murali-Krishna, K., Van Der Most, R. & Ahmed, R. Viral persistence alters CD8 T-cell immunodominance and tissue distribution and results in distinct stages of functional impairment. *Journal of virology* **77**, 4911–4927 (2003).
119. Quigley, M. *et al.* Transcriptional analysis of HIV-specific CD8<sup>+</sup> T cells shows that PD-1 inhibits T cell function by upregulating BATF. *Nature medicine* **16**, 1147–1151 (2010).
120. Angelosanto, J. M., Blackburn, S. D., Crawford, A. & Wherry, E. J. Progressive loss of memory T cell potential and commitment to exhaustion during chronic viral infection. *Journal of virology* **86**, 8161–8170 (2012).
121. Brooks, D. G., McGavern, D. B. & Oldstone, M. B. Reprogramming of antiviral T cells prevents inactivation and restores T cell activity during persistent viral infection. *Journal of Clinical Investigation* **116**, 1675 (2006).
122. Agnellini, P. *et al.* Impaired NFAT nuclear translocation results in split exhaustion of virus-specific CD8<sup>+</sup> T cell functions during chronic viral infection. *Proc Natl Acad Sci USA* **104**, 4565–4570 (2007).
123. Chiu, Y.-L. *et al.* Sprouty-2 regulates HIV-specific T cell polyfunctionality. *J Clin Invest* **124**, 198 (2014).
124. Martinez, G. J. *et al.* The transcription factor NFAT promotes exhaustion of activated CD8<sup>+</sup> T cells. *Immunity* **42**, 265–278 (2015).
125. Parry, R. V. *et al.* CTLA-4 and PD-1 receptors inhibit T-cell activation by distinct mechanisms. *Molecular and cellular biology* **25**, 9543–9553 (2005).
126. Yokosuka, T. *et al.* Programmed cell death 1 forms negative costimulatory microclusters that directly inhibit T cell receptor signaling by recruiting phosphatase SHP2. *J Exp Med* **209**, 1201–1217 (2012).
127. Clayton, K. L. *et al.* T Cell Ig and Mucin Domain-Containing Protein 3 Is Recruited to the Immune Synapse, Disrupts Stable Synapse Formation, and Associates with Receptor Phosphatases. *The Journal of Immunology* **192**, 782–791 (2014).
128. Blackburn, S. D. *et al.* Coregulation of CD8<sup>+</sup> T cell exhaustion by multiple inhibitory receptors during chronic viral infection. *Nat Immunol* **10**, 29–37 (2009).
129. Ejrnaes, M. *et al.* Resolution of a chronic viral infection after interleukin-10 receptor blockade. *J Exp Med* **203**, 2461–2472 (2006).
130. Brooks, D. G. *et al.* Interleukin-10 determines viral clearance or persistence in vivo. *Nature medicine* **12**, 1301 (2006).
131. Brooks, D. G. *et al.* IL-10 and PD-L1 operate through distinct pathways to suppress T-cell activity during persistent viral infection. *Proc Natl Acad Sci USA* **105**, 20428–20433 (2008).
132. Tinoco, R., Alcalde, V., Yang, Y., Sauer, K. & Zuniga, E. I. Cell-intrinsic transforming growth factor- $\beta$  signaling mediates virus-specific CD8<sup>+</sup> T cell deletion and viral persistence in vivo. *Immunity* **31**, 145–157 (2009).
133. Garidou, L., Heydari, S., Gossa, S. & McGavern, D. B. Therapeutic blockade of transforming growth factor beta fails to promote clearance of a persistent viral infection. *Journal of virology* **86**, 7060–7071 (2012).
134. Boettler, T., Cheng, Y., Ehrhardt, K. & Herrath, von, M. TGF- $\beta$  blockade does not improve control of an established persistent viral infection. *Viral immunology* **25**, 232–238 (2012).

135. Teijaro, J. R. *et al.* Persistent LCMV infection is controlled by blockade of type I interferon signaling. *Science* **340**, 207–211 (2013).
136. Wilson, E. B. *et al.* Blockade of chronic type I interferon signaling to control persistent LCMV infection. *Science* **340**, 202–207 (2013).
137. BURNET, M. Cancer: a biological approach. III. Viruses associated with neoplastic conditions. IV. Practical applications. *British medical journal* **1**, 841–847 (1957).
138. Burnet, F. M. in *Immunological Aspects of Neoplasia* **13**, 1–27 (Karger Publishers, 1970).
139. Shankaran, V. *et al.* IFN $\gamma$  and lymphocytes prevent primary tumour development and shape tumour immunogenicity. *Nature* **410**, 1107–1111 (2001).
140. Schreiber, R. D., Old, L. J. & Smyth, M. J. Cancer immunoediting: integrating immunity's roles in cancer suppression and promotion. *Science* **331**, 1565–1570 (2011).
141. Ward, J. P., Gubin, M. M. & Schreiber, R. D. *The Role of Neoantigens in Naturally Occurring and Therapeutically Induced Immune Responses to Cancer. Tumor Immunology* **130**, 25–74 (Elsevier Inc., 2016).
142. Smyth, M. J., Godfrey, D. I. & Trapani, J. A. A fresh look at tumor immunosurveillance and immunotherapy. *Nat Immunol* **2**, 293–299 (2001).
143. Teng, M. W., Galon, J., Fridman, W.-H. & Smyth, M. J. From mice to humans: developments in cancer immunoediting. *J Clin Invest* **125**, 3338–3346 (2015).
144. Diamond, M. S. *et al.* Type I interferon is selectively required by dendritic cells for immune rejection of tumors. *J Exp Med* jem–20101158 (2011).
145. Fuertes, M. B. *et al.* Host type I IFN signals are required for antitumor CD8<sup>+</sup> T cell responses through CD8 $\alpha$ <sup>+</sup> dendritic cells. *J Exp Med* **208**, 2005–2016 (2011).
146. MacKie, R. M., Reid, R. & Junor, B. Fatal melanoma transferred in a donated kidney 16 years after melanoma surgery. *New England Journal of Medicine* **348**, 567–568 (2003).
147. Koebel, C. M. *et al.* Adaptive immunity maintains occult cancer in an equilibrium state. *Nature* **450**, 903–907 (2007).
148. Hanahan, D. & Weinberg, R. A. Hallmarks of Cancer: The Next Generation. *Cell* **144**, 646–674 (2011).
149. Dunn, G. P., Old, L. J. & Schreiber, R. D. The immunobiology of cancer immunosurveillance and immunoediting. *Immunity* **21**, 137–148 (2004).
150. Vesely, M. D., Kershaw, M. H., Schreiber, R. D. & Smyth, M. J. Natural innate and adaptive immunity to cancer. *Annu. Rev. Immunol.* **29**, 235–271 (2011).
151. Yu, H., Pardoll, D. & Jove, R. STATs in cancer inflammation and immunity: a leading role for STAT3. *Nature reviews. Cancer* **9**, 798–809 (2009).
152. Mihm, M. C., Jr, Clemente, C. G. & Cascinelli, N. Tumor infiltrating lymphocytes in lymph node melanoma metastases: a histopathologic prognostic indicator and an expression of local immune response. *Laboratory investigation; a journal of technical methods and pathology* **74**, 43–47 (1996).
153. Anderson, K. G., Stromnes, I. M. & Greenberg, P. D. Obstacles Posed by the Tumor Microenvironment to T cell Activity: A Case for Synergistic Therapies. *Cancer Cell* **31**, 311–325 (2017).

154. Curiel, T. J. *et al.* Specific recruitment of regulatory T cells in ovarian carcinoma fosters immune privilege and predicts reduced survival. *Nature medicine* **10**, 942–949 (2004).
155. Galon, J. *et al.* Type, density, and location of immune cells within human colorectal tumors predict clinical outcome. *Science* **313**, 1960–1964 (2006).
156. Slaney, C. Y., Kershaw, M. H. & Darcy, P. K. Trafficking of T cells into tumors. *Cancer research* **74**, 7168–7174 (2014).
157. Harlin, H. *et al.* Chemokine expression in melanoma metastases associated with CD8<sup>+</sup> T-cell recruitment. *Cancer research* **69**, 3077–3085 (2009).
158. Mulligan, A. M. *et al.* Tumoral lymphocytic infiltration and expression of the chemokine CXCL10 in breast cancers from the Ontario Familial Breast Cancer Registry. *Clinical cancer research : an official journal of the American Association for Cancer Research* **19**, 336–346 (2013).
159. Peng, D. *et al.* Epigenetic silencing of TH1-type chemokines shapes tumour immunity and immunotherapy. *Nature* **527**, 249–253 (2015).
160. Motz, G. T. *et al.* Tumor endothelium FasL establishes a selective immune barrier promoting tolerance in tumors. *Nature medicine* **20**, 607–615 (2014).
161. Stromnes, I. M., Greenberg, P. D. & Hingorani, S. R. Molecular pathways: myeloid complicity in cancer. *Clinical cancer research : an official journal of the American Association for Cancer Research* **20**, 5157–5170 (2014).
162. Chou, C. K. *et al.* Cell-intrinsic abrogation of TGF- $\beta$  signaling delays but does not prevent dysfunction of self/tumor-specific CD8 T cells in a murine model of autochthonous prostate cancer. *The Journal of Immunology* **189**, 3936–3946 (2012).
163. Haddad, R. & Saldanha-Araujo, F. Mechanisms of T-cell immunosuppression by mesenchymal stromal cells: what do we know so far? *BioMed research international* **2014**, (2014).
164. Warburg, O., Wind, F. & Negelein, E. The metabolism of tumors in the body. *The Journal of general physiology* **8**, 519 (1927).
165. Singer, K. *et al.* Warburg phenotype in renal cell carcinoma: High expression of glucose-transporter 1 (GLUT-1) correlates with low CD8<sup>+</sup> T-cell infiltration in the tumor. *International journal of cancer* **128**, 2085–2095 (2011).
166. Yu, M. *et al.* The prognostic value of GLUT1 in cancers: a systematic review and meta-analysis. *Oncotarget* **8**, 43356 (2017).
167. Jacobs, S. R. *et al.* Glucose uptake is limiting in T cell activation and requires CD28-mediated Akt-dependent and independent pathways. *The Journal of Immunology* **180**, 4476–4486 (2008).
168. Cham, C. M., Driessens, G., O'Keefe, J. P. & Gajewski, T. F. Glucose deprivation inhibits multiple key gene expression events and effector functions in CD8<sup>+</sup> T cells. *Eur. J. Immunol.* **38**, 2438–2450 (2008).
169. Ho, P.-C. *et al.* Phosphoenolpyruvate is a metabolic checkpoint of anti-tumor T cell responses. *Cell* **162**, 1217–1228 (2015).
170. Mocellin, S., Bronte, V. & Nitti, D. Nitric oxide, a double edged sword in cancer biology: searching for therapeutic opportunities. *Medicinal research reviews* **27**, 317–352 (2007).
171. Sharda, D. R. *et al.* Regulation of macrophage arginase expression and tumor growth by the Ron receptor tyrosine kinase. *The Journal of Immunology* **187**, 2181–2192 (2011).
172. Pauken, K. E. *et al.* Epigenetic stability of exhausted T cells limits durability

- of reinvigoration by PD-1 blockade. *Science* aaf2807 (2016).
173. Sen, D. R. *et al.* The epigenetic landscape of T cell exhaustion. *Science* **354**, 1165–1169 (2016).
  174. Singer, M. *et al.* A distinct gene module for dysfunction uncoupled from activation in tumor-infiltrating T cells. *Cell* **166**, 1500–1511 (2016).
  175. Schietinger, A. *et al.* Tumor-specific T cell dysfunction is a dynamic antigen-driven differentiation program initiated early during tumorigenesis. *Immunity* **45**, 389–401 (2016).
  176. D'Amico, A. V. US Food and Drug Administration Approval of Drugs for the Treatment of Prostate Cancer: A New Era Has Begun. *JCO* **32**, 362–364 (2014).
  177. Lee, J., Kefford, R. & Carlino, M. PD-1 and PD-L1 inhibitors in melanoma treatment: past success, present application and future challenges. *Immunotherapy* **8**, 733–746 (2016).
  178. Specenier, P. Ipilimumab in melanoma. *Expert review of anticancer therapy* **12**, 1511–1521 (2012).
  179. van der Bruggen, P. *et al.* A gene encoding an antigen recognized by cytolytic T lymphocytes on a human melanoma. *Science* **254**, 1643–1647 (1991).
  180. Coulie, P. G., Van den Eynde, B. J., van der Bruggen, P. & Boon, T. Tumour antigens recognized by T lymphocytes: at the core of cancer immunotherapy. *Nature reviews. Cancer* **14**, 135–146 (2014).
  181. Simpson, A. J., Caballero, O. L., Jungbluth, A., Chen, Y.-T. & Old, L. J. Cancer/testis antigens, gametogenesis and cancer. *Nature reviews. Cancer* **5**, 615–625 (2005).
  182. Melero, I. *et al.* Therapeutic vaccines for cancer: an overview of clinical trials. *Nature reviews Clinical oncology* **11**, 509–524 (2014).
  183. Stone, J. D., Harris, D. T. & Kranz, D. M. TCR affinity for p/MHC formed by tumor antigens that are self-proteins: impact on efficacy and toxicity. *Current opinion in immunology* **33**, 16–22 (2015).
  184. Aleksic, M. *et al.* Different affinity windows for virus and cancer-specific T-cell receptors: Implications for therapeutic strategies. *Eur. J. Immunol.* **42**, 3174–3179 (2012).
  185. Tian, S., Maile, R., Collins, E. J. & Frelinger, J. A. CD8+ T cell activation is governed by TCR-peptide/MHC affinity, not dissociation rate. *The Journal of Immunology* **179**, 2952–2960 (2007).
  186. Morgan, R. A. *et al.* Case report of a serious adverse event following the administration of T cells transduced with a chimeric antigen receptor recognizing ERBB2. *Molecular Therapy* **18**, 843–851 (2010).
  187. Morgan, R. A. *et al.* Cancer regression and neurologic toxicity following anti-MAGE-A3 TCR gene therapy. *J Immunother* **36**, 133 (2013).
  188. Grupp, S. A. *et al.* Chimeric antigen receptor–modified T cells for acute lymphoid leukemia. *New England Journal of Medicine* **368**, 1509–1518 (2013).
  189. Yarchoan, M., Johnson, B. A., Lutz, E. R., Laheru, D. A. & Jaffee, E. M. Targeting neoantigens to augment antitumour immunity. *Nature reviews. Cancer* **17**, 209–222 (2017).
  190. Garraway, L. A. & Lander, E. S. Lessons from the cancer genome. *Cell* **153**, 17–37 (2013).
  191. Rooney, M. S., Shukla, S. A., Wu, C. J., Getz, G. & Hacohen, N. Molecular



- and genetic properties of tumors associated with local immune cytolytic activity. *Cell* **160**, 48–61 (2015).
192. Snyder, A. *et al.* Genetic basis for clinical response to CTLA-4 blockade in melanoma. *New England Journal of Medicine* **371**, 2189–2199 (2014).
  193. Kreiter, S. *et al.* Mutant MHC class II epitopes drive therapeutic immune responses to cancer. *Nature* **520**, 692–696 (2015).
  194. Topalian, S. L., Weiner, G. J. & Pardoll, D. M. Cancer immunotherapy comes of age. *JCO* **29**, 4828–4836 (2011).
  195. Ott, P. A. *et al.* An immunogenic personal neoantigen vaccine for patients with melanoma. *Nature Publishing Group* 1–21 (2017). doi:10.1038/nature22991
  196. Hausen, zur, H. Papillomaviruses in the causation of human cancers—a brief historical account. *Virology* **384**, 260–265 (2009).
  197. Greiner, J., Bullinger, L., Guinn, B.-A., Döhner, H. & Schmitt, M. Leukemia-associated antigens are critical for the proliferation of acute myeloid leukemia cells. *Clinical cancer research : an official journal of the American Association for Cancer Research* **14**, 7161–7166 (2008).
  198. Mahoney, K. M., Freeman, G. J. & McDermott, D. F. The next immune-checkpoint inhibitors: PD-1/PD-L1 blockade in melanoma. *Clinical therapeutics* **37**, 764–782 (2015).
  199. Lee, J. Y. *et al.* Structural basis of checkpoint blockade by monoclonal antibodies in cancer immunotherapy. *Nature communications* **7**, 13354 (2016).
  200. Wolchok, J. D. *et al.* Nivolumab plus ipilimumab in advanced melanoma. *New England Journal of Medicine* **369**, 122–133 (2013).
  201. Rosenberg, S. A., Restifo, N. P., Yang, J. C., Morgan, R. A. & Dudley, M. E. Adoptive cell transfer: a clinical path to effective cancer immunotherapy. *Nature reviews. Cancer* **8**, 299–308 (2008).
  202. Rosenberg, S. A. *et al.* Durable complete responses in heavily pretreated patients with metastatic melanoma using T-cell transfer immunotherapy. *Clinical cancer research : an official journal of the American Association for Cancer Research* **17**, 4550–4557 (2011).
  203. Robbins, P. F. *et al.* Tumor regression in patients with metastatic synovial cell sarcoma and melanoma using genetically engineered lymphocytes reactive with NY-ESO-1. *JCO* **29**, 917–924 (2011).
  204. Wayteck, L., Breckpot, K., Demeester, J., De Smedt, S. C. & Raemdonck, K. A personalized view on cancer immunotherapy. *Cancer Letters* **352**, 113–125 (2014).
  205. Chang, C.-H. *et al.* Metabolic competition in the tumor microenvironment is a driver of cancer progression. *Cell* **162**, 1229–1241 (2015).
  206. Siska, P. J. & Rathmell, J. C. T cell metabolic fitness in antitumor immunity. *Trends in Immunology* **36**, 257–264 (2015).
  207. Pollizzi, K. N. & Powell, J. D. Regulation of T cells by mTOR: the known knowns and the known unknowns. *Trends in Immunology* **36**, 13–20 (2015).
  208. Battaglia, M., Stabilini, A. & Roncarolo, M.-G. Rapamycin selectively expands CD4<sup>+</sup> CD25<sup>+</sup> FoxP3<sup>+</sup> regulatory T cells. *Blood* **105**, 4743–4748 (2005).
  209. Wang, Y., Wang, X. Y., Subjeck, J. R., Shrikant, P. A. & Kim, H. L. Temsirolimus, an mTOR inhibitor, enhances anti-tumour effects of heat shock protein cancer vaccines. *British journal of cancer* **104**, 643 (2011).

210. Chaoul, N. *et al.* Rapamycin impairs antitumor CD8<sup>+</sup> T-cell responses and vaccine-induced tumor eradication. *Cancer research* **75**, 3279–3291 (2015).
211. Patsoukis, N. *et al.* PD-1 alters T-cell metabolic reprogramming by inhibiting glycolysis and promoting lipolysis and fatty acid oxidation. *Nature communications* **6**, (2015).
212. Gerriets, V. A. *et al.* Metabolic programming and PDHK1 control CD4<sup>+</sup> T cell subsets and inflammation. *J Clin Invest* **125**, 194 (2015).
213. Sukumar, M. *et al.* Inhibiting glycolytic metabolism enhances CD8<sup>+</sup> T cell memory and antitumor function. *J Clin Invest* **123**, 4479 (2013).
214. Sukumar, M. *et al.* Mitochondrial membrane potential identifies cells with enhanced stemness for cellular therapy. *Cell metabolism* **23**, 63–76 (2016).
215. Chang, C.-H. & Pearce, E. L. Emerging concepts of T cell metabolism as a target of immunotherapy. *Nat Immunol* **17**, 364–368 (2016).
216. World Health Organization. Cancer.  
<http://www.who.int/mediacentre/factsheets/fs297/en/>
217. Ferlay, J. *et al.* Cancer incidence and mortality worldwide: sources, methods and major patterns in GLOBOCAN 2012. *Int J Cancer* E359–86 (2015). doi:10.1002/ijc.29210
218. Blachier, M., Leleu, H., Peck-Radosavljevic, M., Valla, D.-C. & Roudot-Thoraval, F. The burden of liver disease in Europe: a review of available epidemiological data. *J Hepatol* **58**, 593–608 (2013).
219. Siegel, R., Naishadham, D. & Jemal, A. Cancer statistics, 2013. *CA: A Cancer Journal for Clinicians* **63**, 11–30 (2013).
220. Greten, T. F., Duffy, A. G. & Korangy, F. Hepatocellular Carcinoma from an Immunologic Perspective. *Clinical cancer research : an official journal of the American Association for Cancer Research* **19**, 6678–6685 (2013).
221. Racanelli, V. & Rehermann, B. The liver as an immunological organ. *Hepatology* **43**, (2006).
222. Jenne, C. N. & Kubes, P. Immune surveillance by the liver. *Nat Immunol* **14**, 996–1006 (2013).
223. Sheth, K. & Bankey, P. The liver as an immune organ. *Current opinion in critical care* **7**, 99–104 (2001).
224. Crispe, I. N. Liver antigen-presenting cells. *J Hepatol* **54**, 357–365 (2011).
225. Wisse, E., De Zanger, R. B., Charels, K., Van Der Smissen, P. & McCuskey, R. S. The liver sieve: considerations concerning the structure and function of endothelial fenestrae, the sinusoidal wall and the space of Disse. *Hepatology* **5**, 683–692 (1985).
226. Kempka, G. & Kolb-Bachofen, V. Binding, uptake, and transcytosis of ligands for mannose-specific receptors in rat liver: an electron microscopic study. *Experimental cell research* **176**, 38–48 (1988).
227. Thompson, E. D., Enriquez, H. L., Fu, Y.-X. & Engelhard, V. H. Tumor masses support naive T cell infiltration, activation, and differentiation into effectors. *J Exp Med* jem–20092454 (2010).
228. Sachdeva, M. Immunology of hepatocellular carcinoma. *WJH* **7**, 2080–12 (2015).
229. Attallah, A. M., Tabll, A. A., El-Sadany, M., Ibrahim, T. A. & El-Dosoky, I. Dysregulation of blood lymphocyte subsets and natural killer cells in schistosomal liver cirrhosis and hepatocellular carcinoma. *Clinical and experimental medicine* **3**, 181–185 (2003).
230. Cabrera, R. *et al.* Hepatocellular carcinoma immunopathogenesis: clinical

- evidence for global T cell defects and an immunomodulatory role for soluble CD25 (sCD25). *Digestive diseases and sciences* **55**, 484–495 (2010).
231. Wu, K., Kryczek, I., Chen, L., Zou, W. & Welling, T. H. Kupffer cell suppression of CD8<sup>+</sup> T cells in human hepatocellular carcinoma is mediated by B7-H1/programmed death-1 interactions. *Cancer research* **69**, 8067–8075 (2009).
  232. Jia, Y. *et al.* Impaired function of CD4<sup>+</sup> T follicular helper (T<sub>fh</sub>) cells associated with hepatocellular carcinoma progression. *PLoS One* **10**, e0117458 (2015).
  233. Ormandy, L. A. *et al.* Increased populations of regulatory T cells in peripheral blood of patients with hepatocellular carcinoma. *Cancer research* **65**, 2457–2464 (2005).
  234. Kobayashi, N. *et al.* FOXP3<sup>+</sup> regulatory T cells affect the development and progression of hepatocarcinogenesis. *Clinical cancer research : an official journal of the American Association for Cancer Research* **13**, 902–911 (2007).
  235. Fu, J. *et al.* Increased regulatory T cells correlate with CD8 T-cell impairment and poor survival in hepatocellular carcinoma patients. *Gastroenterology* **132**, 2328–2339 (2007).
  236. Ghiringhelli, F., Ménard, C., Martin, F. & Zitvogel, L. The role of regulatory T cells in the control of natural killer cells: relevance during tumor progression. *Immunological reviews* **214**, 229–238 (2006).
  237. Zhang, J.-P. *et al.* Increased intratumoral IL-17-producing cells correlate with poor survival in hepatocellular carcinoma patients. *J Hepatol* **50**, 980–989 (2009).
  238. Yan, J. *et al.* Prevalence and clinical relevance of T-helper cells, Th17 and Th1, in hepatitis B virus-related hepatocellular carcinoma. *PLoS One* **9**, e96080 (2014).
  239. Murugaiyan, G. & Saha, B. Protumor vs antitumor functions of IL-17. *The Journal of Immunology* **183**, 4169–4175 (2009).
  240. Berzofsky, J. A. & Terabe, M. The contrasting roles of NKT cells in tumor immunity. *Current molecular medicine* **9**, 667–672 (2009).
  241. Bricard, G. *et al.* Enrichment of human CD4<sup>+</sup> V $\alpha$ 24/V $\beta$ 11 invariant NKT cells in intrahepatic malignant tumors. *The Journal of Immunology* **182**, 5140–5151 (2009).
  242. Anson, M. *et al.* Oncogenic  $\beta$ -catenin triggers an inflammatory response that determines the aggressiveness of hepatocellular carcinoma in mice. *J Clin Invest* **122**, 586 (2012).
  243. Zheng, C. *et al.* Landscape of Infiltrating T Cells in Liver Cancer Revealed by Single-Cell Sequencing. *Cell* **169**, 1342–1356.e16 (2017).
  244. Ferradini, L. *et al.* Analysis of T cell receptor variability in tumor-infiltrating lymphocytes from a human regressive melanoma. Evidence for in situ T cell clonal expansion. *Journal of Clinical Investigation* **91**, 1183 (1993).
  245. Hindley, J. P. *et al.* Analysis of the T-cell receptor repertoires of tumor-infiltrating conventional and regulatory T cells reveals no evidence for conversion in carcinogen-induced tumors. *Cancer research* (2010).
  246. El-Serag, H. B., Marrero, J. A., Rudolph, L. & Reddy, K. R. Diagnosis and treatment of hepatocellular carcinoma. *Gastroenterology* **134**, 1752–1763 (2008).
  247. Chan, S. L., Mok, T. & Ma, B. B. Management of hepatocellular carcinoma:

- beyond sorafenib. *Current oncology reports* **14**, 257–266 (2012).
248. Gnoni, A. *et al.* Hepatocellular carcinoma treatment over sorafenib: epigenetics, microRNAs and microenvironment. Is there a light at the end of the tunnel? *Expert opinion on therapeutic targets* **19**, 1623–1635 (2015).
  249. Bruix, J. *et al.* Regorafenib for patients with hepatocellular carcinoma who progressed on sorafenib treatment (RESORCE): a randomised, double-blind, placebo-controlled, phase 3 trial. *The Lancet* **389**, 56–66 (2017).
  250. Shirakawa, H. *et al.* Glypican-3 expression is correlated with poor prognosis in hepatocellular carcinoma. *Cancer science* **100**, 1403–1407 (2009).
  251. Sawada, Y. *et al.* Phase I trial of glypican-3-derived peptide vaccine for advanced hepatocellular carcinoma showed immunological evidence and potential for improving overall survival. *Clinical cancer research : an official journal of the American Association for Cancer Research* clincanres–3044 (2012).
  252. Sawada, Y. *et al.* Phase II study of the GPC3-derived peptide vaccine as an adjuvant therapy for hepatocellular carcinoma patients. *Oncoimmunology* **5**, e1129483 (2016).
  253. Qi, X. *et al.* Development of InCVAX, in situ cancer vaccine, and its immune response in mice with hepatocellular cancer. *Journal of clinical & cellular immunology* **7**, (2016).
  254. Zhou, F. *et al.* InCVAX—A novel strategy for treatment of late-stage, metastatic cancers through photoimmunotherapy induced tumor-specific immunity. *Cancer Letters* **359**, 169–177 (2015).
  255. Wang, X.-P. *et al.* Recombinant heat shock protein 70 functional peptide and alpha-fetoprotein epitope peptide vaccine elicits specific anti-tumor immunity. *Oncotarget* **7**, 71274–71284 (2016).
  256. Aravalli, R. N. & Steer, C. J. Immune-Mediated Therapies for Liver Cancer. *Genes* **8**, 76 (2017).
  257. Gao, H. *et al.* Development of T cells redirected to glypican-3 for the treatment of hepatocellular carcinoma. *Clinical cancer research : an official journal of the American Association for Cancer Research* **20**, 6418–6428 (2014).
  258. Zhang, T. & Herlyn, D. Combination of active specific immunotherapy or adoptive antibody or lymphocyte immunotherapy with chemotherapy in the treatment of cancer. *Cancer Immunology, Immunotherapy* **58**, 475–492 (2009).
  259. Franceschetti, M. *et al.* Cytokine-induced killer cells are terminally differentiated activated CD8 cytotoxic T-EMRA lymphocytes. *Experimental hematology* **37**, 616–628 (2009).
  260. Parkhurst, M. R., Riley, J. P., Dudley, M. E. & Rosenberg, S. A. Adoptive transfer of autologous natural killer cells leads to high levels of circulating natural killer cells but does not mediate tumor regression. *Clinical cancer research : an official journal of the American Association for Cancer Research* (2011).
  261. Hui, D., Qiang, L., Jian, W., Ti, Z. & Da-Lu, K. A randomized, controlled trial of postoperative adjuvant cytokine-induced killer cells immunotherapy after radical resection of hepatocellular carcinoma. *Digestive and liver disease* **41**, 36–41 (2009).
  262. Takayama, T. *et al.* Adoptive immunotherapy to lower postsurgical recurrence rates of hepatocellular carcinoma: a randomised trial. *The Lancet*

- 356**, 802–807 (2000).
263. Ma, Y. *et al.* Cytokine-induced killer (CIK) cell therapy for patients with hepatocellular carcinoma: efficacy and safety. *Experimental hematology & oncology* **1**, 11 (2012).
  264. Weng, D.-S. *et al.* Minimally invasive treatment combined with cytokine-induced killer cells therapy lower the short-term recurrence rates of hepatocellular carcinomas. *J Immunother* **31**, 63–71 (2008).
  265. Yu, X. *et al.* A randomized phase II study of autologous cytokine-induced killer cells in treatment of hepatocellular carcinoma. *Journal of clinical immunology* **34**, 194–203 (2014).
  266. Lee, J. H. *et al.* Adjuvant immunotherapy with autologous cytokine-induced killer cells for hepatocellular carcinoma. *Gastroenterology* **148**, 1383–1391 (2015).
  267. Sangro, B. *et al.* A clinical trial of CTLA-4 blockade with tremelimumab in patients with hepatocellular carcinoma and chronic hepatitis C. *J Hepatol* **59**, 81–88 (2013).
  268. Gardiner, D. *et al.* A randomized, double-blind, placebo-controlled assessment of BMS-936558, a fully human monoclonal antibody to programmed death-1 (PD-1), in patients with chronic hepatitis C virus infection. *PLoS One* **8**, e63818 (2013).
  269. Chen, N. *et al.* Lymphocyte activation gene 3 negatively regulates the function of intrahepatic hepatitis C virus-specific CD8<sup>+</sup> T cells. *Journal of gastroenterology and hepatology* **30**, 1788–1795 (2015).
  270. Li, F.-J., Zhang, Y., Jin, G.-X., Yao, L. & Wu, D.-Q. Expression of LAG-3 is coincident with the impaired effector function of HBV-specific CD8<sup>+</sup> T cell in HCC patients. *Immunology letters* **150**, 116–122 (2013).
  271. McMahan, R. H. *et al.* Tim-3 expression on PD-1<sup>+</sup> HCV-specific human CTLs is associated with viral persistence, and its blockade restores hepatocyte-directed in vitro cytotoxicity. *J Clin Invest* **120**, 4546–4557 (2010).
  272. Geiger, R. *et al.* L-arginine modulates T cell metabolism and enhances survival and anti-tumor activity. *Cell* **167**, 829–842 (2016).
  273. Vriskoop, N. *et al.* Sparse production but preferential incorporation of recently produced naive T cells in the human peripheral pool. *Proc Natl Acad Sci USA* **105**, 6115–6120 (2008).
  274. Grover, W. H. *et al.* Measuring single-cell density. *Proc Natl Acad Sci USA* **108**, 10992–10996 (2011).
  275. Rellahan, B. L. *et al.* Elf-1 regulates basal expression from the T cell antigen receptor  $\zeta$ -chain gene promoter. *The Journal of Immunology* **160**, 2794–2801 (1998).
  276. Grenningloh, R. *et al.* Ets-1 maintains IL-7 receptor expression in peripheral T cells. *The Journal of Immunology* **186**, 969–976 (2011).
  277. Kerdiles, Y. M. *et al.* Foxo1 links homing and survival of naive T cells by regulating L-selectin, CCR7 and interleukin 7 receptor. *Nat Immunol* **10**, 176–184 (2009).
  278. Kakugawa, K. *et al.* Essential Roles of SATB1 in Specifying T Lymphocyte Subsets. *Cell Reports* **19**, 1176–1188 (2017).
  279. Lin, W.-H. W. *et al.* CD8<sup>+</sup> T lymphocyte self-renewal during effector cell determination. *Cell Reports* **17**, 1773–1782 (2016).
  280. Wei, H. *et al.* Cutting edge: Foxp1 controls naive CD8<sup>+</sup> T cell quiescence by

- simultaneously repressing key pathways in cellular metabolism and cell cycle progression. *The Journal of Immunology* **196**, 3537–3541 (2016).
281. Bjørkøy, G. *et al.* p62/SQSTM1 forms protein aggregates degraded by autophagy and has a protective effect on huntingtin-induced cell death. *The Journal of cell biology* **171**, 603–614 (2005).
  282. Xu, X. *et al.* Autophagy is essential for effector CD8<sup>+</sup> T cell survival and memory formation. *Nat Immunol* **15**, 1152–1161 (2014).
  283. Thoreen, C. C. *et al.* A unifying model for mTORC1-mediated regulation of mRNA translation. *Nature* **485**, 109 (2012).
  284. West, M. J., Stoneley, M. & Willis, A. E. Translational induction of the c-myc oncogene via activation of the FRAP/TOR signalling pathway. *Oncogene* **17**, (1998).
  285. Gordan, J. D., Thompson, C. B. & Simon, M. C. HIF and c-Myc: sibling rivals for control of cancer cell metabolism and proliferation. *Cancer Cell* **12**, 108–113 (2007).
  286. Klumpp, S., Scott, M., Pedersen, S. & Hwa, T. Molecular crowding limits translation and cell growth. *Proc Natl Acad Sci USA* **110**, 16754–16759 (2013).
  287. MacDonald, H. R. & Zaech, P. Light scatter analysis and sorting of cells activated in mixed leukocyte culture. *Cytometry Part A* **3**, 55–58 (1982).
  288. Fabre, S. *et al.* FOXO1 regulates L-Selectin and a network of human T cell homing molecules downstream of phosphatidylinositol 3-kinase. *The Journal of Immunology* **181**, 2980–2989 (2008).
  289. Kuo, C. T., Veselits, M. L. & Leiden, J. M. LKLF: A transcriptional regulator of single-positive T cell quiescence and survival. *Science* **277**, 1986–1990 (1997).
  290. Li, C. *et al.* Autophagy is induced in CD4<sup>+</sup> T cells and important for the growth factor-withdrawal cell death. *The Journal of Immunology* **177**, 5163–5168 (2006).
  291. Botbol, Y., Guerrero Ros, I. & Macian, F. Key roles of autophagy in regulating T-cell function. *Eur. J. Immunol.* **46**, 1326–1334 (2016).
  292. Wolf, A. *et al.* Hexokinase 2 is a key mediator of aerobic glycolysis and promotes tumor growth in human glioblastoma multiforme. *J Exp Med* jem–20101470 (2011).
  293. Palmieri, D. *et al.* Analyses of resected human brain metastases of breast cancer reveal the association between up-regulation of hexokinase 2 and poor prognosis. *Molecular Cancer Research* **7**, 1438–1445 (2009).
  294. Monticelli, L. A. *et al.* Arginase 1 is an innate lymphoid cell-intrinsic metabolic checkpoint controlling type 2 inflammation. *Nat Immunol* **17**, 656 (2016).
  295. Feng, Y. *et al.* Global analysis of protein structural changes in complex proteomes. *Nature biotechnology* **32**, 1036–1044 (2014).
  296. Ganapathy, V., Daniels, T. & Casiano, C. A. LEDGF/p75: a novel nuclear autoantigen at the crossroads of cell survival and apoptosis. *Autoimmunity reviews* **2**, 290–297 (2003).
  297. Jaendling, A. & McFarlane, R. J. Biological roles of translin and translin-associated factor-X: RNA metabolism comes to the fore. *Biochemical Journal* **429**, 225–234 (2010).
  298. He, X., Lin, H., Yuan, L. & Li, B. Combination therapy with L-arginine and  $\alpha$ -PD-L1 antibody boosts immune response against osteosarcoma in

- immunocompetent mice. *Cancer Biology & Therapy* **18**, 94–100 (2017).
299. Rui, L. Energy metabolism in the liver. *Comprehensive physiology* (2014).
300. Forman, D. *et al.* Cancer Incidence in Five Continents Vol. X. *IARC Scientific Publication No. . Lyon International Agency for Research on Cancer* 1–1436 (2014).
301. Barber, D. L. *et al.* Restoring function in exhausted CD8 T cells during chronic viral infection. *Nature* **439**, 682 (2006).
302. Rosenberg, S. A. & Restifo, N. P. Adoptive cell transfer as personalized immunotherapy for human cancer. *Science* **348**, 62–68 (2015).
303. Chew, V. *et al.* Inflammatory tumour microenvironment is associated with superior survival in hepatocellular carcinoma patients. *J Hepatol* **52**, 370–379 (2010).
304. Sun, C. *et al.* The predictive value of centre tumour CD8+ T cells in patients with hepatocellular carcinoma: comparison with Immunoscore. *Oncotarget* **6**, 35602 (2015).
305. Boni, C. *et al.* Characterization of Hepatitis B Virus (HBV)-Specific T-Cell Dysfunction in Chronic HBV Infection. *Journal of virology* **81**, 4215–4225 (2007).
306. Blackburn, S. D., Shin, H., Freeman, G. J. & Wherry, E. J. Selective expansion of a subset of exhausted CD8 T cells by  $\alpha$ PD-L1 blockade. *Proc Natl Acad Sci USA* **105**, 15016–15021 (2008).
307. Mognol, G. P. *et al.* Exhaustion-associated regulatory regions in CD8 +tumor-infiltrating T cells. *Proc Natl Acad Sci USA* **114**, E2776–E2785 (2017).
308. Turchaninova, M. A. *et al.* Pairing of T-cell receptor chains via emulsion PCR. *Eur. J. Immunol.* **43**, 2507–2515 (2013).
309. Briggs, A. W. *et al.* Tumor-infiltrating immune repertoires captured by single-cell barcoding in emulsion. 1–34 (2017). doi:10.1101/134841
310. DeKosky, B. J. *et al.* High-throughput sequencing of the paired human immunoglobulin heavy and light chain repertoire. *Nature biotechnology* **31**, 166–169 (2013).
311. Tang, X.-Y. *et al.* Third-generation CD28/4-1BB chimeric antigen receptor T cells for chemotherapy relapsed or refractory acute lymphoblastic leukaemia: a non-randomised, open-label phase I trial protocol. *BMJ open* **6**, e013904 (2016).
312. Messi, M. *et al.* Memory and flexibility of cytokine gene expression as separable properties of human TH1 and TH2 lymphocytes. *Nat Immunol* **4**, 78–87 (2003).
313. Fuhrer, T., Heer, D., Begemann, B. & Zamboni, N. High-throughput, accurate mass metabolome profiling of cellular extracts by flow injection–time-of-flight mass spectrometry. *Analytical chemistry* **83**, 7074–7080 (2011).
314. Link, H., Fuhrer, T., Gerosa, L., Zamboni, N. & Sauer, U. Real-time metabolome profiling of the metabolic switch between starvation and growth. *Nature Methods* **12**, 1091–1100 (2015).
315. Hornburg, D. *et al.* Deep proteomic evaluation of primary and cell line motoneuron disease models delineates major differences in neuronal characteristics. *Molecular & Cellular Proteomics* **13**, 3410–3420 (2014).
316. Rappsilber, J., Mann, M. & Ishihama, Y. Protocol for micro-purification, enrichment, pre-fractionation and storage of peptides for proteomics using

- StageTips. *Nature protocols* **2**, 1896–1906 (2007).
317. Hubner, N. C., Ren, S. & Mann, M. Peptide separation with immobilized pI strips is an attractive alternative to in-gel protein digestion for proteome analysis. *Proteomics* **8**, 4862–4872 (2008).
318. Michalski, A. *et al.* Mass spectrometry-based proteomics using Q Exactive, a high-performance benchtop quadrupole Orbitrap mass spectrometer. *Molecular & Cellular Proteomics* **10**, M111–011015 (2011).
319. Scheltema, R. A. & Mann, M. SprayQc: a real-time LC–MS/MS quality monitoring system to maximize uptime using off the shelf components. *Journal of proteome research* **11**, 3458–3466 (2012).
320. Olsen, J. V. *et al.* Higher-energy C-trap dissociation for peptide modification analysis. *Nature Methods* **4**, 709–713 (2007).
321. Carr, E. L. *et al.* Glutamine uptake and metabolism are coordinately regulated by ERK/MAPK during T lymphocyte activation. *The Journal of Immunology* **185**, 1037–1044 (2010).
322. Sanjana, N. E., Shalem, O. & Zhang, F. Improved vectors and genome-wide libraries for CRISPR screening. *Nature Methods* **11**, 783–784 (2014).
323. Ichida, M. & Finkel, T. Ras regulates NFAT3 activity in cardiac myocytes. *Journal of Biological Chemistry* **276**, 3524–3530 (2001).
324. Schütze, T. *et al.* A streamlined protocol for emulsion polymerase chain reaction and subsequent purification. *Analytical biochemistry* **410**, 155–157 (2011).
325. Malissen, M. *et al.* Altered T cell development in mice with a targeted mutation of the CD3-epsilon gene. *The EMBO journal* **14**, 4641 (1995).
326. Cox, J. & Mann, M. MaxQuant enables high peptide identification rates, individualized ppb-range mass accuracies and proteome-wide protein quantification. *Nature biotechnology* **26**, 1367–1372 (2008).
327. Cox, J. *et al.* Andromeda: a peptide search engine integrated into the MaxQuant environment. *Journal of proteome research* **10**, 1794–1805 (2011).
328. Lubber, C. A. *et al.* Quantitative proteomics reveals subset-specific viral recognition in dendritic cells. *Immunity* **32**, 279–289 (2010).
329. Wiśniewski, J. R. *et al.* Extensive quantitative remodeling of the proteome between normal colon tissue and adenocarcinoma. *Molecular systems biology* **8**, 611 (2012).
330. Subramanian, A. *et al.* Gene set enrichment analysis: a knowledge-based approach for interpreting genome-wide expression profiles. *Proc Natl Acad Sci USA* **102**, 15545–15550 (2005).



## 10 Acknowledgements

Firstly, I would like to express my gratitude to my mentors, Federica Sallusto and Antonio Lanzavecchia, for giving me the opportunity to perform my doctoral thesis in their laboratory. I consider the chance to learn from their expertise as a great privilege. In particular, I would like to thank Antonio Lanzavecchia. His advices and feedback were fundamental for the project.

I want to thank Federica Sallusto, Antonio Lanzavecchia and Manfred Kopf for being members in my PhD committee. The inspiring scientific discussion and support were essential for my PhD project, as well as for my scientific development.

I gratefully acknowledge Roger Geiger for being my mentor throughout my PhD. Beside the countless discussions and his guidance; he helped me to grow as a scientist and person.

Furthermore, I would like to thank Silvia Monticelli. Her outstanding effort during the IRB PhD course allowed me to learn critical thinking, improved my paper reviewing and gave me helpful insights in writing a grant.

I thank my lab mates Marco and Wenjie, as well as all members of institute. During my time in Bellinzona, I performed experiments in almost every lab of the institute. The scientific support represents an important pillar for this project. Especially, I would like to acknowledge Mariagrazia and her lab for hosting me for several months.

My credit goes also to our collaborators Jan Rieckmann, Felix Meissner, Yuehan Feng, Paula Picotti, Tobias Fuhrer, Maria Kogadeeva, Nicola Zamboni, Christopher Bleck, Dirk Bumann, Robert Kimmerling and Scott Manalis. Their efforts were essential for this project.

Special thanks goes to the patients that gave their consent and supported this project. In this context, I would like to give credit to Elisabetta Loggi, Pietro Andreone and Giorgio Ercolani that allowed us access to the clinical samples.

I would like to thank Yun Ding and Andrew DeMello for their collaborative efforts and for designing the microfluidics device.

Moreover, I would like to give credit to Alexander, Antonino, Joshua and Philipp for the fruitful scientific and non-scientific discussions. My gratitude goes also to Eveline, Alessandro M., Alessandro P. and Tim.

In particular, I would like to thank Kathrin. She is an amazing scientist and person. I am thankful to consider she as my friend.

Carla, Esther, Sandra, Acaymo, Gunz, Miguel and Simon, the time we could spend together was a great privilege for me. I hope our paths will cross again.

My special gratitude goes to Gianluca with whom I share my passion for mountains, hiking, hockey and other stuff. He is an outstanding person and contributed to this work more than he thinks.

Last, but not least I am deeply grateful for the support of my entire family. You always believed in me and made all this possible.

# 11 Curriculum Vitae

Tobias Wolf, Dipl. Biochem.

Address Via Fleming 8  
6500 Bellinzona  
Switzerland

Email twolf@student.ethz.ch

Mobile +41 78 819 94 48

Nationality German

## **Education and Qualification**

---

2013 (Nov) - present

### **Doctoral studies in Microbiology and Immunology**

Swiss Federal Institute of Technology (ETHZ), 8092 Zurich, Switzerland

Project title: "New approaches to understand T cell activation and circumvent T cell dysfunction in cancer"

Supervisor: Dr. Antonio Lanzavecchia, director of the Institute for Research in Biomedicine and head of the department of Immune Regulation, Bellinzona, Switzerland

#### Experimental work

- Cell culture (general)
- Human T cell culture
- Processing of primary human tissue and tumor samples
- Molecular biological techniques (Western-blot, transformation, cloning, DNA and RNA purification)
- Primer design, PCR and real-time qPCR
- Design and cloning of CRISPR/Cas9 constructs
- Generation of CRISPR/Cas9 primary human T cell clones via transfection and transduction
- Handling of microfluidic-based systems for mRNA capturing and PCR
- Design and establishment of a NFAT-GFP reporter construct
- Preparation of lentivirus for overexpression of cellular factors in human T cells and Jurkat cells
- Preparation of samples for mass spectrometry analysis
- ELISA
- Preparation of cells for pulsed SILAC
- 3D reconstruction with 3Dmod
- Epifluorescence microscopy
- Multicolor flow cytometry and FACS (BD Canto I, BD Fortessa)
- Flow cytometry applications: FlowJo 7-10

- 2013 (Nov) - present      **Student of the life science Zurich graduate school**  
Microbiology and Immunology PhD program  
Coordinator: Judith Zingg  
ETH Zurich, Switzerland
- 2012 (Nov) – 2013 (Oct)    **Diploma thesis in biochemistry (specialized field: immunology), grade: 1.1 (very good, grading system from 1 (very good) to 5 (fail))**  
University Greifswald, Germany  
Project title: “Impact of obesity on the immune reaction after a primary immunization”  
Supervisor: Prof. Dr. Barbara Broecker, Acting head of the department of Immunology, University Greifswald, Germany
- Experimental work
- Animal experimentation with C57BL/6 and ob/ob mice
  - Isolation of immune cells from adipose tissue
  - Proliferation assay with murine splenocytes
  - ELISA, ELISpot
  - PCR, restriction digests
  - Investigation of T cell subsets and macrophages with the BD™ LSR II flow cytometry system and data analysis with FACSDiva and FlowJo Software
  - Cytometric Bead Array for interleukin measurements
- 2010 – 2013                    Advanced study period with emphasis on biotechnology (Prof. Uwe Bornscheuer) and immunology (Prof. Barbara Broecker)
- 2010                              Pre-diploma in biochemistry, grade: good
- 2000 – 2007                    A-levels (Staedtisches Gymnasium “Werner Seelenbinder”, Fuerstenwalde, Germany)

### **Internships**

- 
- 2012 (Feb) – 2012 (Mar)    Internship at Federal Research Institute for Animal Health, Friedrich-Loeffler-Institute, Riems
- Work group “Biochemistry and Proteomics”, Institute for Molecular Biology
- Experimental work
- “OFFGEL” fractionation of complex peptide mixtures
  - Fractionation of serum proteins by affinity solid

- 
- phase extraction
  - Recording MALDI-TOF mass spectra of peptides and proteins

2010 (Feb-Apr) Tutor for practical course Quantitative Analysis (Dr. Ulrich Hasse, “Analytical Chemistry”, Institute of Biochemistry)

---

### Awards

IRB student Award 2016 – 2017

---

### Personal Skills

Mother Tongue	German
Other Languages	English: advanced Italian: basic

---

### Computer Skills

Operating systems	Windows 7 and earlier versions, Macintosh OS X
Office applications	Windows Office 2007 and earlier versions, GraphPad Prism 7 and earlier versions, CLC Genomic Workbench, Adobe Acrobat, Adobe Illustrator, Papers for Macintosh, Endnote

---

### Social Skills

Organization of the Life Science Zürich Graduate School retreat (Wildhaus, Switzerland 2014) and the IRB PhD Retreat (Weggis, Switzerland 2017)

Member of Student Council (Department Biochemistry, University Greifswald, Germany, 2010 – 2011 public relations officer, 2011 – 2012 treasurer)

---

### Publications

Public antibodies to malaria antigens generated by two LAIR1 insertion modalities  
K. Pieper, J. Tan, L. Piccoli, M. Foglierini, S. Barbieri, Y. Chen, C. Silacci-Fregni, T. Wolf, D. Jarrossay, M. Anderle, A. Abdi, F. M. Ndungu, O. K. Doumbo, B. Traore, T. M. Tran, S. Jongo, I. Zenklusen, P. D. Crompton, C. Daubenberger, P. C. Bull, F. Sallusto, A. Lanzavecchia  
in Nature (2017) vol. 548 pp597-601

Social network architecture of human immune cells unveiled by quantitative proteomics

J. C. Rieckmann, R. Geiger, D. Hornburg, T. Wolf, K. Kveler, D. Jarrossay, F. Sallusto, S. S. Shen-Orr, A. Lanzavecchia, M. Mann, F. Meissner  
in Nat Immunol (2017) vol. 18 pp583-593

L-Arginine Modulates T Cell Metabolism and Enhances Survival and Anti-tumor Activity

R. Geiger, J. C. Rieckmann, T. Wolf, C. Basso, Y. Feng, T. Fuhrer, M. Kogadeeva, P. Picotti, F. Meissner, M. Mann, N. Zamboni, F. Sallusto, A. Lanzavecchia  
in Cell (2016) vol. 167 pp829-842 e13

### **Publications in preparation**

---

Translation profiling reveals regulations underlying T cell naiveté and preparedness  
T. Wolf, C. Bleck, M. Pecoraro, T. Beltraminelli, M. Benevento, J. Rieckmann,  
R. Kimmerling, D. Bumann, S. Manalis, F. Meissner, M. Mann, F. Sallusto,  
A. Lanzavecchia, R. Geiger

### **References**

---

Antonio Lanzavecchia  
IRB, Via Vincenzo Vela 6  
6500 Bellinzona, Switzerland  
lanzavecchia@irb.usi.ch

Federica Sallusto  
IRB, Via Vincenzo Vela 6  
6500 Bellinzona, Switzerland  
federica.sallusto@irb.usi.ch

Manfred Kopf  
ETHZ, HPL G 12, Otto-Stern-Weg 7  
8093 Zürich, Switzerland  
manfred.kopf@biol.ethz.ch

Roger Geiger  
IRB, Via Vincenzo Vela 6  
6500 Bellinzona, Switzerland  
roger.geiger@irb.usi.ch